MACROSPIN MODEL OF MAGNETIZATION DYNAMICS GOVERNED BY LANDAU-LIFSHITZ-BLOCH EQUATION OF MOTION

by

Ufuk Kılıç

B.S., Physics, Yıldız Technical University, 2009

Submitted to the Institute for Graduate Studies in
Science and Engineering in partial fulfillment of
the requirements for the degree of
Master of Science

Graduate Program in Physics

Boğaziçi University

2012

ACKNOWLEDGEMENTS

Foremost, I would like to thank my advisor Assoc. Prof. Ozhan Ozatay for providing me a great opportunity to do my MS. thesis with him. His goal is not just to finish up something on time but is to make the work as perfect as we can and is to create new targets which needs to be discussed or studied. Accordingly, another important point is that he always expects to gain physical insight behind the models that we developed by using COMSOL Multiphysics. So that I cannot forget the presentation parts of the sample models for every Friday morning that we have carried out using COMSOL Multiphysics. All in all, he has been actively interested in my work and has always been available to advise me.

I especially want to thank on the spot, Prof. Giovanni Finnochio, whose support and guidance made my thesis work possible and his neat hostage while I was in Italy for the part of our project. Furthermore, I will not forget the taste of both aranchino and fogatcha. I want to thank present and past members of the BUSPIN lab: Ahmed Salayev, Ismail Volkan Inlek and of course Ibrahim Çinar for sharing their precious time with me for the implementation of this project. In addition to them, I would like to thank other BUSPIN members for their kind behaviors and friendships.

My special thanks go to Haluk Doğan due to his altruistic attempt in converting my thesis into LATEX form and Yemliha Bilal Kalyoncu for doing the proofreading of my thesis. Thanks to Prof. Carlos Garcia Garcia since he shared his invaluable life and academic experiences. For the non-scientific side of my thesis, I particularly want to thank my parents and sister for their neverending faith and support. Particularly, I cannot forget the coffee talks. I was really glad to be a part of these talks. I socialized there and it contributed me many things. I want to tell my family and advisor that your supports are appreciated more than you realize. I am also very grateful for the support given by Turkish Academy of Sciences TUBA-GEBIP award and Boğaziçi University Research Fund under the contract numbers 5051 and 6121.

ABSTRACT

MACROSPIN MODEL OF MAGNETIZATION DYNAMICS GOVERNED BY LANDAU-LIFSHITZ-BLOCH EQUATION OF MOTION

The main physical limitation in the down-scaling of magnetic data storage technologies, namely the superparamagnetic effect, can be pushed back considerably by using high perpendicular magnetic anisotropy materials. The lack of understanding of the nature of such switching dynamics of magnetic bits especially close to Curie temperature (T_C) led to the development of a new formalism that takes into account both longitudinal and transverse magnetization relaxation mechanisms in addition to temperature dependent damping parameters. All such effects are conventionally disregarded within the Landau-Lifshitz-Gilbert framework. In our study, we point out significant changes in the switching process close to $T_C$using the recently proposed stochastic Landau-Lifshitz-Bloch formalism which takes into account thermal excitations at elevated temperatures by including Gaussian stochastic processes. The essential motivation of current work is to develop a Stochastic-LLB based macrospin model, using experimentally measured temperature dependence of intrinsic parameters for an example magnetic system CoNi/Pd multilayers as realistic material parameters. Such a model enables us to determine the temperature dependence of longitudinal susceptibility from single fit simulations of experimental switching data consistent with previous ab-initio calculations. A map of switching time as a function of magnetic field and heating pulses together with a visualization of granular switching process is presented for the evaluation of this and similar material systems for potential thermally assisted recording applications. While using a simple macrospin approach appears effective in describing the average behavior of strongly exchange-coupled magnetic MLs, a good understanding of the detailed switching mechanism and the role of geometry when patterned into nanoscale structures would necessitate an extension of our model to the micromagnetic simulations.

ÖZET

LANDAU-LIFSHITZ-BLOCH HAREKET DENKLEMİ İLE YÖNLENDİRİDİLEN MANYETİZASYON DİNAMİĞİNİN MAKROSPİN MODELLENMESİ

Manyetik veri depolama teknolojilerinin minyatürizasyonunun ardındaki ana fiziksel sınırlama süperparamanyetik etki olarak nitelendirilir. Bu etki dikey manyetik anizotropisi yüksek malzemeler kullanıldığında kaydadeğer ölçüde geri itelenebilir. Manyetik bitlerin anahtarlama dinamiğinin doğasının, özellikle Curie sıcaklığına yakın sıcaklıklarda bilinmezliği, yeni bir formalizmanın geliştirilmesine yol açtı. Bu yeni formalizma, sıcaklığa bağlı sönümleme parametrelerine ek olarak, hem boylamsal hem de dikey olarak manyetizasyon yatışma/gevşeme mekanizmasını göz önünde bulundurmaktadır. Tüm bu etkiler, Landau-Lifshitz-Gilbert (LLG) çercevesi içinde alışıla gelmiş biçimde gözardı edilmektedir. Çalışmamızda, son zamanlarda önerilen stokastik Landau-Lifshitz-Bloch formalizmini kullanarak, Curie sıcaklığı civarında anahtarlama işleminde çok önemli değişimler olduğunu gösterdik. Stokastik tipteki bu denklem, yüksek sıcaklıklardaki termal uyarılmaları Gaussiyan stokastik işlemleri içererek göz önünde bulundurmaktadır. Şu anki çalışmanın temel motivasyonu, örnek bir manyetik sistem için deneysel yöntemlerle ölçülmüş olunan esas/intrinsik parametrelerin sıcaklığa bağlılıklarını kullanarak, stokastik LLB bazlı makrospin modelini geliştirmektir. Gerçek malzeme parametreleri olarak CoNi/Pd çok katmanlı ince film alınmıştır. Böyle bir modellemeyle, önceki ab-initio hesaplamalarıyla tutarlılık gösteren, tek fitli deneysel anahtarlama simülasyonlarından elde edilen boylamsal manyetik duygunluğun sıcaklığa bağlı fonksiyonunu saptamayı sağlamıştır. Anahtarlama için gerekli zamanın haritası, manyetik alan ve ısı darbesinin bir fonksiyonu olarak tanımlanmış ve bu harita granülün anahtarlama işleminin görselleştirmesiyle sunulmuştur. Bu gösterim ısı destekli kayıt uygulamalarındaki potansiyel kullanımı mümkün olan bu ve buna benzer malzemeli sistemlerin değerlendirilmesini sağlamaktadır. Basit bir makrospin yaklaşımı kuvvetli

değiş tokuş çiftli, manyetik çoklu katman yapıdaki ortalama davranışı gözlemlemede etkilidir. Nanoyapılara ayrıldığındaki geometrinin rolünün ve anahtarlama mekanizmasının kapsamlı olarak anlaşılması için modelimizin mikromanyetik simülasyonlara uyarlanması gerekecektir.

TABLE OF CONTENTS

LIST OF FIGURES

LIST OF TABLES

LIST OF SYMBOLS

e	Electron Charge
$f(\boldsymbol{N}, t)$	Distribution Function
g	g-factor
$\boldsymbol{h}_{an}$	Reduced Anisotropy Field
$\boldsymbol{h}_{app}$	Reduced Applied Magnetic Field (Zeeman Field)
$\boldsymbol{h}_{eff}$	Reduced Effective Magnetic Field
$\boldsymbol{h}_{exc}$	Reduced Exchange Field
$\boldsymbol{h}_{long}$	Reduced Form Of The Field Term That Controls The Longitudinal Fluctuations In The Magnetization Magnitude
$\boldsymbol{h}_{Lang}$ or $\boldsymbol{h}_{th}$	Reduced Form Of Langevin Field (Reduced Form Of Stochastic Thermal Field)
$\boldsymbol{k}_B$	Boltzman Constant
m	Reduced Magnetization Vector
$\boldsymbol{m}_0$	Equilibrium Magnetization
m_e	Electron Mass
$\boldsymbol{m}_e$	Reduced Form Of Equilibrium Magnetization
$\boldsymbol{s}_i$	Spin Magnetic Moment On i^{th} Site In The lattice
A	Area
$B(\xi)$	Langevin Function
D_x, D_y, D_z	Demagnetization Factors
$\boldsymbol{H}$	Hamiltonian Of The Spin System
$\boldsymbol{H}_{an}$	Anisotropy Field
$\boldsymbol{H}_{app}$	Applied Magnetic Field (Zeeman Field)
$\boldsymbol{H}_{eff}$	Effective Magnetic Field
$\boldsymbol{H}_{exc}$	Exchange Field
$\boldsymbol{H}_{long}$	A Field Term That Controls The Longitudinal Fluctuations In The Magnetization Magnitude
$\boldsymbol{H}_{Lang}$	Langevin Field (Stochastic Thermal Field)
$\boldsymbol{H}^E$	External Magnetic Field

$\boldsymbol{H}^{MFA}$	MFA Magnetic Field
J_0	Temperature Dependent Coefficient
$\boldsymbol{L}$	Angular Momentum
$\boldsymbol{M}$	Magnetization Vector
M_S	Saturation Magnetization
T	System Temperature
T_c	Curie Temperature
$\boldsymbol{T}_S$	Temperature Of The Magnetic Material (Sample Temperature)
$Z(\boldsymbol{\xi})$	Helmholtz Partition Function
α	Gilbert Damping Parameter
$\alpha_{//}$	Longitudinal Damping Parameter
$\alpha_{\perp}$	Transverse Damping Parameter
γ	Gyromagnetic Ratio
η_x, η_y	Anisotropy Factors
λ	Damping Coefficient
μ	Magnetic Moment
μ_e	Magnetic Moment of Electron
$\boldsymbol{\mu}_0$	Permeability Of Free Space
$\boldsymbol{\xi}$	Gaussian Stochastic Process (Gaussian Function)
$\boldsymbol{\xi}_0$	Reduced Effective Field Includes MFA Field And An External Field
$\boldsymbol{\chi}_{//}$	Longitudinal Susceptibility
$\boldsymbol{\chi}_{\perp}$	Transverse Susceptibility
$\boldsymbol{\Delta}t$	Time Step
$\boldsymbol{\Delta}V$	Volume Of The Computational Cubic Cell
Λ_N	Temperature Dependent Coefficient Of Expected Value Of Damping Torque Term In LLG Equation
$\hbar$	Planck Constant Divided By 2 π

LIST OF ACRONYMS/ABBREVIATIONS

ns	nanosecond
vs.	versus
BCC	Body Centered Cubic
HAMR	Heat Assisted Magnetic Recording
HCP	Hexagonal Close Packed
LL	Landau Lifshitz
LLB	Landau Lifshitz Bloch
LLG	Landau Lifshitz Gilbert
MFA	Mean Field Approximation
ML	MultiLayer
ODE	Ordinary Differential Equation
PDE	Partial Differential Equation
TAMR	Thermally Assisted Magnetic Recording
VSM	Vibrating Sample Magnetometry

1. INTRODUCTION

Nanomagnetism research applications include heat assisted magnetic recording (HAMR), magnetic logic devices, spin based devices. Especially, the ultrahigh density data storage is attainable using magnetic materials or their alloys. The data storage capacity is mainly determined by the magnetization dynamics of the reversal.

Since the perpendicular magnetic recording method (where magnetic bits are perpendicular to the recording medium) provides higher areal density than the longitudinal magnetic recording method (where the magnetic bits are parallel to the recording medium), the perpendicular magnetic recording method is preferred in the latest magnetic recording technologies.

As the need for higher data storage capacity increases, search for suitable magnetic materials to be used in novel magnetic recording applications is inevitably attracting attention of many research groups and companies. Yet, the main problem in increasing areal density is to tune three important correlated parameters of the material. These are the readability, the writability and thermal stability of the magnetic medium, which are setting up the trilemma of magnetic data storage [2]. The figure below shows schematic representation of this phenomena.

It is reported that, three correlated physical factors must be taken under control in achiving higher areal density data storage. These are data storage density (is possible by decreasing the volume of the bit size), thermal stability (based upon anisotropy of the material) and write heads (rely on the coercivity of the material). The interrelationships between these important factors form the trilemma of magnetic data storage. So as to reach high density data storage capacity, these three crucial points must be taken into account. However, recent advancements in the spin based reasearches, in addition to these three crucial issues another significant factor, the bit error rate, plays an undeniable role if the bit size is submicrocron scale. The bit error rate is related to the probability of thermally writing a bit to a submicron scale medium. By the

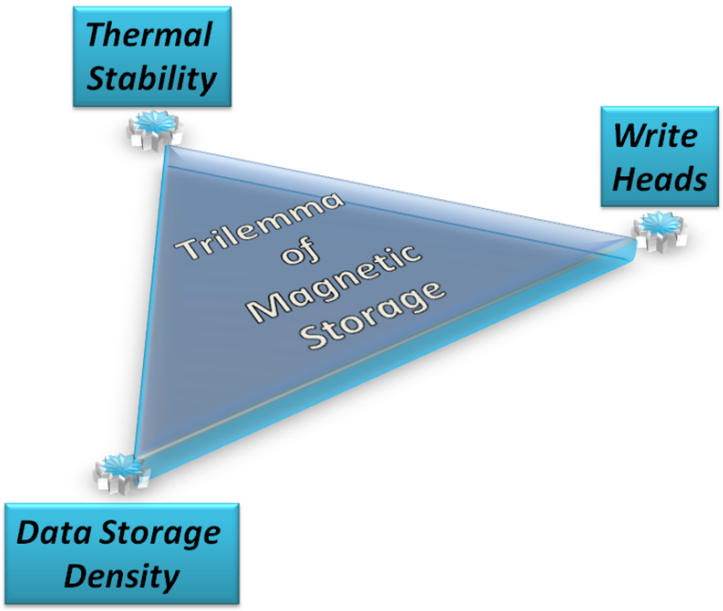

Figure 1.1. Schematic illustration of trilemma of magnetic data storage.

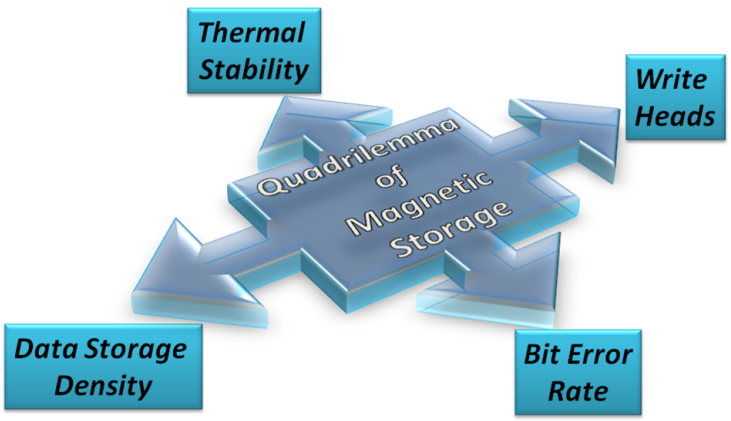

Figure 1.2. Schematic illustration of quadrilemma of magnetic data storage.

addition of the latter factor, the usual trilemma turns out to be the quadrilemma of the magnetic data storage [3].

After the clear description of problems in front of achiving high density data staorage, one solution to this quadrilemma is the energy assisted magnetic recording (it has two different ways but the most accepted one is the heat assisted or the thermally assisted magnetic recording system). Theoretical expressions predict that a large thermal stability with high density data recording is possible with the usage of magnetic materials with high perpendicular magnetic anisotropy [2, 4]. Yet, this type of material preference makes the switching of the magnetization for each bit subtle within the conventional perpendicular magnetic recording (PMR) method. One of the proposed methods not merely pushes back the superparamagnetic effect considerably, but also ensures a boost in storage density. This novel data storage method is called Thermally/Heat Assisted Magnetic Recording (TAR/HAMR) system. It potentially allows recording densities higher than 1 Tb/in^2 [2,5]. Its schematic illustration is shown in the Figure 1.3. This epoch making new method, TAR/HAMR procedure, near the magnetic field involves application of a laser heating pulse with a small spot, inducing local heating up to the Curie temperature (T_c) (which is the phase change point between ferromagnetic and paramagnetic phases). Simultaneously, the coercivity of magnetic material is reduced significantly allowing a reasonable writing magnetic field. TAR/HAMR process writes the bits at elevated temperature close to T_c and stores them at an ambient temperature (i.e. at room temperature) with superior thermal stability and data retention. Eventually, due to the preference of high perpendicular magnetic anisotropy material, both nonvolatility and areal density improvements can be achieved. A magnetic material with high saturation magnetization and strong anisotropy is effective against the thermal fluctuations which cause serious increase in the bit error rate [3].

To sum up, a study of the modeling of magnetization dynamics for the prospective materials to be used in data storage technologies is a hot research field. Plus, in all of the conventional studies numerical analysis of magnetization has been implemented using either a micromagnetic or macrospin approach with the Landau-Lifshitz-Gilbert

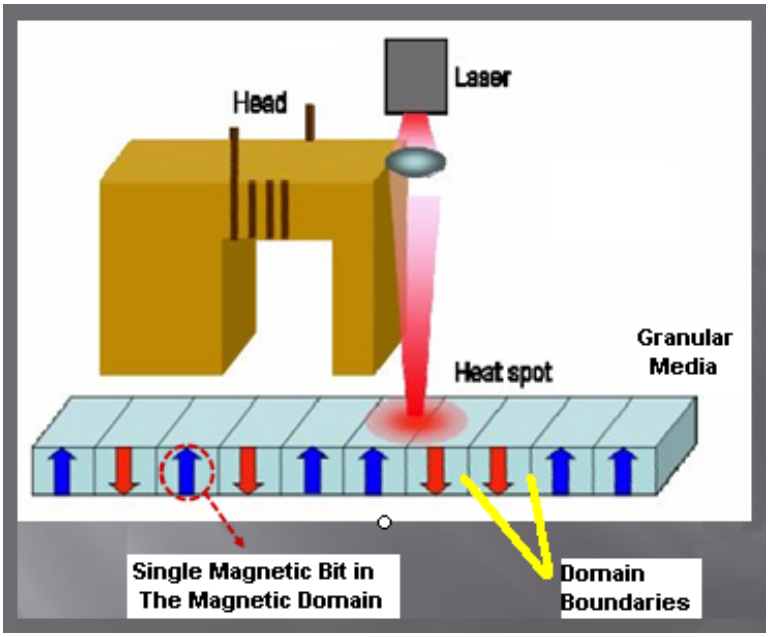

Figure 1.3. The schematic representation of a novel data storage technology, the Heat Assisted Magnetic Recording (HAMR) system which uses laser spot near the magnetic field pulse to write bits on the media with the perpendicular anisotropy.

(LLG) equation of motion. Eventhough, the Landau Lifshitz Gilbert (LLG) equation involves a phenomenological estimation for the magnetization and works successfully at zero temperature, the finite temperature stochastic effects are not accurately described as the magnetization vector is subject to an effective magnetic field.

If we simulate the magnetization dynamics exploiting LLB equation, the longitudinal damping term also acts on the magnetization together with both precession and (transverse) damping torque terms of the conventional LLG equation [6]. Due to this additional term, LLB equation predicts longitudinal fluctuations in the length of magnetization vector in addition to the transverse fluctuations [6]. Moreover, whilst LLG equation only includes the material dependent Gilbert Damping Parameter, LLB equation contains both transverse and longitudinal damping parameters which depend on both temperature and the phenomenological Gilbert damping parameter.

Although the atomistic modeling based on LLB equation describes many significant physical aspects of the behavior of nanoscale magnetic systems, including the damping phenomena, longitudinal fluctuations and the effect of thermal agitations, these effects can alternatively be described by a simple macrospin model based on LLB equation. The latter model is considerably more efficient.

In this study, we have implemented a full macrospin model of magnetization dynamics using LLB equation of motion. After successive tests of the LLB model, instead of applying our model for extensively analyzed $L1_0$ phase intermallic FePt, we applied LLB equation based macrospin approach for strongly exchange coupled CoNi/Pd multilayers with strong perpendicular anisotropy. This alloy possesses lower Curie Temperature ($T_c = 448$ K), a high squareness of the magnetic hysteresis and considerably high perpendicular anisotropy $H_k = 18$ kOe (corresponding $\sim 2 \times 10^6 \quad erg/cm^3$). These nice magnetic characteristics makes it a leading candidate for the magnetic medium to be used in TAR/HAMR technology. In our systematic analysis, initially, CoNi/Pd MLs was experimentally investigated [7]. In other words, the temperature dependence of intrinsic parameters such as zero temperature equilibrium magnetization, saturation magnetization and coercivity values were taken from the experimental results [7]. After sufficient investigation of experimental data of these essential parameters of CoNi/Pd MLs, the LLB based macrospin model is implemented by using simulations to fit to the experimental data. Further, to achieve a successful modeling of the TAR/HAMR technique, we applied almost rectangular (or smoothed step function) shaped heating pulse. In addition to this, a magnetic field pulse is also applied to the material as a representation of the magnetic field applied by the writing heads to the magnetic media. The response of the magnetization to the application of pulsed forms of heat and magnetic field is studied in detail for different combinations of peak values and durations. An entire switching time distribution with respect to peak values of both heating and field pulses has been achieved. For certain temperature values, we examined the switching probabilities. The experimentally taken hysteresis measurements are plotted with their corresponding LLB simulation results. Another part of this thesis encompasses hysteresis loop creation by sweeping the magnetic field. Using our LLB model, hysteresis loops are plotted together with the corresponding experimental

hysteresis loops for different temperature values.

We began with an LLB based model using the magnetic properties of hcp type Co and at the same time, many control simulations have been performed to understand whether the LLB based macrospin model gives plausible results or not. Right after that the model is extended to a real potential candidate for the recording layer of HAMR system which is CoNi/Pd multilayers [7].

In our LLB based magnetization modeling, we used two different programs. First of all, we preferred to use COMSOL Multiphysics [8] which is one of the reasonable modeling programs that has the ability to process different physical variable at the same time As a secondary approach, we preferred to use Mathematica 8 version.

However, in COMSOL Multiphysics due to meshing problems and higher computation time of the simulations of magnetization dynamics based on LLB equation made us choose Mathematica as the major program. Yet, most of the macrospin simulations were carried out in both of these two programming languages to check whether they are giving similar results or not. The details of the codes in COMSOL Multiphysics and Mathethematica are given in Appendix E and Appendix F. The COMSOL approach also has the advangtage that it can be extended to micromagnetic simulations.

2. THEORETICAL BACKGROUND

2.1. Magnetization Dynamics: Landau-Lifshitz-Gilbert Equation

The magnetization dynamics is an attractive field of study. This complex problem requires a clear formulation to understand the subtitles involved. In early 1930s, L.D. Landau and E.M. Lifshitz have described a primitive equation of motion for spins and their interaction with the magnetic field [9].

The magnetic moment has a well-known relation with spin angular momentum (**S**): $\boldsymbol{\mu} = -(\frac{g\mu_B}{\hbar})\boldsymbol{S} = \gamma \boldsymbol{S}$ where g is called g-factor and is approximately equal to 2 for ferromagnets, μ_B is Bohr Magneton and $\hbar$ is obtained by dividing Planck constant h by 2π. Lastly, γ is the ratio of the magnetic moment to its spin angular momentum called gyromagnetic ratio, see Appendix A for detailed information. When the magnetic field is applied to the material, it directly interacts with the magnetic moment of material which causes the creation of a torque acting on the magnetic moment in the following form:

$$\boldsymbol{\tau} = \boldsymbol{\mu} \times \boldsymbol{H} \tag{2.1}$$

Since torque is the time differentiation of angular momentum and $\boldsymbol{S} = \frac{\boldsymbol{\mu}}{\gamma}$, we can write torque as $\boldsymbol{\tau} = \frac{d\boldsymbol{S}}{dt} = \frac{1}{\gamma}(\frac{d\boldsymbol{\mu}}{dt})$. Thus, the equation below is obtained;

$$\frac{d\boldsymbol{\mu}}{dt} = -\left|\gamma\right| \boldsymbol{\mu} \times \boldsymbol{H} \tag{2.2}$$

For the spin system, in the absence of damping mechanism, this leads to the Larmor precession with a well-defined frequency(called Larmor precession frequency) and Equation 2.2 is called damping-free equation (undamped form of Landau-Lifshitz equation) and reveals that the spin system doesn't exchange their energy with the environment so according to the conservations of both energy and angular momentum, a permanent

precession occurs. In that case, the schematic illustration of magnetization vector time evolution is shown in the figure below.

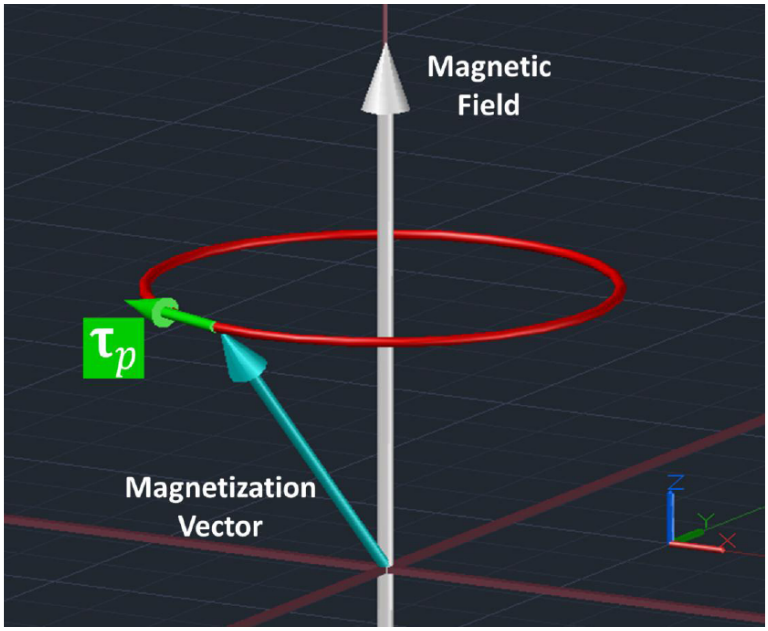

Figure 2.1. This is a schematic representation of the motion of a magnetization vector (cyan color). The motion of magnetization vector is governed by the undamped form LL equation (as the external magnetic field (gray colored arrow) is applied through +z direction). In the presence of the precessional torque $\boldsymbol{\tau}_p$ the magnetization vector follows the trajectory (red color) depicted above.

Yet, the spin systems are in a viscous like medium which causes exchange of energy with the environment. The dissipation of energy which is directly related to the relaxation of magnetization was first taken into account in 1935 by L.D. Landau and E.M. Lifshitz. To describe this non-linear motion of the spins in the presence of an effective magnetic field, they proposed an ordinary differential equation (ODE) called Landau-Lifshitz (LL) equation. By taking the energy dissipation processes into account due to phenomenological reasons, they preferred to write damped form Landau-Lifshitz equation as follows;

$$\frac{d\boldsymbol{M}}{dt} = -|\gamma|\,(\boldsymbol{M} \times \boldsymbol{H}_{eff}) + |\gamma|\,(\frac{\lambda}{\boldsymbol{M}_s})(\boldsymbol{M} \times (\boldsymbol{M} \times \boldsymbol{H}_{eff})) \tag{2.3}$$

where H_{eff} is the effective magnetic field which includes contributions from the external applied magnetic field (i.e. Zeeman Field), anisotropy and some interaction fields such as dipole-dipole and exchange interactions. **M** is a macroscopic magnetic moment density (or macroscopic magnetization vector) and it is equal to $\boldsymbol{M} = (\frac{N}{V})\boldsymbol{\mu}$. V is the volume of the sample and N is number of magnetic moments. As it is stated above, the first term describes purely precessional motion of the magnetization vector without damping. The second one has been proposed to create a damping mechanism during the precessional motion. It is important to note that this form of the second term is chosen to drive the magnetization toward the effective field direction. This direction is the minimal energy state for the magnetization vector. Yet, there is a substantial problem which leads the Landau-Lifshitz equation to restrict itself in a region depending on the value of λ. Since λ is is a parameter introduce to describe the energy dissipation processes, it cannot take a large value ($\lambda \geq 1$ is called over-damped regime) which would dominate the magnetization trajectory. Moreover, it is clear in Equation 2.3 that when the damping torque term increases, the magnetization will move faster but this gives an unphysical result which can easily be seen by taking limit of Equation 2.3 as $\lambda \to \infty$ [10].

Therefore, in 1955, Gilbert modified the LL equation by including phenomenological damping constant obtained from the experimental observations. Unlike the LL equation, Landau-Lifshitz-Gilbert (LLG) equation imposes a different meaning to the damping constant λ, which is the fact that damping constant is not a universal constant but it depends on the magnetic medium and it has a weak temperature dependence [6, 11, 12]. The inclusion of the material dependent damping constant is an important step to get the accurate description of the magnetization dynamics for the low temperature regime. The equation below Equation 2.4 is LLG equation of motion.

$$\frac{\partial \boldsymbol{M}}{dt} = \underbrace{-\gamma\left(\boldsymbol{M} \times \boldsymbol{H}_{eff}\right)}_{\substack{\textbf{\textit{Precessional}} \\ \textbf{\textit{Torque}}}} + \underbrace{\frac{\alpha}{M_s}\left(\boldsymbol{M} \times \frac{d\boldsymbol{M}}{dt}\right)}_{\substack{\textbf{\textit{Damping}} \\ \textbf{\textit{Torque}}}} \tag{2.4}$$

where Like LL equation, for Landau-Lifshitz-Gilbert equation of motion, there are two

Table 2.1. The Symbols And Corresponding Names Used In Conventional LLG Equation.

Symbol	**Name**
$\boldsymbol{M}$	Magnetization Vector
$\boldsymbol{H}_{eff}$	Effective Field
γ	Gyromagnetic Ratio
α	Gilbert Damping Constant
M_S	Saturation Magnetization

types of torque terms that affect the motion of the magnetization vector (Equation 2.4). These are the precessional torque term that arises due to the interaction between the magnetic field and magnetic moments causing a precessional motion with a frequency $w_{prec} = \gamma\mu_0 H_{eff}$, the other one is the phenomenological damping torque term which arises due to the spin lattice interaction. The damping torque term is responsible for the energy dissipation during magnetization precession [10]. The analogy between the LL equation and LLG equation can be seen when LLG Equation 2.4 is written in the form of LL Equation 2.3. After the exhaustive derivations which are shown in detail in Appendix B, the equation below 2.5 can be obtained which is similar to the LL equation.

$$\frac{d\boldsymbol{M}}{dt} = -\left(\frac{\gamma}{1+\alpha^2}\right)\left(\boldsymbol{M} \times \boldsymbol{H}_{eff}\right) + \gamma\left(\frac{1}{M_S}\left(\frac{\alpha}{1+\alpha^2}\right)\right)\boldsymbol{M} \times \left(\boldsymbol{M} \times \boldsymbol{H}_{eff}\right) \tag{2.5}$$

LLG equation is written above by using the macroscopic magnetization vector $\boldsymbol{M}$ as the dependent variable and $\boldsymbol{H}_{eff}$ as a functional. α is called Gilbert damping constant

which has a significant influence on the relaxation time of the spins. That is to say, the higher the damping and the higher the phenomenological Gilbert damping constant, the faster magnetization of the system aligns itself in the same direction as the effective field and thus, the faster the relaxation of magnetization occurs.

2.1.1. Magnetic Damping

The Gilbert damping is used to describe the dissipation of both energy and angular momentum out of the magnetization system. However, the origin of the damping phenomena is still an intensive research topic. However, it can be revealed that the phenomenological damping constant is roughly proportional to Z^4 (Z atomic number, number of protons in the nucleus) suggesting that the damping mechanism mainly arises from energy exchange between the spin system and the crystal lattice(spin-orbit coupling) [13]. That is why, particularly rare earth materials with high Z values possess high damping. It means that the angular momentum of the spin system is transferred into the lattice via spin-orbit coupling. Finally, the energy is dissipated through the fixed lattice spins.

Figure 2.2 is the schematic illustration of time evolution of magnetization vector in the presence of an external magnetic field. The magnetization vector dissipates its energy which is gained via the interaction between the external magnetic field and the magnetization vector (which is called as Zeeman energy). During the application of external magnetic field, there are two torques that act on the magnetization vector. They are precesional and damping torques. If the external magnetic field is high enough then the magnetization vector aligns along the external magnetic field direction. This direction can be attributed to a new easy direction for the magnetization vector.

2.1.2. The Dimensionless Form of LLG Equation

LLG equation can also be written in terms of the spin polarization vector $\boldsymbol{m}$ that is related to the spin vector $\boldsymbol{s}_i$ with the following relation $\boldsymbol{m} = \frac{1}{N}\sum_i \langle \boldsymbol{s}_i \rangle$ (and i is the lattice site index (i=1, 2, 3, ..., N)). Using $\boldsymbol{m}_i = \langle \boldsymbol{s}_i \rangle$ relation (which comes from the

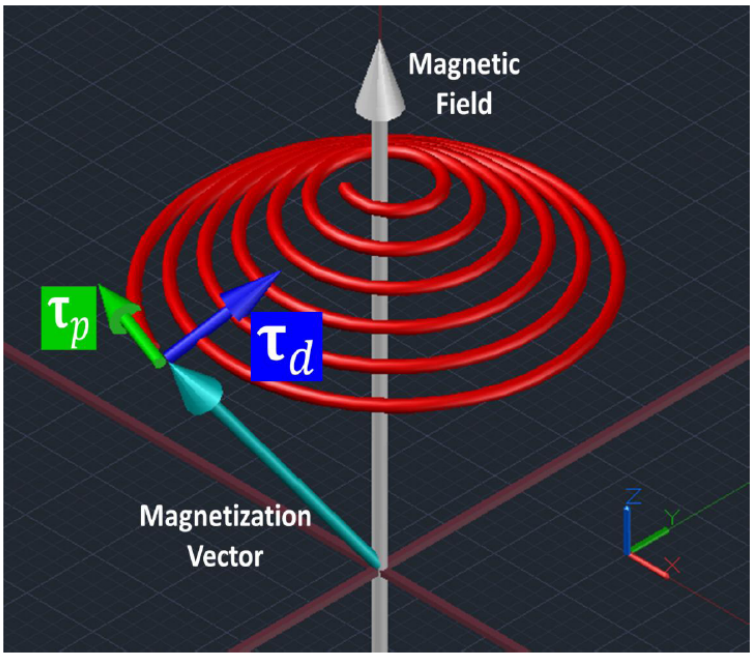

Figure 2.2. This is a schematic representation of the motion of a magnetization vector (blue color) when the motion of magnetization vector is governed by LLG equation (as the external magnetic field (pink color arrows) is applied through the z direction), there are two types of torque which affect this motion: damping torque τ_d and precessional torque τ_p.

Mean Field Approximation [1,6,12,14,15]), the spin polarization vector can be written as $\boldsymbol{m} = \frac{1}{N}\sum_i \boldsymbol{m}_i$ [6]. Furthermore, this equation is written considering a fixed length $|\boldsymbol{m}| = 1$ throughout the relaxation process. That means that the magnitude of the spin polarization vector doesn't change with the other parameters such as magnetic field, temperature etc.

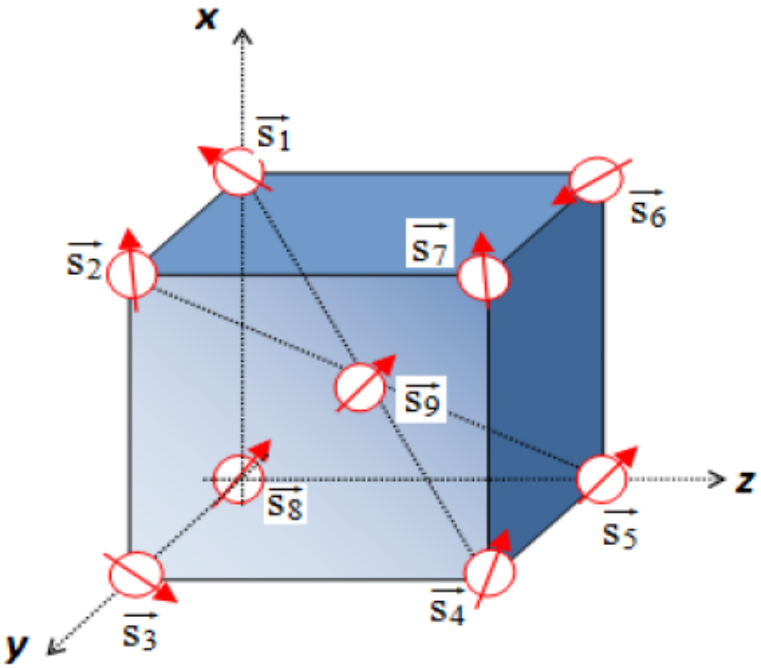

Figure 2.3. That is a lattice structure of the BCC type unit cell; at each corner and in the center, there is an atom with $\boldsymbol{s}_\mathrm{i}$ spin. By taking the average value of all spins in this structure, we can simply reach to unit magnetization vector $\boldsymbol{m}_\mathrm{i}$.

First of all, by using the relation where ν_0 is the volume of the unit cell in the lattice system and μ_0 is the magnetic moment; above LLG equation can be written using another dependent variable, the spin polarization vector $\boldsymbol{m}$ [6, 12, 14] as follows;

$$\frac{d\left(\left(\frac{\mu_0}{\nu_0}\right)\boldsymbol{m}\right)}{dt} = -\gamma\left(\left(\frac{\mu_0}{\nu_0}\right)\boldsymbol{m}\right) \times \boldsymbol{H}_{eff} + \frac{\alpha}{M_s}\left(\left(\frac{\mu_0}{\nu_0}\right)\boldsymbol{m}\right) \times \frac{d\left(\left(\frac{\mu_0}{\nu_0}\right)\boldsymbol{m}\right)}{dt}$$

$$\left(\frac{\cancel{\mu_0}}{\cancel{\nu_0}}\right)\frac{d\left(\boldsymbol{m}\right)}{dt} = -\gamma\left(\frac{\cancel{\mu_0}}{\cancel{\nu_0}}\right)\left(\boldsymbol{m}\right)\times\boldsymbol{H}_{eff} + \left(\frac{\alpha}{M_s}\left(\frac{\mu_0}{\nu_0}\right)^{\cancel{2}}\right)\boldsymbol{m}\times\frac{d\left(\boldsymbol{m}\right)}{dt}$$

$$\frac{d\boldsymbol{m}}{dt} = -\gamma\boldsymbol{m}\times\boldsymbol{H}_{eff} + \left(\frac{\alpha}{M_s}\left(\frac{\mu_0}{\nu_0}\right)\right)\boldsymbol{m}\times\frac{d\boldsymbol{m}}{dt} \tag{2.6}$$

The maximum value of the magnetization is its saturation value M_S. This value differs from material to material $|\mathbf{M}| = M_S$ (where M_S is the saturation magnetization) and in this sense, the maximum value of normalized magnetization is $|\mathbf{m}| = 1$.

$$\boldsymbol{M} = \left(\left(\frac{\mu_0}{\nu_0}\right)\boldsymbol{m}\right) \Rightarrow M_S = \left(\frac{\mu_0}{\nu_0}\right) \tag{2.7}$$

By using Equation 2.7, Equation 2.6 turns into the following form:

$$\frac{dm}{dt} = -\gamma\left(m\times H_{eff}\right) + \left(\frac{\alpha}{\left(\frac{\mu_0}{\nu_0}\right)}\left(\frac{\cancel{\mu_0}}{\cancel{\nu_0}}\right)\right)\left(m\times\frac{dm}{dt}\right)$$

Thus;

$$\frac{\partial\boldsymbol{m}}{dt} = \underbrace{-\gamma\left(\boldsymbol{m}\times\boldsymbol{H}_{eff}\right)}_{\substack{\textbf{\textit{Precessional}}\\ \textbf{\textit{Torque}}}} + \underbrace{\alpha\left(\boldsymbol{m}\times\frac{d\boldsymbol{m}}{dt}\right)}_{\substack{\textbf{\textit{Damping}}\\ \textbf{\textit{Torque}}}} \tag{2.8}$$

The spin polarization vector or the normalized magnetization vector $\boldsymbol{m}$ is in unitless form. Thus, the units of these two torque terms must equal to the inverse of the time (1/s) because the unit of the right hand side of the Equation 2.8 is already the inverse of the time (1/s). Moreover, after some calculations, we can obtain the unit for the gyromagnetic ratio as $\frac{m}{As} \equiv \frac{m}{C}$ [16]. The detailed information about the gyromagnetic ratio is given in Appendix A.

When the magnetization vector is governed by the Landau-Lifshitz-Gilbert Equation of motion, two torque terms are driving the magnetization relaxation but during

the relaxation process magnetization magnitude is preserved [1, 6, 10–12, 14, 15, 17]. To put it in another way, LLG equation doesn't take into consideration the variation in the magnetization magnitude due to the thermal fluctuations. The LLG based micromagnetic (or the macrospin) simulations of magnetization time evolution is disregarding the change in the length of magnetization causes to give reasonable results only at the low temperature regime. Thermal fluctuations are indeed insignificant at low temperatures. Therefore, LLG equation is accuratein this regime (far from Curie point) [6, 11]. However, it is especially problematic for temperatures close to Curie temperature. The longitudinal fluctuations in the magnetization are enhanced by increasing the temperature [6, 11, 12].

In the final analysis, the finite temperature effects are not described well in LL or LLG equation. This can be regarded as a major drawback of the conventional LLG equation.

2.2. Magnetization Dynamics: Landau-Lifshitz-Bloch Equation

The aforementioned lack of crucial points in both LL and LLG equations brings about a restriction for the applicability/reliability of magnetization simulation based on these equations. As the temperature of the sample approaches near the Curie Temperature, the taken from the LLG equation based models are no longer accurate in describing for the experiments [6, 11, 14]. These undesirable predictions about the LLG equation of motion lead researchers to construct a more generalized equation of motion for the understanding of spin dynamics. Consequently, in late 90's, the Landau Lifshitz Bloch (LLB) equation was derived by a reduction of the Fokker-Planck equation using mean field approximation for classical and the density matrix equations for quantum spins in ferromagnets by D. Garanin [6]. Within the framework of LLB equation, changes in magnetization vector length are allowed. This particular consideration within the LLB framework creates a respectable difference from the conventional LLG framework. Another remarkable point is that the Gilbert damping parameter in the LLG equation is replaced with two different damping parameters in the LLB equation called as longitudinal and transverse damping parameters. Moreover, they are

both functions of temperature and are directly proportional to the Gilbert damping parameter. Whereas strictly speaking the Gilbert damping parameter is temperature independent. Thus, especially the inclusion of thermal effects by direct substitution of Gilbert Damping parameter with the linearly temperature dependent two damping parameters which contributes the LLB equation of motion to consider the thermal fluctuation effects on the magnetization dynamics, correctly [6]. These two damping parameters are controlling two separate relaxation processes which are longitudinal and transverse relaxation processes. Moreover, unlike the LLG equation, there are two different relaxation times for the magnetization in the LLB equation. One of them is the time period until the magnetization aligns itself to the same direction with the external magnetic field which is called as transverse relaxation time. The second one is called longitudinal relaxation time, which is directly related to the relaxation of magnetization length. The latter one is principally affected by the heating procedure of the material which brings about the partial/complete demagnetization of material [6].

Usually, solving these underlying equations of magnetization dynamics can only be achieved by numerical methods. What's more, the brief concept of the micromagnetism is that it supports the mathematical framework to describe magnetic and static properties of the structures and it can be regarded as a finite element modeling. When we restrict the number of elements to one a single average spin, which implies not considering the spin-spin interactions we can call this special case of the micromagnetic modeling as the macrospin modeling.

In the macrospin approach all individual spins are locked in phase and are rotating in unison. In other words, while the macrospin approximation is capable of describing the coherent rotation of the spins, it fails to describe micromagnetic phenomena such as the domain wall motion.

If a single bit in the nanomagnetic material is considered as a macrospin where all spins within the spin system are strongly coupled then, such a macrospin is subject to three different terms; the first one is called as damping torque term that arises due to the magnetic field (it has two components one is called as transverse damping torque

term $\boldsymbol{\tau}_{\perp}$ and the other is called as longitudinal damping term $\boldsymbol{\tau}_{//}$), the second one is called as precessional torque term $\boldsymbol{\tau}_{p}$ that arises due to the crystal lattice system itself and the last one is called as spin torque term $\boldsymbol{\tau}_{s}$ that exists if a current is applied to the macrospin [6]. Here, we don't take into consideration the spin torque because no current flows over it. Under this condition, the motion of the magnetization vector of the spin is shown in the figure below.

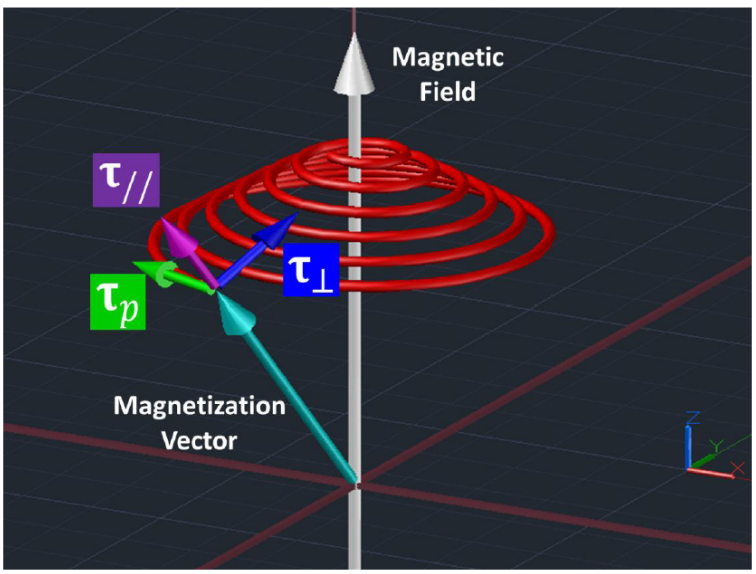

Figure 2.4. As the external magnetic field (gray color) is applied through the z direction, the magnetization vector (cyan color) is affected by three torque terms (the spin torque excluded). They are transverse $\boldsymbol{\tau}_{\perp}$ and longitudinal $\boldsymbol{\tau}_{//}$ damping terms and also the precessional torque term $\boldsymbol{\tau}_{p}$ iff the time evolution of magnetization vector is governed by the LLB equation of motion.

By using the spin polarization vector as a dependent variable, LLB equation of motion is written below;

$$\frac{d\boldsymbol{m}}{dt} = \underbrace{-\gamma\left(\boldsymbol{m}\times\boldsymbol{H}_{eff}\right)}_{\textbf{Precessional Torque Term}} + \underbrace{\gamma\alpha_{//}\left(\frac{\left(\boldsymbol{m}\cdot\boldsymbol{H}_{eff}\right)\boldsymbol{m}}{m^2}\right)}_{\textbf{Longitudinal Damping Term}} - \underbrace{\alpha_{\perp}\gamma\left(\frac{\boldsymbol{m}\times\left(\boldsymbol{m}\times\boldsymbol{H}_{eff}\right)}{m^2}\right)}_{\textbf{Transverse Damping Torque Term}} \tag{2.9}$$

where

$$m^2 \leq 1$$

and Gilbert Stochastic Damping parameters;

Table 2.2. Symbols And Corresponding Names Used In LLB Equation.

Symbol	**Name**
$\boldsymbol{m}$	$\boldsymbol{m} = \frac{1}{N}\sum_i \boldsymbol{m}_i$
$\boldsymbol{H}_{eff}$	Effective Field
γ	Gyromagnetic Ratio
$\alpha_{//}$	Longitudinal Relaxation Parameter
$\alpha_{\perp}$	Transverse Relaxation Parameter
T_c	Curie temperature of the magnetic material

$$\alpha_{//} = \left\{ \alpha\left(\frac{2T}{3T_c}\right), \alpha_{\perp} = \begin{cases} \alpha\left(1 - \frac{T}{3T_c}\right) & \Rightarrow T < T_c \\ \alpha\left(\frac{2T}{3T_c}\right) & \Rightarrow T \geq T_c \end{cases} \right. \tag{2.10}$$

Figure 2.5 shows us the variations in these three damping parameters with respect to the temperature. It is apparent from the figure that, as the temperature is varied there is no change in the Gilbert damping parameter. Yet, according to the equations above, the other two damping parameters (dashed blue and solid red in the Figure 2.5) have an obvious dependence on temperature.

While the temperature is increased, the transverse damping parameter decreases, below T_c. However, the longitudinal damping parameter is directly proportional to the temperature at both above and below T_c. Moreover, above T_c, the transverse damping parameter and the longitudinal damping parameter behaves similarly. These can be seen from the Figure 2.5.

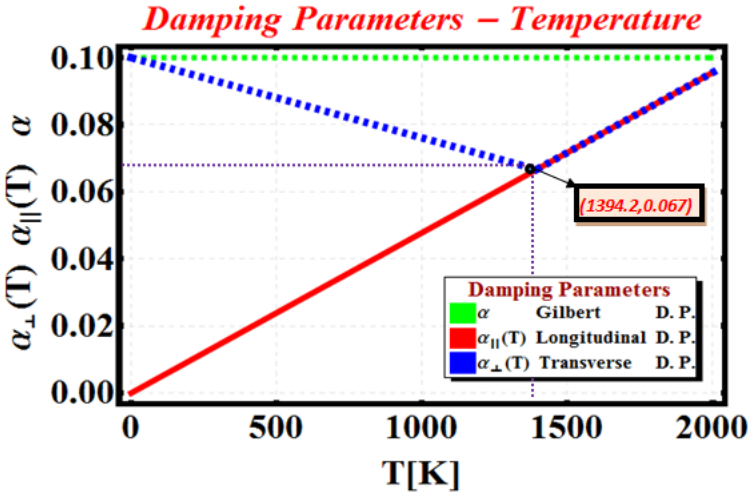

Figure 2.5. Temperature dependence of Gilbert Damping parameter (dashed green), Longitudinal (solid red) and Transverse (dashed blue) damping parameters. 1394.2 K is the Curie temperature for hcp Co.

Unlike the conventional LLG equation, the LLB equation allocates two different relaxation times for the time evolution of magnetization dynamics. Whilst the one is called transverse relaxation time, the other is the longitudinal relaxation time. Furthermore, they are characterized by the transverse susceptibility and the longitudinal susceptibility, respectively. They have one general relation which is written in the following form;

$$\chi_l = \frac{\partial \mathbf{m}(\mathbf{H}, T)}{\partial \mathbf{H}} \tag{2.11}$$

where $\boldsymbol{l}$ is either // or $\perp$ [1, 6, 14, 15].

Similar to the intrinsic magnetic properties such as temperature dependence of saturation magnetization of prospective materials which are potential candidates for spintronic devices, the values of the susceptibilities are mostly calculated by using ab-initio calculations based on first principle method [6].

The other important parameter in LLB equation is the effective field which can

be written in the following form;

$$\boldsymbol{H}_{eff} = \boldsymbol{H}_{app} + \boldsymbol{H}_{an} + \boldsymbol{H}_{Lang} + \boldsymbol{H}_{exc} + \boldsymbol{H}_{long} \tag{2.12}$$

Above Equation 2.12 shows that the effective magnetic field $\boldsymbol{H}_{eff}$ contains terms which are called applied magnetic field(Zeeman field) $\boldsymbol{H}_{app}$, anisotropy field $\boldsymbol{H}_{an}$, Langevin field (stochastic dimensionless thermal field that causes the fluctuation of the magnetization vector from its equilibrium position [6]). $\boldsymbol{H}_{Lang}$, exchange field $\boldsymbol{H}_{exc}$ and a term that controls the longitudinal fluctuations in the magnetization magnitude $\boldsymbol{H}_{long}$. Occasionally, the each component of the effective field is normalized by M_s. This form of the effective field is called reduced effective field and is mostly shown in the following form: $\boldsymbol{h}_{eff} = \boldsymbol{h}_{app} + \boldsymbol{h}_{an} + \boldsymbol{h}_{Lang} + \boldsymbol{h}_{exc} + \boldsymbol{h}_{long}$

The following Equation 2.13 is the anisotropy field. This type of construction of the anisotropy field is valid, when the external magnetic field is acting through the +z direction which is perpendicular to the plane of the thin film sample. Therefore, out of plane anisotropy is z component of the anisotropy field. The remaining components are forming the in-plane anisotropy. Yet, always one of them is dominant.

$$\boldsymbol{H}_{an} = \boldsymbol{H}_{out} + \boldsymbol{H}_{in} = -(D_x \boldsymbol{m}_x + D_y \boldsymbol{m}_y + D_z \boldsymbol{m}_z) \tag{2.13}$$

where $\boldsymbol{m}_x$, $\boldsymbol{m}_y$, and $\boldsymbol{m}_z$ represent x ,y, and z spatial components of the spin polarization vector, respectively and D_x, D_y, D_z are just multipliers of spatial components.

$\boldsymbol{H}_{long}$ is an additional field that contributes to the longitudinal damping of magnetization vector and has a relation as follows;

$$\boldsymbol{H}_{long} = \begin{cases} \frac{1}{2\chi_{//}} \left(1 - \frac{m^2}{m_e^2}\right) \boldsymbol{m} & \Rightarrow \quad T < T_c \\ -\frac{1}{\chi_{//}} \left(1 + \frac{3T_c}{5(T-T_c)} m^2\right) \boldsymbol{m} & \Rightarrow \quad T \geq T_c \end{cases} \tag{2.14}$$

Up to now, all field terms of the effective field are shown with their relations.

Several papers determined their principal topic as the stochastic behavior of the magnetization dynamics [11, 12, 14, 18]. The stochasticity is a random effect that depends on temperature and causes small aberrations from the main trajectory of the magnetization vector during the precessional motion as it is under the influence of the effective magnetic field. In these studies, they preferred to add this stochasticity by using two different ways.

2.2.1. Stochastic Nature Of Magnetization Dynamics

There are two types of representation for the stochastic behavior of the magnetization. The first one is the inclusion of the thermal fluctuations as a component of effective field. In such methods, the field which accounts for this behavior is called Langevin Field or Stochastic Gaussian Field. The following descriptions are written for the purpose of clarifying each point about the inclusion of stochasticity by that way. Langevin Field $\boldsymbol{H}_{Lang}$ is pointed out as a randomly fluctuating field with three dimensional vector components [6, 14, 17, 18] and it is given by; $\boldsymbol{H}_{Lang} \Rightarrow \boldsymbol{\zeta}(t)$ or $\boldsymbol{h}_{th}$: $\boldsymbol{h}_{th} = (\boldsymbol{h}_{th,x}, \boldsymbol{h}_{th,y}, \boldsymbol{h}_{th,z})$

The reduced form of Langevin field has the following general relation;

$$h_{th} = \frac{\xi}{M_s}\sqrt{2\left(\frac{\alpha k_B T}{\mu_0 \gamma_0 \Delta V M_s \Delta t}\right)} = \xi\sqrt{P_t} \tag{2.15}$$

and h_{th} should conform two conditions which are described below;

$$\begin{cases} \langle h_{th,k}(t)\rangle = 0 \\ \langle h_{th,k}(t), h_{th,l}(t')\rangle = P_t \delta_{kl}\delta(t-t') \end{cases}$$

where

The Gaussian Stochastic process ξ has zero mean and unit variance features. By using above space and time dependent Gaussian process relations, we reach the below

Table 2.3. Symbols And Corresponding Names Used In The Definition Of Stochastic Process.

Symbol	**Name**
$\boldsymbol{M_s}$	Saturation Magnetization
k and l	represent the Cartesian Coordinates x, y and z
Δt	Time step
ΔV	Volume of the computational cubic cell
μ_0	Permeability of free space
T	Temperature of the magnetic material
k_B	Boltzman Constant
ξ	A Gaussian Stochastic function

result for ξ;

$$\xi = \frac{1}{\sqrt{2\pi}} \cdot \left(e^{-\left(\frac{t^2}{2}\right)} \right)$$

Then, if we plug this equation into the main equation Equation 2.15 of Langevin field;

$$h_{th} = \left(\frac{1}{\sqrt{2\pi}} e^{-\left(\frac{t^2}{2}\right)} \sqrt{P_t} \right) = \frac{1}{\sqrt{2\pi}} \left(\frac{e^{-\left(\frac{t^2}{2}\right)}}{M_s} \right) \sqrt{2 \left(\frac{\alpha K_B T_s}{\mu_0 \gamma_0 \Delta V M_s \Delta T} \right)} \tag{2.16}$$

The second way of representing the thermal excitations of the magnetization vector is implemented by addressing two uncorrelated, isotropic and three dimensionless terms into the LLB equation. The first one is included in the effective field which is acting on the transverse damping torque term. The second one is acting as an additional torque term. The superior accuracy of the second way in describing near T_c behavior has recently been reported by Evans *et al.* in 2012 [12]. Briefly, this form satisfies the Boltzmann statistical distribution not only at the low temperature regime but also at the elevated temperatures.

Furthermore, the stochastic field and torque terms satisfy the following relations:

$$< \zeta_{\mathrm{i}}^{//}(0)\zeta_{\mathrm{j}}^{\perp}(\mathrm{t}) >= \left(\frac{2\mathrm{k_B T}(\alpha_{\perp} - \alpha_{//})}{\mu_0 \left|\gamma\right| \Delta \mathrm{V M_s} {\alpha_{\perp}}^2}\right) \delta_{\mathrm{ij}}\delta(\mathrm{t}) \;\; < \zeta_i^{\mu} >= 0 \tag{2.17}$$

and

$$< \zeta_{\mathrm{i}}^{//}(0)\zeta_{\mathrm{j}}^{//}(\mathrm{t}) >= \left(\frac{2\mathrm{k_B T}\gamma\alpha_{//}}{\Delta \mathrm{V M_s}}\right) \delta_{\mathrm{ij}}\delta(\mathrm{t}) \;\; < \zeta_{\mathrm{i}}^{//}\zeta_{\mathrm{j}}^{\perp} >= 0 \tag{2.18}$$

where M_s is the saturation magnetization, k_B is the Boltzman constant, μ_0 is the permeability of free space, ΔV is the volume of the computational cubic cell, δt is the time step, i and j represent spatial components in Cartesian coordinates x, y and z. For the Gaussian stochastic process denoted as ζ_{μ} where μ can either be $\perp$ or //. It also has zero mean and unit variance [12].

$$\begin{aligned} \zeta_j^{\perp} &= \frac{1}{\sqrt{2\pi}} \left(\frac{e^{-\left(\frac{t^2}{2}\right)}}{M_s}\right) \sqrt{\left(\frac{2\mathrm{k_B T}(\alpha_{\perp} - \alpha_{//})}{\mu_0 \left|\gamma\right| \Delta \mathrm{V M_s} {\alpha_{\perp}}^2}\right)} \\ \zeta_{\mathrm{i}}^{//} &= \frac{1}{\sqrt{2\pi}} \left(\frac{e^{-\left(\frac{t^2}{2}\right)}}{M_s}\right) \sqrt{\left(\frac{2\mathrm{k_B T}\gamma\alpha_{//}}{\Delta \mathrm{V M_s}}\right)} \end{aligned} \tag{2.19}$$

As a conclusion, LLB equation, which is written above Equation 2.11 is not taking into account the thermal agitations due to the absence of either the Gaussian stochastic process or the Langevin field. Since we gave detailed information about the stochasticity, by the inclusion of this crucial point, the new equation is addressed as the stochastic form LLB (s-LLB) equation [12]. This promising form is written for a macrospin describes the time evolution of the average spin polarization $\boldsymbol{m} = \boldsymbol{M}$ / M_S (T=0) ($\boldsymbol{M}$ is the magnetization vector and M_S is the temperature dependent saturation magnetization) as it is under the influence of an effective field such that;

$$\dot{\boldsymbol{m}} = \frac{\partial \boldsymbol{m}}{\partial \mathrm{t}} = \tilde{\gamma}(\boldsymbol{m} \times \boldsymbol{H_{eff}}) + \frac{\left|\tilde{\gamma}\right| \alpha_{//}}{\mathrm{m}^2} \left[\boldsymbol{m} \cdot \boldsymbol{H_{eff}}\right] \boldsymbol{m} - \frac{\left|\tilde{\gamma}\right| \alpha_{\perp}}{\mathrm{m}^2} \boldsymbol{m} \times [\boldsymbol{m} \times (\boldsymbol{H_{eff}} + \boldsymbol{\zeta}_{\perp})] + \boldsymbol{\zeta}_{//} \tag{2.20}$$

Therefore, LLB equation allows fluctuations in the magnitude of $\boldsymbol{m}$. Involving the thermal agitations is necessary for the accurateness of the simulation as the temperature is far below or close to T_c. As it is mentioned above that one of the crucial differences between the LLG and LLB equations of motion is that in LLB equation, the phenomenological Gilbert damping constant α is replaced by temperature dependent longitudinal and transverse damping terms [6].

In addition, if we take the limit of LLB as T goes to zero, LLB equation turns into LLG equation because, in this limit the LLB equation loses its temperature dependent properties. For this case whilst the longitudinal damping term goes to zero, the transverse damping term turns into the Gilbert damping term of LLG equation [14].

However, for the high temperature regime, in the vicinity of the phase transition point (T_c), the LLB equation gives an accurate description of the thermal effects during the relaxation process of magnetization. As a consequence, it can be said that the LLB equation is a more generalized version of LLG equation of motion valid for all temperatures.

3. LLB SIMULATION RESULTS BASED ON Hcp TYPE Co THIN FILM

As it is stated before, within the framework of LLB formalism, there are three important variables which affect the behavior of the spin system. These are temperature, applied magnetic field and magnetic material properties.

In this part, we shall show the response of magnetization via macrospin model governed by the LLB equation of motion. In the macrospin model where the interactions between the neighboring spins (or the boundaries) aren't taken into account and therefore, the time evolution of the average magnetization of entire system will be considered. However, in this case we will use the intrinsic properties of hcp Co (a well-studied material). We used hcp type Co with intrinsic values taken from the literature as a control system for LLB macrospin calculations, we checked if the outcome of the LLB model was plausible and consistent with previous reports.

3.1. Control Simulations

In the model of magnetization dynamics, the optimization of accurateness and the reproducibility of the results are the staple part of this computational analysis. We developed the modeling in COMSOL Multiphysics, MATLAB and Mathematica programming languages.

For the case of Comsol Multiphysics, each spatial component of the macrospin is solved initially as a time dependent function. Eventually, the LLB equation is converted into an appropriate form to enter in the subdomain-expression-field of COMSOL Multiphysics. Right after that, both the initial values of the macrospin and the period of time length for the evaluation are determined and we make LLB equation of motion solved under these conditions. As the COMSOL Multiphysics evaluates the solution, the time evolution of the each spatial component can be plotted as magnetization ver-

sus time (see Appendix D for details). It is worth mentioning that the results taken from the COMSOL Multiphysics, have some extra assumptions. These additional assumptions of COMSOL Multiphysics (number of meshing time step, internal solver type etc.) causes slight differences in numerical analysis results. This inevitably forced us to develop the LLB based macrospin model in Mathematica, as well.

During the development of the simulations, we tried to add all special features of the terms of the effective field to our system one by one. Thus, we could have a chance to observe the effects of all terms on the magnetization relaxation process. This way leads us to analyze the results of each case, easily.

3.1.1. Convergence Of LLB To LLG Equation For Zero Temperature

The conventional methodology for the investigation of the magnetization dynamics relies on the solution of the Landau-Lifshitz-Gilbert (LLG) equation. The inclusion of effective stochastic Langevin field term ensures the understanding of the finite temperature effects on magnetization [18, 19]. On the one hand, the micromagnetic simulations based on this conventional approach have been used in describing the magnetization behavior for decades but unfortunately it can be regarded as accurate in describing this behavior just for the low temperature regime. On the other hand, whilst the conventional LLG equation has proven applicable for the low temperature regime, it cannot explain well the inclusion of ultrafast changes in temperature via laser pulse which heats the sample close to the Curie point momentarily. Moreover, the need to cinvolute a heating laser pulse with a write field results in a complicated magnetization reversal path as in TAR/HAMR. This issue creates a considerable change in the magnetization dynamics [1, 3, 14]. Therefore, the main drawback of the LLG based micromagnetic approach is the incorrect assumption of conservation of magnetization length during the dynamical excitations at elevated temperatures. The Figure 3.1 and Figure 3.2 shows the result of LLB simulation as the temperature of the system is set to zero temperature. While Figure 3.1 shows the time evolution of components of the magnetization vector (m_x(black), m_y(blue) and m_z(brown)) and the magnitude of magnetization vector(red color).

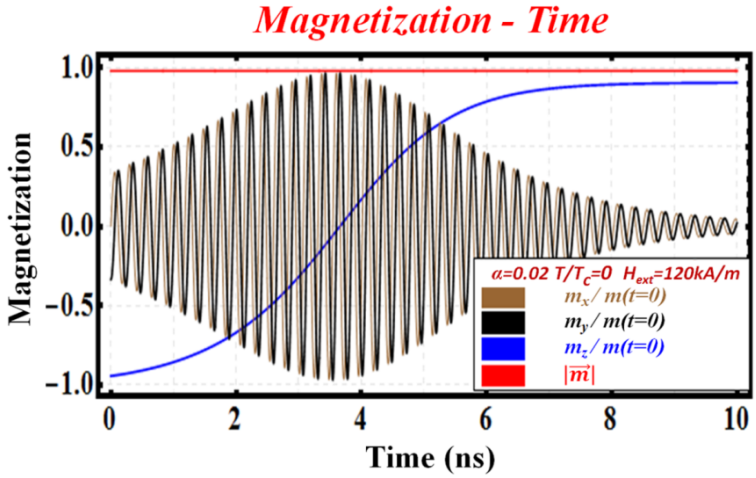

Figure 3.1. Time evolution of magnetization vector components as the temperature of the system set to zero.

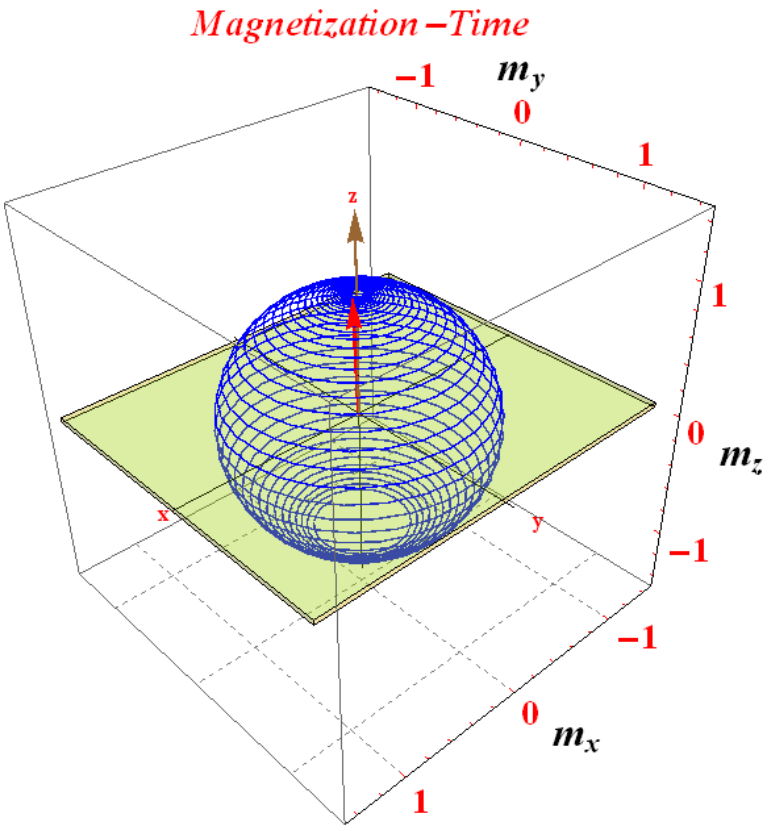

Figure 3.2. 3D trajectory of magnetization vector (blue), red arrow shows the magnetization vector and brown arrow shows the direction of magnetic field.

To investigate the change in the 3-D trajectory of the magnetization vector, the stochastic Langevin field is included in the LLG formalism. It is important to emphasize that the magnetization vector precesses around the effective magnetic field by keeping the magnetization length constant which leads to draw a spherical path.

3.1.2. The Effect Of External Magnetic Field

The increase in the effective field causes an increase in the Larmor precession frequency which leads the magnetization vector to precess around the effective field faster. Thus, this results in a faster relaxation of the magnetization vector. In other words, by increasing the precessional motion the magnetization vector aligns in the same direction with the external field pulse, faster.

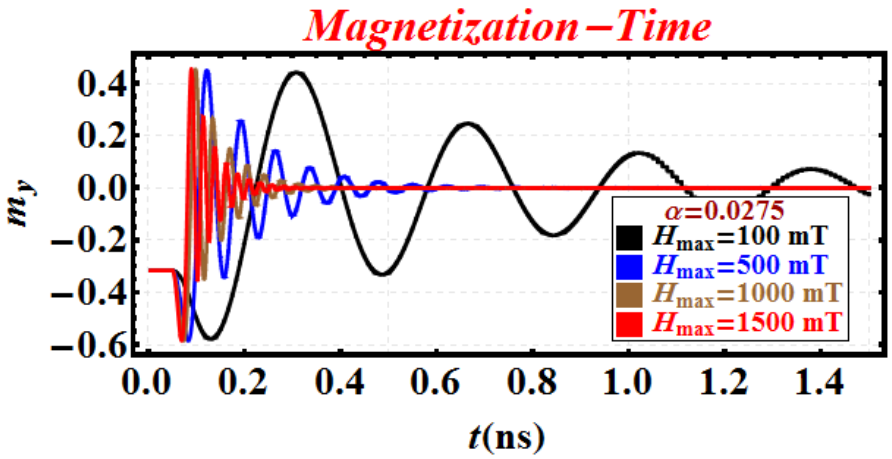

Figure 3.3. Time evolution of x component of magnetization vector for different external magnetic field values ($\boldsymbol{H}_{eff}$: 100 ⇒ 1500 mT). Gilbert damping parameter is taken as $\alpha = 0.05$ and this simulation temperature is 700 K. The considerable decrease can be observed as the external magnetic field is increased.

Figure 3.3 is obtained for different constant effective field values as Gilbert damping parameter is taken as 0.05, and also the system temperature is held at 700 K.

Table 3.1. Constant Effective Field Case.

Assumptions	
Temperature of the sample	**set to room temperature**
Gilbert Damping Parameter	**Constant**
Effective Field	**Variable**
Anisotropy Term	**Constant**
Langevin Field	**taken as zero**
The goal of this assumption is to see how the variation in effective field will affect the relaxation process of the magnetization vector as the Gilbert damping parameter is taken as 0.05. Moreover, the temperature of the macrospin is 700 K. In other words, for a certain value of the Gilbert damping parameter, by varying the effective field, we want to see how the relaxation process of the macrospin will be affected by this change. Besides, the temperature dependence of both saturation magnetization and anisotropy constant are also taken into account. Plus, the transverse and the longitudinal damping parameters vary with temperature.	
Expectation	
An increase in the effective field causes an increase in Larmor precession frequency brings with itself faster damping process.	

Initially, the magnetization vector is slightly tilted from –z direction so that m_x is one of the transverse components of the magnetization vector. When we increase the field pulse from 80 kA/m ($\sim$ 100mT) to 140 kA/m (1500mT), the relaxation time decreases. The demonstration of this physical fact via LLB based macrospin modeling asserts that our LLB simulation developed in Mathematica (8^{th} version) is able to describe the behavior of the magnetization dynamics.

3.1.3. The Effect Of Gilbert Damping Parameter

A brief introduction on the importance of the phenomenological Gilbert damping parameter (α) was given in Chapter 2. The Gilbert damping parameter which is included in both the conventional Landau Lifshitz Gilbert equation and the Landau Lifshitz Bloch equation has a material dependent and has a weak temperature dependence which is mostly neglected in the computation and experimental analysis.

Being able to control the magnetization damping mechanism is important in the operation of many nanomagnetic structures. It is very critical that we will be able to analyze the effect of magnetic damping behaviour described by the phenomenological Gilbert damping parameter.

Table 3.2. The Case Of Gilbert Damping Parameter Variation.

Assumptions	
Temperature of the sample	**set to room temperature**
Gilbert Damping Parameter	**Variable**
Effective Field	**Constant**
Anisotropy Term	**Constant**
Langevin Field	**taken as zero**
The goal of this assumption is to see the consequences of the Gilbert damping parameter variation in the magnetization reversal mechanism. The increase in the Gilbert damping parameter causes to a direct increase in the longitudinal and transverse damping parameters. These increments in the temperature dependent damping parameters give rise to an enhanced damping process (faster relaxation).	
Expectation	
As we increase the Gilbert Damping Parameter; a faster damping process will occur.	

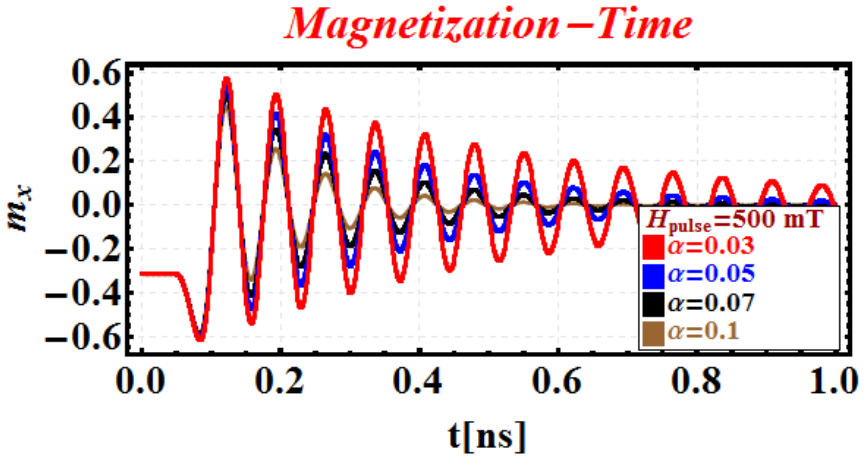

Figure 3.4. The time evolution of the x component of magnetization vector for different Gilbert Damping Parameters. To figure out the effect of variation in the Gilbert damping parameter on the magnetization dynamics, the effective field is set to a constant value ($\boldsymbol{H}_{eff}$: 120 kA/m). For this simulation temperature is set to the room temperature (T=300 K).

According to the reports about the Gilbert damping parameter, it has weakly temperature dependency and its strength is proportional to the strength of coupling between the spin system and its orbit. Moreover, both longitudinal and transverse damping parameters are directly proportional to the Gilbert damping parameter. Then, it can be asserted that the increase in the Gilbert damping directly affects the magnitude of the terms which are driving the time evolution of the magnetization vector. Therefore, the response of magnetization against this increase is to complete the relaxation process faster.

3.2. The Effective Magnetic Field

The effective field is one of the most important segments which plays a key role in describing the magnetization dynamics of a magnetic structure. It involves the characteristic properties of the material. In addition to this, it is the part in which some of the external effects are described. To sum up, in this subchapter the features of effective field components are extensively analyzed by including them one by one.

This results in a great insight meaning about the behavior of the magnetic moments against the modifications to the effective field.

3.2.1. Constant Effective Field With Non-zero Temperature Value

The LLB formalism considers two types of fluctuations. The first one is the longitudinal fluctuations mainly caused by thermal agitations. In other words, the rapid change in the temperature of the system brings about a change in the magnitude of the magnetization vector. The second one is indeed the field driven transverse fluctuations.

In the LLB formalism, the longitudinal fluctuations are included with an additional damping term which is itself temperature dependent. This allows a longitudinal relaxation mechanism in the model. The transverse fluctuations are also represented by the temperature dependent transverse damping term. The table below shows us the detailed description of the model and the assumptions that are made to obtain the following results.

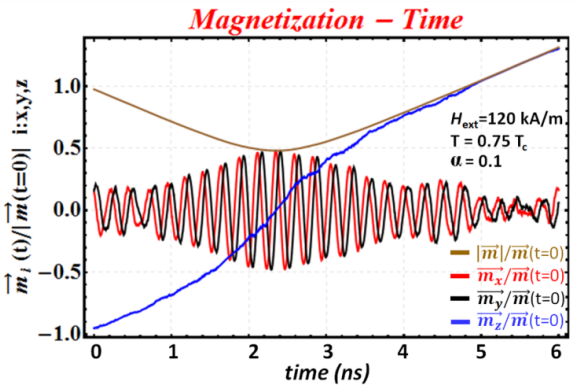

Figure 3.5. The time evolution of both magnetization magnitude and its x, y, and z components as Langevin field is included in the effective field.

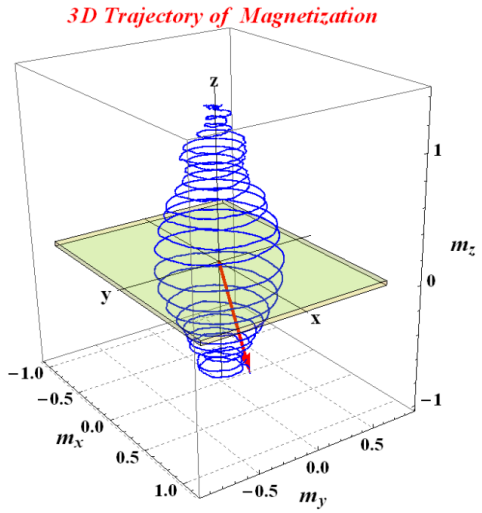

Figure 3.6. 3D path of the magnetization and change in the magnetization magnitude is evident.

As it is specified in the assumption section, we disregarded the temperature dependent features of the effective field except the thermal effects of the Langevin field. In fact, it contains the terms which are the anisotropy field and the field that controls the longitudinal damping of the magnetization. Yet, we set them to a constant value. Therefore, the alignment of magnetization with this effective field, which is through +z direction can be clearly realized in Figure 3.5.

Figure 3.5 shows that all components of the magnetization die out except for z component of the magnetization vector. In addition, the LLB equation allows for a variation of the magnetization magnitude due to the presence of longitudinal relaxation and above Figure 3.5 and Figure 3.6 shows us this change, clearly. In Figure 3.6 red arrow shows the initial position of magnetization vector and the field is acting through +z direction. Since it is high enough, the new alignment of the magnetization vector is achieved through the same direction with the external magnetic field.

However, incorrect part of the results is to have a gradual increase in the magnetization magnitude which is only physical up to its normalized saturation magnetization value. This issue will be addressed in the following discussion.

3.2.2. The Field Which Controls The Longitudinal Fluctuations

Since LLB equation considers the change in the magnetization magnitude throughout the precession motion due to the thermal agitations, to prohibit the unphysical results due to these longitudinal fluctuations a term is coupled to the effective field which is responsible for changes in the magnetization magnitude. Figure 3.7 and Figure 3.8 are the replots of Figure 3.5 and Figure 3.6 respectively, after the longitudinal fluctuations in the magnitude of the magnetization are taken under control. The inclusion of this field led us to prevent the macrospin LLB modeling from giving unphysical magnetization length due to the gradual increase in it during the magnetization precession.

A permanent increase in the magnetization length can also be asserted as somehow incomplete relaxation process. Up to a threshold which is the saturation magneti-

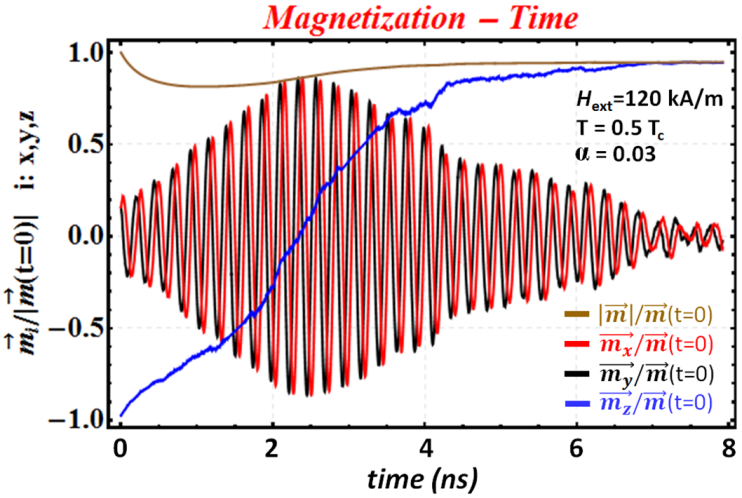

Figure 3.7. The relaxation process of magnetization vector components together with the magnetization magnitude(brown solid line) during the reversal of the magnetization vector. Since x and y components (red and black solid lines) are relaxing to zero z component (blue solid line) aligns same direction with the external field.

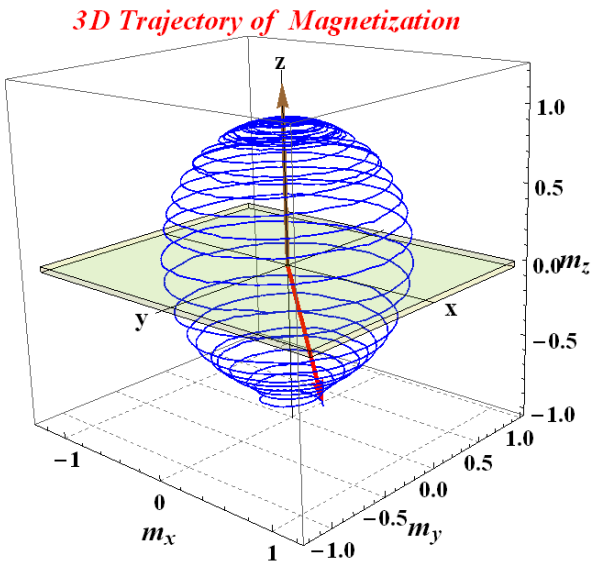

Figure 3.8. 3D trajectory of the magnetization vector (blue solid line), red arrow shows the initial position of magnetization vector and brown arrow show the direction of external magnetic field.

zation value everything can be regarded as physical but to exceed this limit is directly attributed to an unphysical result. Since the LLB equation is a perturbative approach which works accurately in non-equilibrium state of magnetization, in equilibrium state the LLB equation needs to be coupled with Curie Weiss equation to achive an accurate description of magnetization behavior as it is under the influence of a magnetic field even at the equilibrium state. This caused the addition of a new field term which is Equation 2.14:

$$\boldsymbol{H}_{long} = \begin{cases} \frac{1}{2\chi_{//}} \left(1 - \frac{m^2}{m_e^2}\right) \boldsymbol{m} & \Rightarrow \quad T < T_c \\ -\frac{1}{\chi_{//}} \left(1 + \frac{3T_c}{5(T-T_c)} m^2\right) \boldsymbol{m} & \Rightarrow \quad T \geq T_c \end{cases}$$

This new field allows the restriction of the magnetization length to have a maximum value of M_s.

3.2.3. Gaussian Stochastic Process

Another significant addition to the effective field is the Langevin field (random noise term) which is mentioned within detail in Appendix D. The inclusion of thermal noise field enables addressing the thermal agitations of the magnetization vector as it precesses around the effective field. In addition to this, we will also look at the impact of the Langevin Stochastic Field term on the relaxation process of magnetization as we add the special properties of the other terms of the effective field. In short, the last thing is to see the effect of the Langevin field to the time evolution of the magnetization. Yet, according to a recently published paper [12] the thermal excitations of magnetic moments need to be identified by different formalism to satisfy the Boltzman distribution. This new formalism is expressed in detail in Chapter 2 (Stochasticity Process for the Magnetization Dynamics part) and in Appendix E and F, the Gaussian stochastic formalism and a pair of sample plots of stochastic processes can be seen. Figure 3.9 and Figure 3.10 time evolution of magnetization vector transverse components in the absence of Gaussian Stochastic process and in the presence of Gaussian Stochastic Process. These figures are obtained when The external field 120 kA/m, T= 0.5 T_c and the Gilbert damping parameter is taken as 0.03.

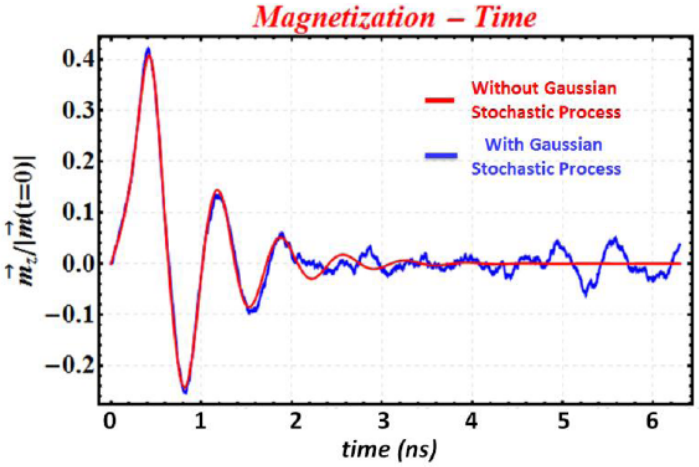

Figure 3.9. The time evolution of magnetization vector z component in the presence and in the absence of Gaussian stochastic process.

In the latter case, the small aberration from the main trajectory of magnetization results from the thermal excitations. If these thermal excitations are strong enough, they will result in random alignment of magnetic moment leading to demagnetization.

3.3. Systems With Different Magnetic Anisotropies

Many magnetic properties of the materials are based upon a preferential direction. This directional dependence stems from the magnetic anisotropy. Whilst the magnetic moments in a magnetically anisotropic material tend to align themselves through a preferential direction, for the case of magnetically isotropic materials, however, the dependence on a preferential direction for their magnetic moments does not exist. This preferential direction (which is one of the easy axes) of spontaneous magnetization leads the magnetic moments to have an opportunity of minimizing their energy. This energetically favorable alignment is determined by the sources of magnetic anisotropies.

Ferromagnetic material has net magnetic moments even in the absence of magnetic field because the entire volume of a ferromagnet is divided into lots of small subvolumes which are called domains and each domain is spontaneously magnetized and has a net alignment. Even though the direction of magnetization changes from

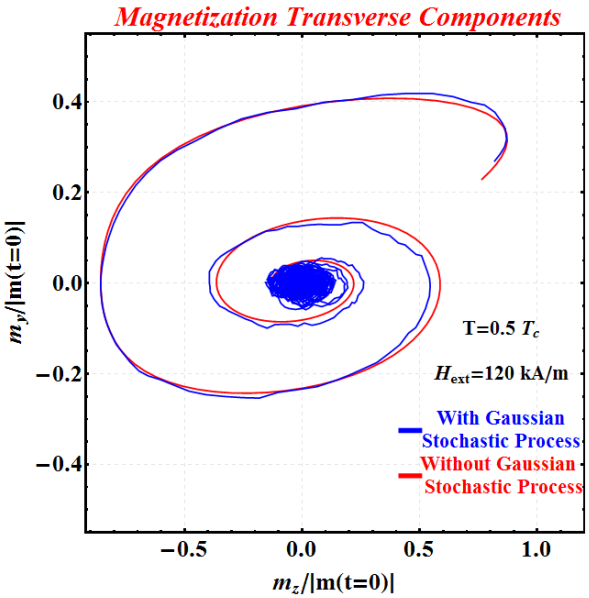

Figure 3.10. The time evolution of transverse components in the presence and in the absence of stochastic process. The thermal agitations bring about small vibrations around the predicted path of magnetization.

domain to domain, the vector sum of all domains produces nonzero magnetization.

In this part, we will implement the inclusion of principal magnetic anisotropies in our macrospin model for the purpose of discerning how the direction based properties of the magnetic material affect the relaxation process of the magnetic system.

3.3.1. In-Plane Anisotropy

As it is stated above that the magnetic anisotropy permits the magnetic moments to minimize their energy when they are aligned along a particular crystal direction. In the presence of a magnetic field the Zeeman energy of the magnetic moments reaches its lowest value when they lie parallel to the magnetic field direction.

According to the magnetic material preference, the preferential orientation of the magnetization shows variety due to the dominant magnetic anisotropy mechanism. In other words, there are several types of anisotropies possesses by each magnetic material

but there is just one anisotropy that dominates over the other anisotropies. If the plane of the thin film sample is energetically favorable rather than the out of plane, for this particular case the in plane anisotropy of the material is the dominant anisotropy.

Towards a more realistic model, the sample is taken as a thin film ferromagnetic material. This gives rise to take the shape anisotropy into account, inevitably. As a consequence of this, a demagnetizing field in the direction which is perpendicular to the thin film surface is included as it is described in chapter 2 within detail. The plane of thin film sample is favorable. Therefore, magnetization vector spends less time out of the thin film plane and hence this brings with itself of having a more elliptical trajectory rather than a spherical one.

As a result, the theoretically predicted (elliptical) trajectory is observed in the simulations as shown in Figure 3.12. Brown and red arrows represent the external magnetic field and the initial position of magnetization vector, respectively. Thin film shape is shown by square region.

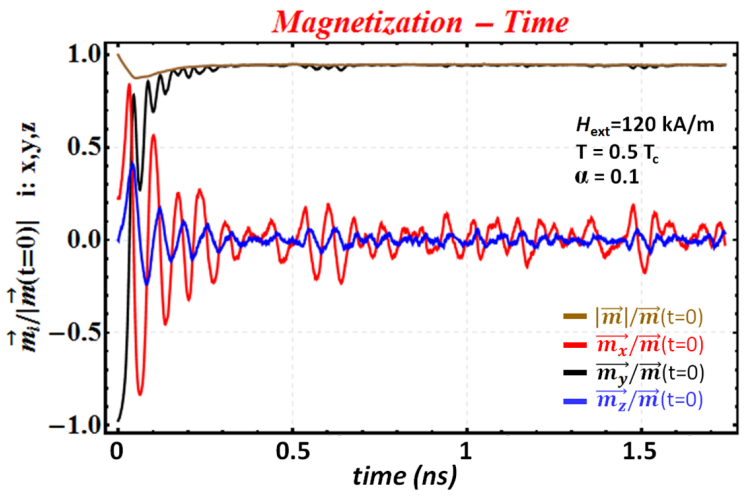

Figure 3.11. The time evolution of magnetization vector components (red, black, and blue solid lines are for x, y, and z components of magnetization vector) together with the magnetization magnitude (brown solid line).

Therefore, effects of both in plane anisotropy and stochastic random process

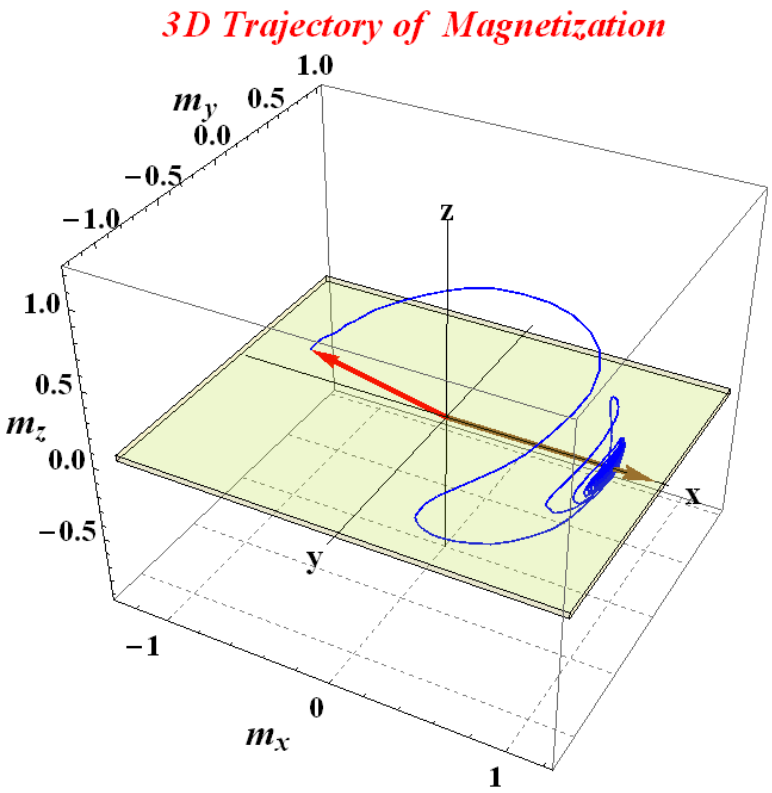

Figure 3.12. The 3D trajectory of magnetization vector as the magnetic thin film has a dominant in-plane anisotropy.

on the behavior of the magnetization are studied as it is under the influence of an external magnetic field. Accordingly, since the field which controls the longitudinal fluctuations in the magnetization length is also included in the effective field, we prevent unphysical gradual increment in the magnetization magnitude during the precessional motion. When the magnetization vector has completed its switching the saturation of magnetization is completed as well. Moreover, since this is an LLB modeling the change in magnetization magnitude which is shown with brown solid line in Figure 3.11 is evident.

3.3.2. Out Of Plane Anisotropy

One of the hot research topics is to study the behavior of magnetic moments in the magnetic thin films and magnetic multilayer structures which can potentially be used in the development of new solid state electronic devices.

Moreover, a great effort has been devoted to the study of tailoring the preferential direction of magnetization orientation in the absence of magnetic field which may cause the development of new recording systems. The possession of high perpendicular magnetic anisotropy (PMA) results in the orientation of magnetization to be the out of the plane helps to record more data in the same size [2,4]. The anisotropy energy defines the easy axis of magnetic moments. Although there are many types of anisotropy which have more or less contribution to the anisotropy energy for a magnetic structure, there is only one term which is the strongest among them. If the dominant anisotropy is perpendicular magnetic anisotropy (which originates from the competition between the magnetostatic energy and the out-of-plane anisotropy energy), the easy axis of the magnetization is normal to the thin film plane. In this part, we included both in plane and out of plane anisotropy but the out of plane anisotropy is determined as the dominant anisotropy.

Figure 3.13 and Figure 3.14 show the time evolution of magnetization vector components and three dimensional trajectory of the magnetization vector respectively. Since the applied magnetic field is normal to the thin film plane and the material has

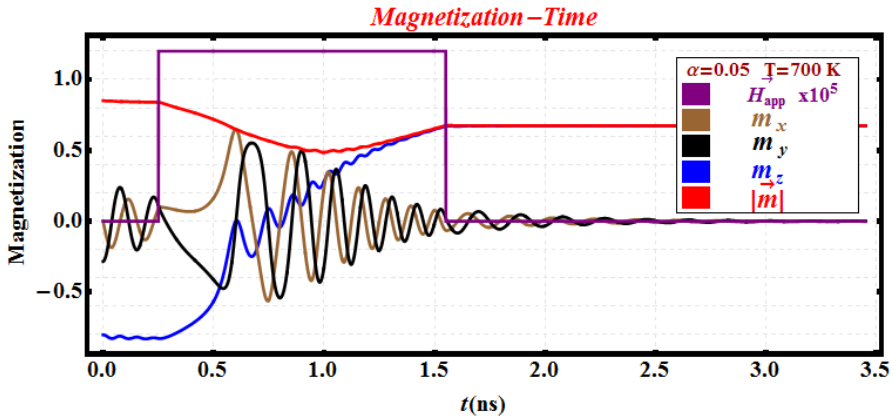

Figure 3.13. Time evolution of magnetization vector for a magnetic thin film with high perpendicular anisotropy. The variation in all components of the magnetization vector. In this figure the purple one shows us the applied field pulse ($\boldsymbol{H}_{app}$) (pulse width is approximately 1.3 nanoseconds and the amplitude of the pulse is 120 kA/m).

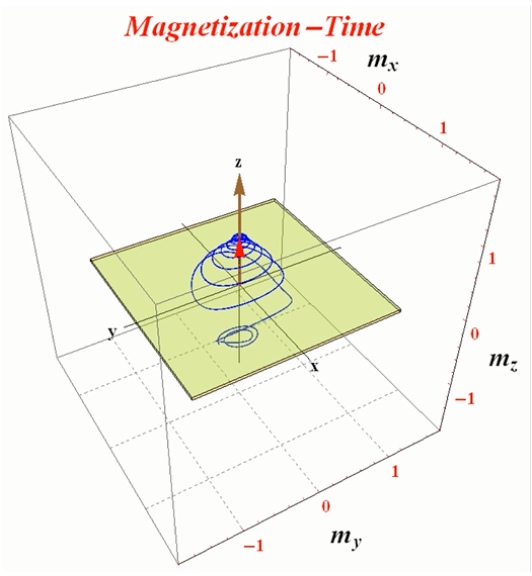

Figure 3.14. The strong perpendicular anisotropy addition to the effective field makes the surface of the thin film sample energetically unfavorable. While the red arrow shows the direction of magnetization vector, the brown one is in the magnetic field direction.

inherently high PMA, the magnetization vector does not prefer to stay much time in the plane of thin film.

4. LLB SIMULATIONS BASED UPON EXPERIMENTAL RESULTS: HIGH PERPENDICULAR ANISOTROPY CoNi/Pd MLs

The write stage in the TAR/HAMR process involves a sequential application of a writing magnetic field pulse (whose magnitude entails to be larger than the coercivity of the heated region in order to ensure magnetization reversal) and a laser pulse (which is increasing the temperature of a localized region momentarily).

By means of localized heating, a momentarily decrease in the coercivity of this region is achieved. This brings with itself more energy-efficient data write-process than the conventional recording techniques since the reduction in the coercivity means that the magnetic moments can be aligned by applying less external magnetic field.

Hence, the possession of high perpendicular anisotropy made the CoNi/Pd multilayer magnetic structure a strong recording-layer candidate for the HAMR/TAR applications. Further, its high coercivity decreases in the vicinity of Curie point as in the case of FePt multilayers.

The switching mechanism of magnetization dynamics has been studied before relying upon material parameters determined from ab initio calculations. In this chapter, an LLB based macrospin approach is applied to a CoNi/Pd magnetic multilayer (ML) thin film. The goal is to extract the temperature dependent switching behavior with realistic input parameters which are exracted from the experimental measurements.

In other words, the temperature dependencies of intrinsic parameters such as zero temperature equilibrium magnetization, saturation magnetization and coercivity values were obtained from the experimental data.

Further, to achieve a successful model of TAR/HAMR process, both heating pulse

(which is the simplification of electron temperature profiles as they occur in pump-probe experiments) and magnetic field pulse (which can be regarded as a representation of magnetic field applied by the writing heads to the magnetic media) are taken to be almost in the form of rectangular (or smoothed step function) shape pulses. To see detailed description about how we can create a pulse with adjustable width, height, and slopes please see Appendix D for codes written in Mathematica and Appendix E for the codes written in COMSOL Multiphysics.

The response of magnetization to the applications of heating and magnetic field pulses are studied in detail for different peak values and durations. Lastly, an entire switching time distribution as a function of both heating and field pulse amplitudes have been calculated. Plus, all simulations are carried out in the presence and absence of the Gaussian stochastic process.

4.1. Experimental Analysis Of CoNi/Pd MLs

The CoNi/Pd MLs were sputter deposited onto a Si/SiO_2 substrate with a stack consisting of Ta (1.5nm) / Pd (3nm) / [$Co_{55}Ni_{45}$ (0.22nm) /Pd (1.2nm)] x 22 repeats /Pd (2nm). The films exhibited strong perpendicular anisotropy field H_k=18 kOe (corresponding to $\sim 2 \times 10^6 erg/cm^3$) and saturation magnetization M_S=220 emu/cm^3 as determined from vibrating specimen magnetometry (VSM) measurements at room temperature. A striking feature of such magnetic material systems is the strong exchange coupling (exchange lengths in the 20-30nm range with an effective exchange constant $A = 3 - 6 \times 10^{-6} ergs/cm$) which makes them a good candidate for macrospin like switching behavior in granular thin films or bit patterned media. Figure 4.1 (where an out of plane magnetic field of 1 kOe was applied to avoid demagnetization by breaking into domains above 400K).

The Curie temperature is determined by measuring $M_S(T)$ in the presence of an applied field and finding the point where M_S approaches zero. The first one is based on the measurements that are carried out in the presence of a small external magnetic field. The second one is obtained in the absence of external magnetic field (no Zeeman

Energy).

Unlike the magnetization temperature trend obtained under a non-dominant external field (1kOe), for the zero field case the magnetization value drops abruptly after $100°C$ which can be seen from Figure 4.1 (red point markers) [20]. This implies that for the case of zero field, out-ofplane anisotropy still exists near $100 - 125°C$ and the magnetization relaxation occurs due to the demagnetization by breaking into domains with perpendicular orientation. The blue point markers shown in Figure 4.1 is obtained [20]. As a result, the intersection point of data which is taken in the absence of magnetic field and in the presence of magnetic field which determines the Curie temperature of CoNi/Pd MLs as $175°C$ (448 K).

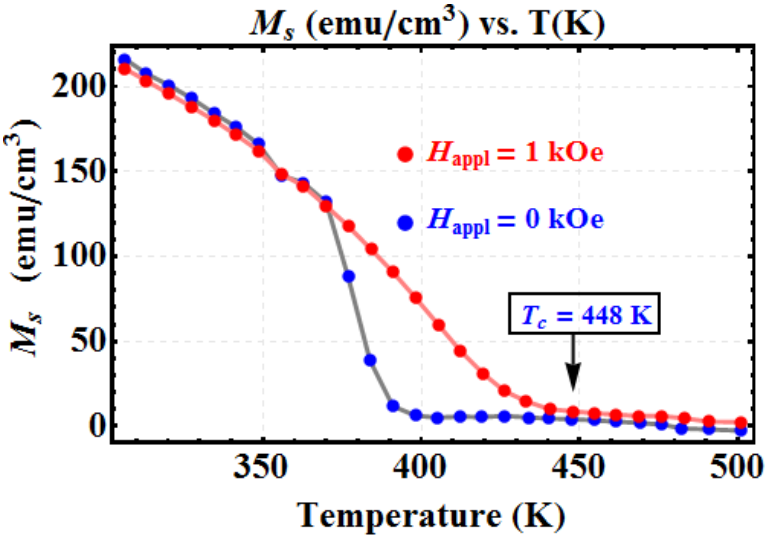

Figure 4.1. Temperature dependence of saturation magnetization as the material is under the influence of magnetic field (red point markers) and as no magnetic field is acting on the material (blue point markers). The solid lines are showing the interpolation functions of saturation magnetization for both nonzero and zero magnetic field.

The temperature dependence of coercivity is extracted from the hysteresis measurements for CoNi/Pd MLs which correspond to different temperature values. Figure 4.2 (the point markers) shows this experimental data [20]. Therefore, we can easily assert that if both coercivity and its corresponding temperature values are plugged

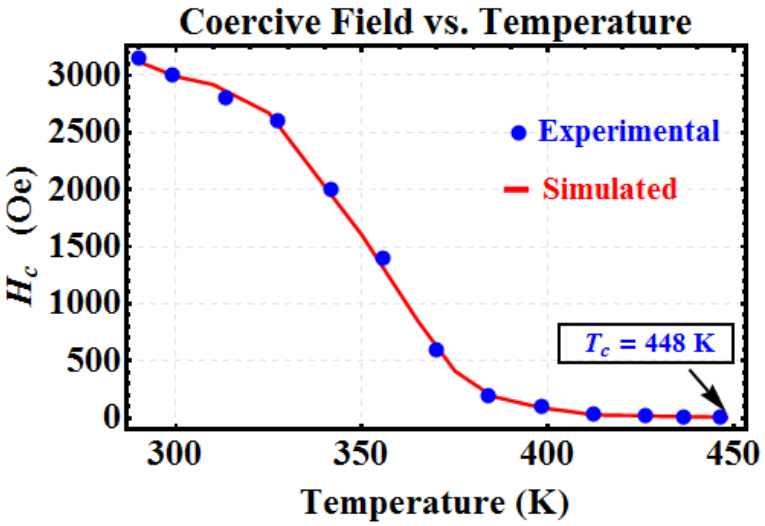

Figure 4.2. Experimental determination of temperature dependence of coercivity(blue point markers). Red solid line shows the simulated magnetic field which is sufficient to reverse the magnetization vector from one preferred direction to the other.

into the LLB simulation, more or less we need to see the magnetization reversal from one preferred direction (determined by the anisotropy of the material) to the other direction (stimulated by the external field). As a result, in Figure 4.2 (solid lines), these values agree with the trend of experimental data.

4.2. The Temperature Dependence Of Longitudinal Susceptibility

As it is stated before, the temperature dependency of coercivity can certainly be accepted as an interpolating function into the simulation. The details of the creation of an interpolation function are shown in Appendix D. This function is obtained isung a single fit parameter. This parameter is called longitudinal susceptibility ($\chi_{//}$). By following this simple logic, the temperature dependence of longitudinal susceptibility is obtained. Thus, we extracted its temperature dependence by including the experimental coercivity and its corresponding temperature values as our inputs to the LLB based simulations. In Figure 4.3, it is apparent that when the system temperature approaches Tc, there is a considerable rise in the longitudinal susceptibility value [20].

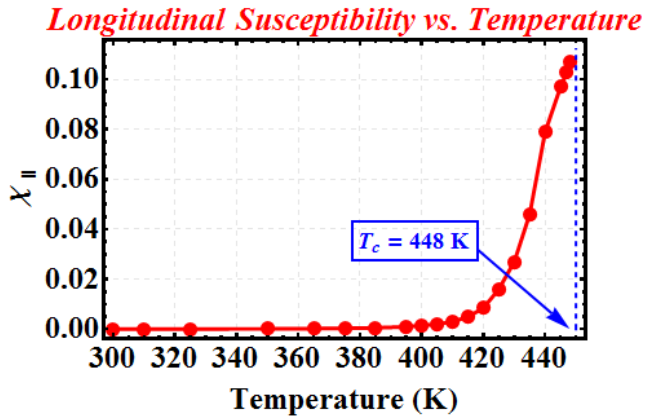

Figure 4.3. The temperature dependence of longitudinal susceptibility extracted from single fit parameter fit to the LLB model.

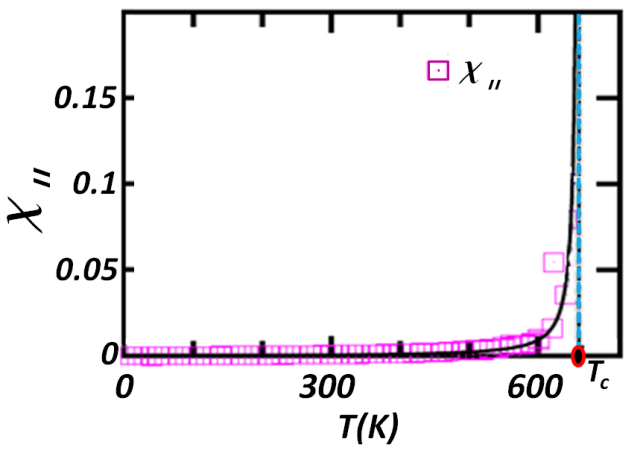

Figure 4.4. The temperature dependence of longitudinal susceptibility extracted from the ab-inito calculations [for detailed information [1]].

Most importantly, the result obtained by following this simple logic is remarkably consistent with the previously reported *ab initio* studies see Figure 4.4.

4.3. LLB Simulations Of Magnetic Hysteresis Loop Of CoNi/Pd MLs

The application of an alternating magnetic field through the ferromagnetic magnetic material makes the trajectory of the magnetization draw an irreversible path. In other words, the magnetization vector traces out a loop which is called as the magnetic

hysteresis loop which is a measure of magnetization versus field as the field is swept between two extremes. This behavior results from the existence of magnetic domains inside the magnetic material.

Figure 4.5 shows the experimentally determined hysteresis loop (blue solid line) on top of the simulated hysteresis loop at T=344 K. The simulations were performed with the longitudinal susceptibility value obtained from fitting the switching field to the coercive field and sweeping the field through the range used in the experiment. This procedure was repeated for all temperatures and checked against the experimental measurements.

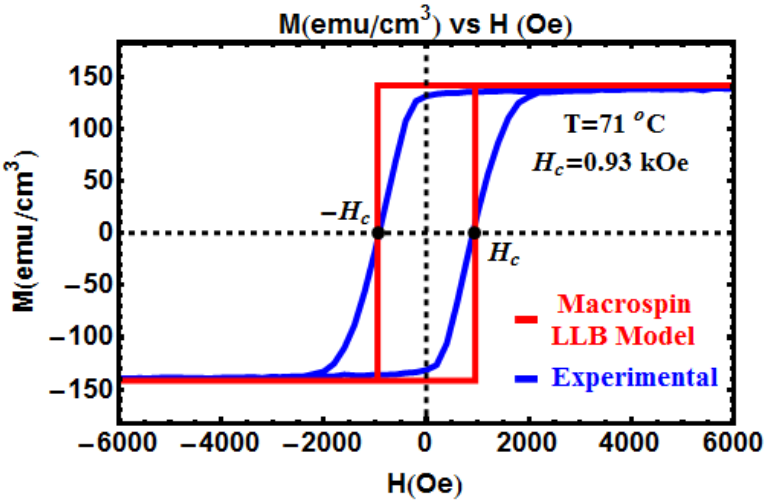

Figure 4.5. The blue solid line shows the hysteresis loop measurement which is experimentally determined. The red solid line is the macrospin simulation result for the same circumstance.

We have consistently been able to reproduce the switching in both directions at the correct applied field value. However, a careful comparison between the experimental and simulated hysteresis loops reveals that there is a clear discrepancy in the squareness of hystesis loops probably due to the detailed switching mechanism that is not considered in a simple macrospin approach as can be seen in Figure 4.5. This can be attributed to an inaccurate thin film demagnetization correction in the experimental data (-4πM for an infinite sheet but somewhat lower for finite dimensions) which results

in a finite slope of the M vs. H curve perhaps in addition to the micromagnetic reversal mechanism which was reported to be nucleation dominated in a previous study [7].

4.4. The Time Evolution Of Magnetization Dynamics In The Presence Of Heating And Magnetic Field Pulses (A Simplified HAMR Simulations)

Like the other intrinsic parameters, the temperature dependence of longitudinal susceptibility is employed in the model as an interpolating function. The detailed information about the inclusion of longitudinal susceptibility as an interpolating function can be seen in Appendix E. Thus, even for a certain temperature value (but not investigated experimentally) has its corresponding M_s, m_e, $\chi_{//}$, and H_c values inside the model.

We choose a set of realistic field and temperature values which can be used during the data recording process. Figure 4.6 shows an example set of magnetic field (blue colored) and heating (red colored) pulses.

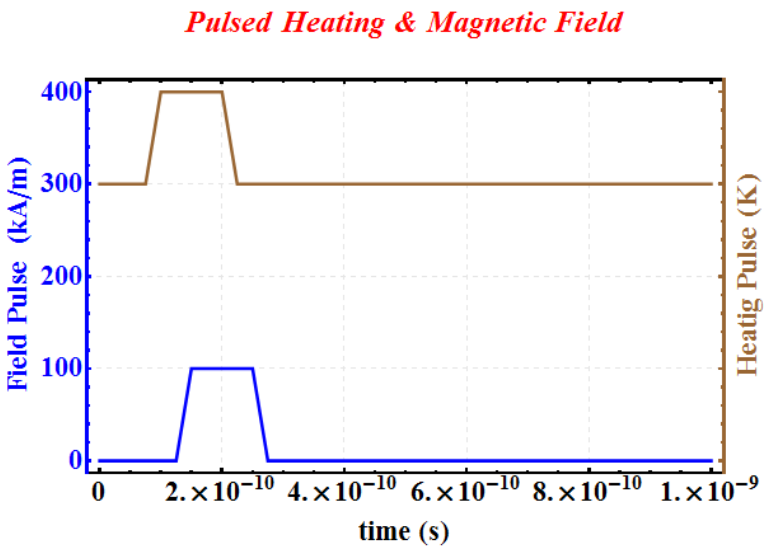

Figure 4.6. An example heating and magnetic field pulse set. Initially the heating pulse(brown solid line) is opened. After 0.5 ns delay magnetic field pulse(blue solid line) is applied to the material.

Figure 4.7 shows the time evolution of normalized (by zero temperature saturation magnetization M_s(T = 0K) = 250 emu/cm^3) magnetization vector components (blue solid line z component, black solid line y component and brown solid line x component) together with the magnetization length (red solid line) as a response to the application of heating and field pulses. In these simulations, the initial position of the magnetization vector is slightly tilted (10°) from -z direction (the easy axis determined by the strong perpendicular anisotropy). The reason behind tilting magnetization from –z direction with a small angle is that within the perfect alignment of magnetization along –z direction the magnetic moments find themselves the most possible energetically favorable direction and this cannot be changed by appliying an external magnetic field.

In Figure 4.7, it is shown that the magnetization has completed its longitudinal relaxation (in a few nanoseconds) and its transverse relaxation (in a few tens of nanoseconds). Since the external field is through +z direction, both x and y components (blue and brown colored lines) of the magnetization vector die out and the z component of magnetization aligns along the direction of external field [20]. In the final analysis, the ambient temperature of the system was taken as room temperature (300 K). Heating pulses with different pulse amplitudes were applied to the material to study the magnetization response. The delay between two pulses is 0.5 ns. The duration of the external magnetic field pulse is 1.25 nanoseconds (between 50% transition points). The inset of 4.7 shows the change in magnetization length with in response to heating pulses with different amplitudes [20].

Thanks to the existence of high perpendicular magnetic anisotropy, the plane of the thin film sample is not energetically favorable. Therefore, the magnetization minimizes the time spent in the plane of thin film sample during the precessional motion around the magnetic field. In Figure 4.8, the 3-D trajectory of magnetization vector is represented as it is under the influence of an effective magnetic field which includes an external field pulse (which aligns the magnetization along a preferred direction), anisotropy field (including in-plane anisotropy and dominant perpendicular anisotropy) and lastly, the field which is responsible for the longitudinal fluctuations [20]. Since

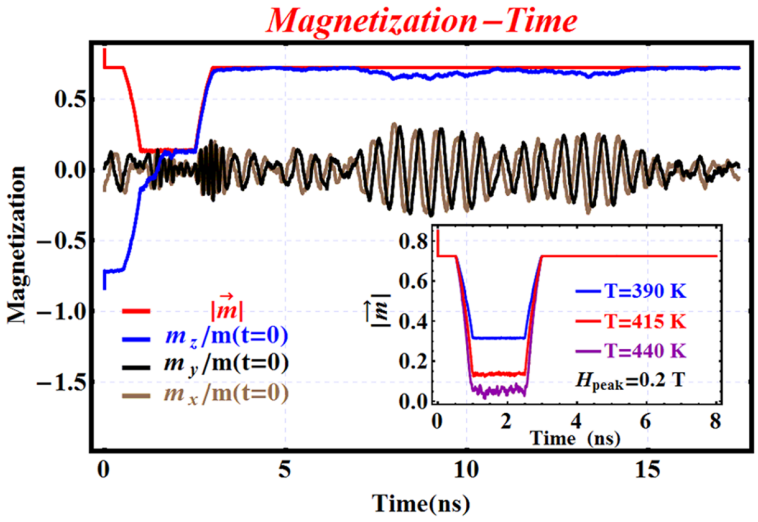

Figure 4.7. The time evolution of magnetization vector components together with the magnitude of magnetization vector. The inset shows the response of the magnetization magnitude for different heating pulse amplitudes.

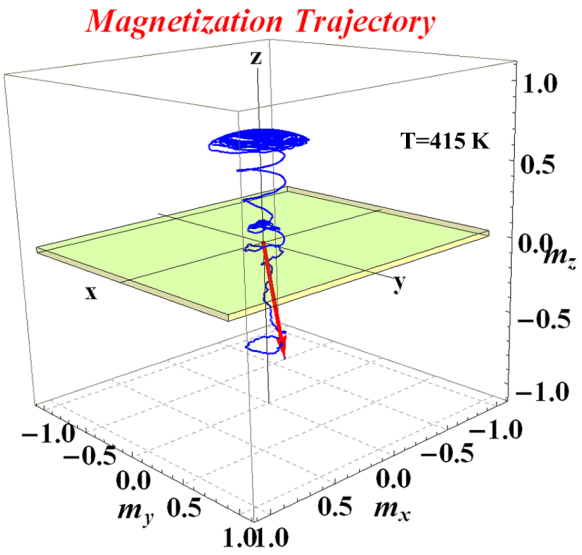

Figure 4.8. 3-D trajectory of magnetization vector. While red arrow shows the initial position of magnetization vector, blue colored solid line represents the trajectory of magnetization vector.

this is a macrospin approach, the field which accounts for the interaction between the magnetic moments called exchange field is not considered [15]. The trajectory is also slightly elliptically distorted due to the thin film demagnetizing field effect. The exchange field is required for the alignment of magnetic moments along a direction.

4.5. Switching Time Distribution

The considerable decrease in the coercivity of the material can only be achieved as the temperature of the system approaches T_c (see 4.2). Therefore, the physical mechanism of magnetic recording at elevated temperatures needs to be investigated in detail. In pursuit of this goal, we investigated the switching process as a function of both heating and writing field pulses systematically. Whilst the peak value of laser pulse ranges from 300 K to 450 K, the peak value of magnetic field pulse ranges from 0 A/m to 150 kA/m. In Figure 4.9, the pulse width (1.25ns), the rise and fall times (0.25 ns), and the delay between between pulses (0.5 ns) are fixed throughout the simulations while the pulse amplitudes varied [20].

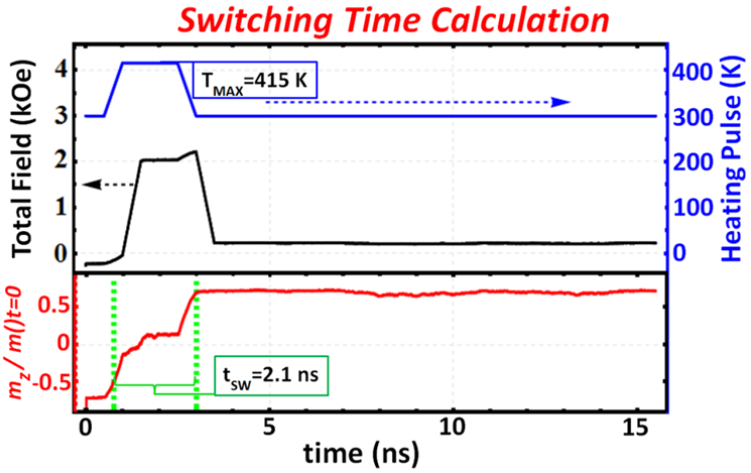

Figure 4.9. An example set of total effective field and heating pulses (black and blue solid lines respetively). The red solid line is the response of z component of magnetization vector to this field and heating pulse combination. The switching time for this case is about 2.1 ns.

Heating the system by using a laser pulse is a rather complicated process. Heating of the recording region initially affects the electron system (in a few femtoseconds). Due to the coupling between electron and lattice system, the energy exchange between them starts. During this energy transfer lattice temperature and the electron temperature relaxes to a new eqilibrium temperature value. The thermal exchange between the electron and lattice systems is described by the two temperature model [15]. After the application of heating pulse electron temperature increases drastically and then the dissipation of the energy (possessed by the electrons) heats the lattice system (hundreds of picoseconds) [15]. Therefore, in one of the prior studies, it is reported that by employing the experimentally determined temperature dependence of thermal conductivity in the finite element calculations, the estimated thermal relaxation time for CoNi/Pd ML system is on the order of 100 ps which is comparable to the typical electron-lattice thermal relaxation time. The cooling time is set to 250 ps in our simulations.

After the determination of pulse properties, the next focus is about how to get the switching time distribution. The details of switching time calculation are presented in Appendix F. The switching time is defined as the time elapsed between the onset of the heating pulse and the instant when %90 of the equilibrium magnetization value is achieved. It is worth noting that since the actual switching time calculation is intermixed with the longitudinal relaxation process during heating and cooling, the switching time obtained with this procedure gives an upper bound to the actual switching time.

4.5.1. The Case Of Non-Stochastic LLB Model

In the final analysis, Figure 4.10 shows the calculated switching times as a function of the heating pulse and writing pulse amplitudes (averaged over 200 iterations). The switching times are color coded. While the black color implies no switching, the red color implies ultrafast switching.

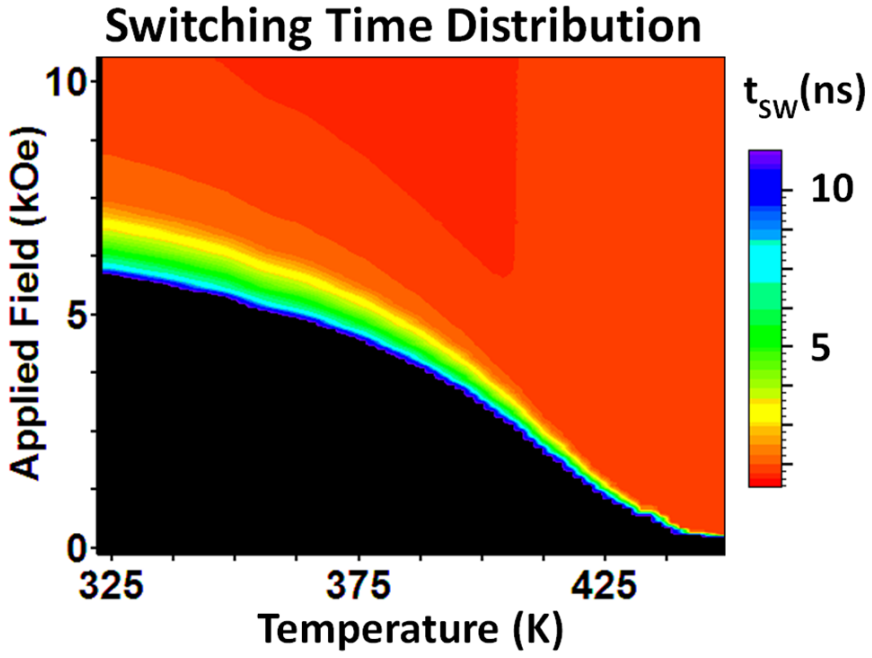

Figure 4.10. For different field and heating pulse combinations, the switching time is calculated. The black region is showing the non-switching region and the red one shows the ultrafast switching. For this case, the Gaussian stochastic process in not taken into account.

It can be inferred from the numerical analysis based on the LLB formalism that for a given heating pulse, the switching time can be reduced considerably by applying magnetic fields well above the coercive field value. Furthermore, as the temperature of the system exceeds 425 K (close to $T_c = 448$ K), the ultrafast switching (sub-ns scale) is observed with very small magnetic fields (in the order of less than an Oersted).

According to the reports on ultrafast manipulation of magnetization [21] the actual time required for the switching is expected to be controllable down to 10-100s of fs. 4.10 suggests that at any temperature value, by over-driving the switching with an external magnetic field pulse which is higher than the coercive field, the switching can be achieved in sub-nanosecond scale.

4.5.2. The Case Of Stochastic LLB Model (S-LLB II)

Particularly, stochastic processes play an important role at finite temperatures. In our study, since system temperature needs to be increased up to the phase transition point (which is in between the ferromagnetic and paramagnetic transition), the implementation of stochasticity is a requirement of obtaining a probabilistic point of view to the magnetization reversal process. So the thermally induced noise effects are significant at especially temperature regime close to T_c. For this purpose, the LLB equation has been modified by including the Gaussian Stochastic process (resulting in S-LLB II) which is described within detail in Chapter 2.

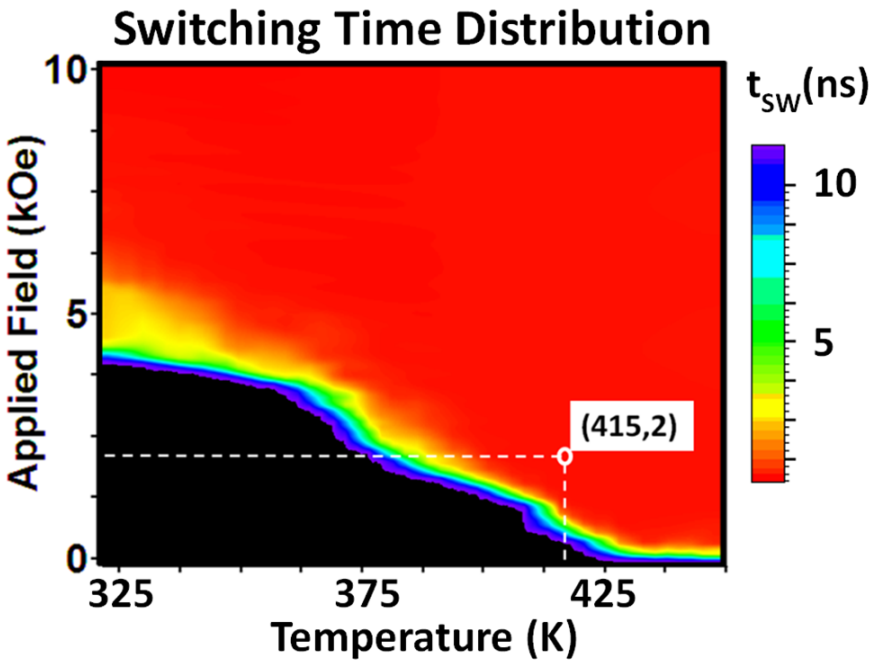

Figure 4.11. The average switching time (obtained from 200 iterations) is represented as a function of heating and magnetic field pulses. The red region is showing ultrafast switching and the black region shows non switching case. In this case, the Gaussian stochastic process is taken into account.

Due to the probabilistic nature of the switching process, we have repeated our simulations to obtain the switching time 200 times [20]. Figure A.1 shows the switching time distribution as the magnetization dynamics is governed by the stochastic LLB

equation of motion (S-LLB II). While the black color means the combination of field and heating pulses are not capable of switching the magnetization vector, the red one implies the ultrafast reversal of the magnetization vector. It is worth noting here that for higher temperature values, the switching can be achieved by moderately high magnetic fields.

5. CONCLUSION

In this study, we have implemented a comprehensive model to understand the nature of switching dynamics in the existence of both external magnetic field and heating pulses. Consistent with previous reports, an enhanced damping is observed by increasing the temperature of the magnetic medium. Another significant result is the extraction of temperature trend of longitudinal susceptibility by addressing it as the single fitting parameter of our macrospin approach while the other inputs are experimentally taken bulk properties of a strong candidate (CoNi/Pd MLs) for the recording layer of TAR/HAMR technique. Moreover, the temperature profile of longitudinal susceptibility obtained in this way has a considerable consistency with the reports that they have employed ab-intio calculations. Accordingly, as a unique study the entire switching time distribution as a function of both heating and magnetic field pulses is created by taking these essential guidelines (temperature dependence of both intrinsic properties of CoNi/Pd MLs and the longitudinal susceptibility) into account. As a consequence of this, it can be said that the LLB based macrospin model is able to shed a comprehensive light on the underlying mechanism of the magnetization reversal during the writing process of up-coming magnetic data storage techniques (such as TAR/HAMR). On the one hand, the macrospin model has the requisite qualities to give detailed description about the coherent rotation of magnetic moments. On the other hand, the effect of spin spin interactions can be seen by the extension of this simplistic model to the micromagnetic LLB model. This enables for example the observation of slower recovery process in response to the enhanced temperature values. Nevertheless, this simple approach allows a qualified evaluation of the switching properties of CoNi/Pd MLs with a relatively low Curie temperature and strong perpendicular anisotropy at room temperature and other similar thin film structures as a candidate for granular or bit patterned TAR/HAMR applications.

APPENDIX A: THE UNIT OF THE GYROMAGNETIC RATIO

The unit of γ is evidently C/kg but in lots of papers call the unit of γ as $\frac{m}{A \cdot s}$. Now, in this appendix, we show that these two units are equal.

In general, it is known that gyromagnetic ratio is the ratio of the magnetic moment of an electron $\boldsymbol{\mu}_e$ to the angular momentum $\boldsymbol{L}$

$$\gamma_0 = \frac{\boldsymbol{\mu}_e}{\boldsymbol{L}} = \frac{\frac{e\cancel{v}\cancel{r}}{2}}{m_e\cancel{v}\cancel{r}} = \left(\frac{e}{2m_e}\right) \tag{A.1}$$

$$\gamma = g \cdot \gamma_0 = g \cdot \left(\frac{e}{2m_e}\right) \tag{A.2}$$

When we assume an infinitesimally narrow circular ring has radius r, area $A = \pi r^2$,

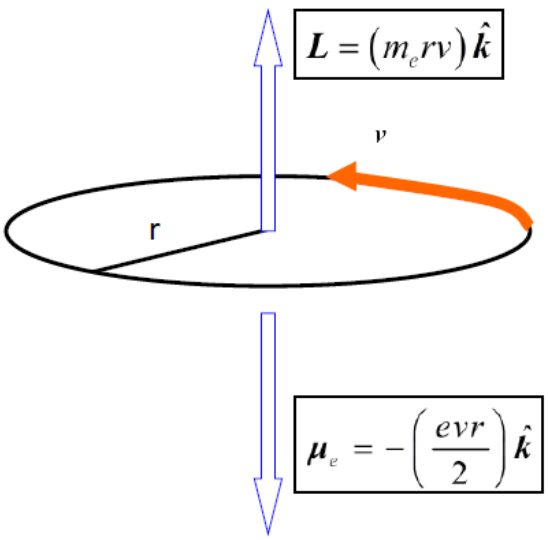

Figure A.1. Components of the classical gyromagnetic ratio of the obiting electron.

mass m, charge q, and angular momentum defined as $L = mvr$. Then, the magnitude

of the magnetic dipole moment is

$$\mu = IA = \left(\left(\frac{q}{2\pi r}\right)v\right)\pi r^2 = \left(\frac{q}{2m}\right)mvr = \left(\frac{q}{2m}\right)L \tag{A.3}$$

The orbital motion of an electron can be regarded as the flow of current in a circular wire. Thus, the last form of the equation above can be written in the following form;

$$\mu_e = \left(\frac{e}{2m}\right)L \tag{A.4}$$

The value of the g-factor is 2.002290... for all ferromagnetic materials. Furthermore, our primary objective is to carry out these simulations by using a special ferromagnetic material. Thus, this g-factor will be used as one of our constants in our simulation. By using the last equation A.2 for gyromagnetic ratio, we can reach the gyromagnetic ratio value for both free electrons and ferromagnetic materials;

$$\gamma = g \cdot \gamma_0 = g \cdot \left(\frac{e}{2m_e}\right) = g \cdot \left(\frac{\mu_e}{\hbar}\right) \tag{A.5}$$

By means of the above formula A.5, the electron gyromagnetic ratio of a ferromagnet is calculated within the following form;

$$\gamma = g \cdot \gamma_0 = g \cdot \left(\frac{e}{2m_e}\right) = g \cdot \left(\frac{\mu_e}{\hbar}\right) = 1.760859770 \times 10^{11} s^{-1} T^{-1} \tag{A.6}$$

Here, there is also a mixed unit computation so for T (Tesla) is used as a unit of magnetic field strength; $1T = 10^4$ Gauss and 1 Gauss (G) corresponds to 1 Oersted (Oe). By using this convention and the relation between Oersted and A/m: $1Oe = \left(\frac{1000}{4\pi}\right)\frac{4}{m}$, the unit for external magnetic field can be turned into the unit for the magnetic field inside the material within the following form; $1T \equiv 10^4 Oe = 79.57747155 \times 10^4 \frac{A}{m}$ then, if the gyromagnetic ratio unit is analyzed, we firstly need the inverse of the Tesla $(T)^{-1}$ so that

$$T^{-1} = \frac{1}{79.57747155 \times 10^4}\left(\frac{A}{m}\right)^{-1} = 1.25663706 \times 10^{-2}\left(\frac{A}{m}\right)^{-1}$$

The value of the gyromagnetic ratio for both free electrons and ferromagnetic materials

$$\begin{aligned}\gamma &= g \cdot \left(\frac{\mu_e}{\hbar}\right) = 1.760859770 \times 10^{11} s^{-1} T^{-1} \\ &= \left(1.760859770 \times 10^{11} (s)^{-1}\right) \cdot \left(1.25663706 \times 10^{-6} \left(\frac{A}{m}\right)^{-1}\right) \\ &= 2.212761647 \times 10^{5} \left(\frac{m}{A \cdot s}\right)\end{aligned} \tag{A.7}$$

APPENDIX B: BRIEF DERIVATION OF LANDAU LIFSHITZ GILBERT EQUATION OF MOTION

Equation 4 is the LLG equation but it is different from the form of LL equation.

$$\frac{\partial \mathbf{M}}{dt} = -\gamma \left(\mathbf{M} \times \mathbf{H}_{eff}\right) + \frac{\alpha}{M_s}\left(\mathbf{M} \times \frac{d\mathbf{M}}{dt}\right) \tag{B.1}$$

By vector multiplying both sides of the equation above by $\mathbf{M}$;

$$\mathbf{M} \times \left(\frac{\partial \mathbf{M}}{dt} = -\gamma \left(\mathbf{M} \times \mathbf{H}_{eff}\right) + \frac{\alpha}{M_s}\left(\mathbf{M} \times \frac{d\mathbf{M}}{dt}\right)\right)$$

$$\mathbf{M} \times \frac{\partial \mathbf{M}}{dt} = -\gamma \mathbf{M} \times \left(\mathbf{M} \times \mathbf{H}_{eff}\right) + \frac{\alpha}{M_s}\mathbf{M} \times \left(\mathbf{M} \times \frac{d\mathbf{M}}{dt}\right) \tag{B.2}$$

Using the following vector product identity;

$$\mathbf{a} \times \mathbf{b} \times \mathbf{c} = \mathbf{b}\left(\mathbf{a} \cdot \mathbf{c}\right) - \mathbf{c}\left(\mathbf{a} \cdot \mathbf{b}\right) \tag{B.3}$$

The second term of the last equation B.3 can be written in the following form;

$$\mathbf{M} \times \left(\mathbf{M} \times \frac{d\mathbf{M}}{dt}\right) = \mathbf{M}\left(\mathbf{M} \cdot \frac{d\mathbf{M}}{dt}\right) - \frac{d\mathbf{M}}{dt}\left(\mathbf{M} \cdot \mathbf{M}\right) \tag{B.4}$$

To reach more precise relation, if we take the scalar (inner) product of both sides of Equation B.3 with $\mathbf{M}$;

$$\mathbf{M} \cdot \left(\frac{\partial \mathbf{M}}{dt} = -\gamma \left(\mathbf{M} \times \mathbf{H}_{eff}\right) + \frac{\alpha}{M_s}\left(\mathbf{M} \times \frac{d\mathbf{M}}{dt}\right)\right)$$

$$\mathbf{M} \cdot \frac{\partial \mathbf{M}}{dt} = -\gamma \mathbf{M} \cdot \left(\mathbf{M} \times \mathbf{H}_{eff}\right) + \frac{\alpha}{M_s}\mathbf{M} \cdot \left(\mathbf{M} \times \frac{d\mathbf{M}}{dt}\right) \tag{B.5}$$

$$\text{Since } \mathbf{M}\perp \begin{cases} (\mathbf{M}\times\mathbf{H}_{eff}) \\ \left(\mathbf{M}\times\frac{d\mathbf{M}}{dt}\right) \end{cases} \Rightarrow \mathbf{M}\cdot\frac{\partial\mathbf{M}}{dt}=0$$

$$\mathbf{M}\cdot\frac{\partial\mathbf{M}}{dt}=-\gamma\left|\mathbf{M}\right|\left|(\mathbf{M}\times\mathbf{H}_{eff})\right|\cos(\pi/2)+\frac{\alpha}{M_s}\left|\mathbf{M}\right|\left|\left(\mathbf{M}\times\frac{d\mathbf{M}}{dt}\right)\right|\cos(\pi/2)=0$$

The principal knowledge has been used in both LL and LLG equation is that the magnetization magnitude is constant in time $|\mathbf{M}|=M_s$. Thus, we can write down the second term of the Equation B.4 in following form;

$$\mathbf{M}\times\left(\mathbf{M}\times\frac{d\mathbf{M}}{dt}\right)=\mathbf{M}\left(\mathbf{M}\cdot\frac{d\mathbf{M}}{dt}\right)-\frac{d\mathbf{M}}{dt}\left(\mathbf{M}\cdot\mathbf{M}\right)$$

$$=-\frac{d\mathbf{M}}{dt}\left(\left|\mathbf{M}\right|\left|\mathbf{M}\right|\cos(0)\right)=-{M_s}^2\left(\frac{d\mathbf{M}}{dt}\right) \tag{B.6}$$

Therefore, the Equation B.6 becomes

$$\begin{aligned}
\mathbf{M}\times\frac{\partial\mathbf{M}}{dt} &= -\gamma\mathbf{M}\times(\mathbf{M}\times\mathbf{H}_{eff})+\frac{\alpha}{M_s}\mathbf{M}\times\left(\mathbf{M}\times\frac{d\mathbf{M}}{dt}\right) \\
&= -\gamma\mathbf{M}\times(\mathbf{M}\times\mathbf{H}_{eff})+\frac{\alpha}{M_s}\left(-{M_s}^2\left(\frac{d\mathbf{M}}{dt}\right)\right) \\
\mathbf{M}\times\frac{\partial\mathbf{M}}{dt} &= -\gamma\mathbf{M}\times(\mathbf{M}\times\mathbf{H}_{eff})+\frac{\alpha}{\cancel{M_s}}\left(-{M_s}^{\cancel{2}}\left(\frac{d\mathbf{M}}{dt}\right)\right) \\
&= -\gamma\mathbf{M}\times(\mathbf{M}\times\mathbf{H}_{eff})-\alpha M_s\left(\frac{d\mathbf{M}}{dt}\right)
\end{aligned} \tag{B.7}$$

$\mathbf{M}\times\frac{\partial\mathbf{M}}{dt}=-\gamma\mathbf{M}\times(\mathbf{M}\times\mathbf{H}_{eff})-\alpha M_s\left(\frac{d\mathbf{M}}{dt}\right)$ B.7

Moreover, we can have one more relation for using the B.1;

$$\left(\mathbf{M}\times\frac{d\mathbf{M}}{dt}\right)=\frac{M_s}{\alpha}\left(\frac{\partial\mathbf{M}}{dt}+\gamma\left(\mathbf{M}\times\mathbf{H}_{eff}\right)\right) \tag{B.8}$$

By equating last two equations B.7 and B.8 to each other;

$-\gamma \mathbf{M} \times (\mathbf{M} \times \mathbf{H}_{eff}) - \alpha M_s \left(\frac{d\mathbf{M}}{dt}\right) = \frac{M_s}{\alpha} \left(\frac{\partial \mathbf{M}}{dt} + \gamma (\mathbf{M} \times \mathbf{H}_{eff})\right)$

$\left(M_s \left(\frac{1}{\alpha} + \alpha\right)\right) \frac{\partial \mathbf{M}}{dt} = \gamma \mathbf{M} \times (\mathbf{M} \times \mathbf{H}_{eff}) - \frac{\gamma M_s}{\alpha} (\mathbf{M} \times \mathbf{H}_{eff})$

$\frac{\partial \mathbf{M}}{dt} = \gamma \left(\frac{1}{M_s} \left(\frac{\alpha}{1+\alpha^2}\right)\right) \mathbf{M} \times (\mathbf{M} \times \mathbf{H}_{eff}) - \frac{\gamma \cancel{M_s}}{\cancel{\alpha}} \left(\frac{1}{\cancel{M_s}} \left(\frac{\cancel{\alpha}}{1+\alpha^2}\right)\right) (\mathbf{M} \times \mathbf{H}_{eff})$

Thus;

$$\frac{\partial \mathbf{M}}{dt} = -\left(\frac{\gamma}{1+\alpha^2}\right) (\mathbf{M} \times \mathbf{H}_{eff}) + \gamma \left(\frac{1}{M_s} \left(\frac{\alpha}{1+\alpha^2}\right)\right) \mathbf{M} \times (\mathbf{M} \times \mathbf{H}_{eff}) \tag{B.9}$$

$$\frac{d\mathbf{M}}{dt} = -|\gamma| (\mathbf{M} \times \mathbf{H}_{eff}) + |\gamma| \left(\frac{\lambda}{M_s}\right) (\mathbf{M} \times (\mathbf{M} \times \mathbf{H}_{eff})) \tag{B.10}$$

Equation B.9 is another form of LLG equation and the similarity between the components of the LL Equation B.10 and LLG equation can be seen, easily.

Yet, there is a huge difference between them. While the LL equation can describe the magnetization dynamics as the damping constant (α) is less than 1, LLG equation gives a new description to damping constant and thus even for larger damping regime the LLG equation gives the true result.

Using Equation B.9, as $\alpha \Rightarrow \infty$, all terms at the left hand side vanish thus, $\frac{dM}{dt} \Rightarrow 0$

However, in Equation B.10 (LL equation) as $\alpha \Rightarrow \infty$ the second term of the LL equation (damping term) energy dissipation becomes dominant and therefore, $\frac{dM}{dt} \Rightarrow \infty$ which is unphysical.

It is important to note that when the thermal interactions are taken into account, these two conventional equations give accurate results just for the low temperature regime [1, 6, 11, 14, 15].

APPENDIX C: THE CLASSICAL DERIVATION OF LANDAU LIFSHITZ BLOCH EQUATION OF MOTION

The conventional LLG equation has crucial drawbacks as opposed to the LLB equation. For example, the latter one involves a field term to control the longitudinal fluctuations in the magnetization length which brings with itself additional relaxation time called as the longitudinal relaxation time. Whereas, there is just one relaxation time for the magnetization relaxation process which is called as transverse relaxation time in the former one. Furthermore, in LLB equation there are two damping parameters called as longitudinal damping parameter and transverse damping parameter which depend on both macroscopic Gilbert damping parameter and the temperature of the system.

In this appendix, the goal is to derive this equation of motion which is valid for classical ferromagnets for the whole temperature range starting from the Fokker-Planck formalism which is a methodology to describe the evolution of probability density function;

$$\frac{\partial f}{\partial t}+\frac{\partial}{\partial \mathbf{N}}\left\{\gamma\left(\mathbf{N}\times\mathbf{H}\right)-\gamma\lambda\left(\mathbf{N}\times\left[\mathbf{N}\times\mathbf{H}\right]\right)+\frac{\gamma\lambda T}{\mu_0}\left(\mathbf{N}\times\left[\mathbf{N}\times\frac{\partial}{\partial \mathbf{N}}\right]\right)\right\}f=0 \quad \text{(C.1)}$$

where $f(\boldsymbol{N},t)$ is the distribution function $f(\boldsymbol{N},t)=\langle\delta^3(\boldsymbol{N}-\boldsymbol{s}(t))\rangle$ and $\boldsymbol{m}=\langle\boldsymbol{s}\rangle$ is the spin polarization vector which is dimensionless and it has a clear expression in terms of the distribution function.

$$\int d^3N\mathbf{N}f(\mathbf{N},t)=\langle\mathbf{s}\rangle=\mathbf{m} \quad \text{(C.2)}$$

This can be proved trivially by plugging the general relation of distribution function written within the mean field approach:

$$\int d^3N\mathbf{N}f(\mathbf{N},t) = \int d^3N\mathbf{N}\left\langle \delta^3(\mathbf{N}-\mathbf{s}(t))\right\rangle = \left\langle \int d^3N\mathbf{N}\delta^3(\mathbf{N}-\mathbf{s}(t))\right\rangle = \langle \mathbf{s}\rangle = \mathbf{m}$$

When the magnetization vector is differentiated, we can combine Fokker-Planck Equation C.1 with the following differential equation. In this way, the first stage of LLB equation can be obtained.

$$\frac{d\mathbf{m}}{dt} = \frac{d}{dt}\left(\int d^3N\mathbf{N}f(\mathbf{N},t)\right) = \int d^3N\mathbf{N}\frac{\partial}{\partial t}\left(f(\mathbf{N},t)\right)$$

Therefore, instead of $\frac{\partial}{\partial t}\left(f(\mathbf{N},t)\right)$, we can write its equivalence which were taken from the Equation C.1

$$\begin{aligned}
&\textstyle\int d^3\boldsymbol{N}\boldsymbol{N}\frac{\partial}{\partial t}\left(f(\boldsymbol{N},t)\right) = \\
&\textstyle\int d^3\boldsymbol{N}\boldsymbol{N}\left\{-\frac{\partial}{\partial \boldsymbol{N}}\left\{\gamma\left(\boldsymbol{N}\times\boldsymbol{H}\right)-\gamma\lambda\left(\boldsymbol{N}\times\left[\boldsymbol{N}\times\boldsymbol{H}\right]\right)+\frac{\gamma\lambda k_BT}{\mu_0}\left(\boldsymbol{N}\times\left[\boldsymbol{N}\times\frac{\partial}{\partial \boldsymbol{N}}\right]\right)\right\}f\right\} \\
&= -\gamma\textstyle\int d^3\boldsymbol{N}\boldsymbol{N}\frac{\partial}{\partial \boldsymbol{N}}\left(\boldsymbol{N}\times\boldsymbol{H}\right)f+ \\
&-\gamma\lambda\textstyle\int d^3\boldsymbol{N}\boldsymbol{N}\frac{\partial}{\partial \boldsymbol{N}}\left(\boldsymbol{N}\times\left[\boldsymbol{N}\times\boldsymbol{H}\right]\right)f+\frac{\gamma\lambda k_BT}{\mu_0}\int d^3\boldsymbol{N}\boldsymbol{N}\frac{\partial}{\partial \boldsymbol{N}}\left(\boldsymbol{N}\times\left[\boldsymbol{N}\times\frac{\partial}{\partial \boldsymbol{N}}\right]\right)f \\
&= -\gamma\textstyle\int d^3\boldsymbol{N}\left(\boldsymbol{N}\times\boldsymbol{H}\right)f-\gamma\lambda\int d^3\boldsymbol{N}\left(\boldsymbol{N}\times\left[\boldsymbol{N}\times\boldsymbol{H}\right]\right)f+ \\
&\textstyle\frac{\gamma\lambda k_BT}{\mu_0}\int d^3\boldsymbol{N}\left(\boldsymbol{N}\times\left[\boldsymbol{N}\times\frac{\partial}{\partial \boldsymbol{N}}\right]\right)f
\end{aligned} \tag{C.3}$$

As a result of this, we can reach the following expression;

$$\int d^3N\mathbf{N}\frac{\partial}{\partial t}\left(f(\mathbf{N},t)\right) = -\gamma\left(\mathbf{m}\times\mathbf{H}\right)-\gamma\lambda\left\langle \mathbf{s}\times\left[\mathbf{s}\times\mathbf{H}\right]\right\rangle+\frac{\gamma\lambda k_BT}{\mu_0}\int d^3N\left(\mathbf{N}\times\left[\mathbf{N}\times\frac{\partial}{\partial\mathbf{N}}\right]\right)f \tag{C.4}$$

Detailed analysis of the third term at the right hand side of the Equation C.4: Inside the last integral (third term), instead of cross product representation, we can make use of two Levi Civita mathematical identities. Simultaneously, we did partial by parts integration after we played with dummy indices by lowering and raising them

all for each LeviCivita symbol $\left(\varepsilon^{\alpha}{}_{i\beta},\, \varepsilon^{\beta}{}_{jk}\right)$ over the Equation C.4

$$\frac{\gamma\lambda k_B T}{\mu_0}\int d^3\mathbf{N}\left(\mathbf{N}\times\left[\mathbf{N}\times\frac{\partial}{\partial\mathbf{N}}\right]\right)f(\mathbf{N},t)=\frac{\gamma\lambda k_B T}{\mu_0}\int d^3\mathbf{N}\varepsilon^{\alpha}{}_{i\beta}\varepsilon^{\beta}{}_{jk}\mathbf{N}^i\mathbf{N}^j\frac{\partial}{\partial\mathbf{N}}^k f(\mathbf{N},t) \tag{C.5}$$

While we are dealing with a tensor problem, the following three main features are extensively used which leads to raise or to lower the indices;

$$\varepsilon^{\alpha i\beta}=\varepsilon_{\alpha i\beta}\ and\ \delta_{j\alpha}=-\delta_{\alpha j} \tag{C.6}$$

$$X^i=\delta^{ij}X_j\ and\ X_j=\delta_{ij}X^i \tag{C.7}$$

$$\left\{\begin{array}{c}\varepsilon^{\alpha i\beta}\varepsilon_{\beta jk}=2\delta^{\alpha i}_{jk}=\delta^{\alpha}{}_{j}\delta^{i}{}_{k}-\delta^{\alpha}{}_{k}\delta^{i}{}_{j}\\ or\\ \varepsilon^{\alpha i\beta}\varepsilon_{\beta jk}=\varepsilon_{\alpha i\beta}\varepsilon_{\beta jk}=\delta_{j\alpha}\delta_{ik}-\delta_{\alpha k}\delta_{ij}\end{array}\right\} \tag{C.8}$$

So we obtain;

$$\frac{\gamma\lambda k_B T}{\mu_0}\int d^3\mathbf{N}\varepsilon^{\alpha}{}_{i\beta}\varepsilon^{\beta}{}_{jk}\mathbf{N}^i\mathbf{N}^j\frac{\partial}{\partial\mathbf{N}}^k f(\mathbf{N},t)=\frac{\gamma\lambda k_B T}{\mu_0}\int d^3\mathbf{N}\varepsilon^{\alpha i\beta}\varepsilon_{\beta jk}\left(\delta^{ik}\mathbf{N}^i+\mathbf{N}^j\delta^{jk}\right)\frac{\partial}{\partial\mathbf{N}}^k f(\mathbf{N},t)$$

The product of two Levi-Civita symbols can be expressed as the combinations of the Kronecker's symbols Equation C.8. As a result, we can write this term with tensors in the following form;

$$\begin{array}{l}\frac{\gamma\lambda k_B T}{\mu_0}\int d^3\mathbf{N}\varepsilon^{\alpha i\beta}\varepsilon_{\beta jk}\left(\delta^{ik}\mathbf{N}^j+\mathbf{N}^i\delta^{jk}\right)\frac{\partial}{\partial\mathbf{N}}^k f(\mathbf{N},t)=\\ \quad=\frac{\gamma\lambda k_B T}{\mu_0}\int d^3\mathbf{N}\left(\delta^{\alpha}{}_{j}\delta^{i}{}_{k}-\delta^{\alpha}{}_{k}\delta^{i}{}_{j}\right)\left(\delta^{ik}\mathbf{N}^j+\mathbf{N}^i\delta^{jk}\right)\frac{\partial}{\partial\mathbf{N}}^k f(\mathbf{N},t)\end{array} \tag{C.9}$$

Now, we are ready to analyze Equation C.9 by looking at the values of indices;
By setting $\alpha=k\ and\ i=j$, solution is zero.

By setting $\alpha = j \; and \; i = k$, solution is in the following form;

$$\begin{aligned}
&\tfrac{\gamma\lambda k_B T}{\mu_0} \int d^3\mathbf{N} \left(\delta^{\alpha}{}_{j}\delta^{i}{}_{k} - \delta^{\alpha}{}_{k}\delta^{i}{}_{j}\right) \left(\delta^{ik}\mathbf{N}^{j} + \mathbf{N}^{i}\delta^{jk}\right) \tfrac{\partial}{\partial \mathbf{N}}{}^{k} f(\mathbf{N},t) = \\
&\quad = \tfrac{\gamma\lambda k_B T}{\mu_0} \int d^3\mathbf{N} \left(\delta^{\alpha}{}_{\alpha}\delta^{k}{}_{k} - \delta^{\alpha}{}_{k}\delta^{k}{}_{\alpha}\right) \left(\delta^{kk}\mathbf{N}^{\alpha} + \mathbf{N}^{i}\delta^{\alpha k}\right) \tfrac{\partial}{\partial \mathbf{N}}{}^{k} f(\mathbf{N},t) \\
&\quad = \tfrac{2\gamma\lambda k_B T}{\mu_0} \int d^3\mathbf{N}\mathbf{N}^{\alpha} \tfrac{\partial}{\partial \mathbf{N}}{}^{k} f(\mathbf{N},t)
\end{aligned}$$

The equation written above is last form the third term in Equation C.4. Yet, there is another way of getting the same result. Classically, we can reach this result by the help of a trivial method which is a special feature of Levi Civita: two consecutive vector products with three different vectors can be written as follows:

$$\mathbf{a} \times (\mathbf{b} \times \mathbf{c}) = \mathbf{b}\,(\mathbf{a} \cdot \mathbf{c}) - \mathbf{c}\,(\mathbf{a} \cdot \mathbf{b}) \tag{C.10}$$

The proof of this relation:

$$\begin{aligned}
\mathbf{d} = \mathbf{a} \times (\mathbf{b} \times \mathbf{c}) &= \varepsilon_{mni} a_n \left(\varepsilon_{ijk} b_j c_k\right) = \varepsilon_{mni}\varepsilon_{ijk} a_n b_j c_k \\
&= \left(\delta_{mj}\delta_{nk} - \delta_{mk}\delta_{nj}\right) a_n b_j c_k = a_m b_k c_k - c_m a_j b_j \\
&= \left[\mathbf{b}\,(\mathbf{a} \cdot \mathbf{c})\right]_m - \left[\mathbf{c}\,(\mathbf{a} \cdot \mathbf{b})\right]_m
\end{aligned}$$

Then, we can apply this to our case;

$$\begin{aligned}
&\tfrac{\gamma\lambda k_B T}{\mu_0} \int d^3N \left(\mathbf{N} \times \left[\mathbf{N} \times \tfrac{\partial}{\partial \mathbf{N}}\right]\right) f = \tfrac{\gamma\lambda k_B T}{\mu_0} \int d^3N \left(\mathbf{N}\left[\mathbf{N}\tfrac{\partial f(\mathbf{N},t)}{\partial \mathbf{N}}\right] - \tfrac{\partial}{\partial \mathbf{N}}\left(f(\mathbf{N},t)N^2\right)\right) = \\
&\quad = \tfrac{\gamma\lambda k_B T}{\mu_0} \int d^3N \left(\mathbf{N}\left[\mathbf{N}\tfrac{\partial f(\mathbf{N},t)}{\partial \mathbf{N}}\right] - N^2\tfrac{\partial f(\mathbf{N},t)}{\partial \mathbf{N}} - 2N\tfrac{\partial f(\mathbf{N},t)}{\partial \mathbf{N}}\right) \\
&\quad = \tfrac{\gamma\lambda k_B T}{\mu_0} \int d^3N \left(\cancel{\tfrac{\partial f(\mathbf{N},t)}{\partial \mathbf{N}}} - \cancel{\tfrac{\partial f(\mathbf{N},t)}{\partial \mathbf{N}}} - 2N\tfrac{\partial f(\mathbf{N},t)}{\partial \mathbf{N}}\right) \\
&\quad = -\tfrac{\gamma\lambda k_B T}{\mu_0} 2 \int d^3N \left(N\tfrac{\partial f(\mathbf{N},t)}{\partial \mathbf{N}}\right)
\end{aligned}$$

As a result we obtained the same result ;

$$\frac{\gamma\lambda k_B T}{\mu_0} \int d^3N \left(\mathbf{N} \times \left[\mathbf{N} \times \frac{\partial}{\partial \mathbf{N}}\right]\right) f = -\frac{\gamma\lambda k_B T}{\mu_0} 2 \int d^3N \left(N\frac{\partial f(\mathbf{N},t)}{\partial \mathbf{N}}\right)$$

By doing integration by parts, the first derivative of the distribution function disappears;

Integration by parts: $\int udv = uv - \int vdu$

$u = \boldsymbol{N}^{\alpha}$
$\int \frac{\partial}{\partial \boldsymbol{N}}^{k} f(\boldsymbol{N},t) d^3\boldsymbol{N} = \int dv$
$v = f(\boldsymbol{N},t)$
$\frac{2\gamma\lambda k_B T}{\mu_0} \int d^3\boldsymbol{N}\boldsymbol{N}^{\alpha} \frac{\partial}{\partial \boldsymbol{N}}^{k} f(\boldsymbol{N},t) = \frac{2\gamma\lambda k_B T}{\mu_0} \left(\boldsymbol{N}^{\alpha} f(\boldsymbol{N},t)|_{-\infty}^{+\infty} - \int d^3\boldsymbol{N}\boldsymbol{N}^{\alpha} f(\boldsymbol{N},t) \right)$
$= -\frac{2\gamma\lambda k_B T}{\mu_0} \int d^3\boldsymbol{N}\boldsymbol{N}^{\alpha} f(\boldsymbol{N},t)$

By making use of Equation C.2 and under the light of this equation written above, we can revise Equation C.11;

$\frac{\gamma\lambda k_B T}{\mu_0} \int d^3N \left(\mathbf{N} \times \left[\mathbf{N} \times \frac{\partial}{\partial \mathbf{N}} \right] \right) f = -\frac{\gamma\lambda k_B T}{\mu_0} 2 \int d^3N \left(N \frac{\partial f(\mathbf{N},t)}{\partial \mathbf{N}} \right) = -\frac{2\gamma\lambda k_B T}{\mu_0} \int d^3\mathbf{N}\mathbf{N}^{\alpha} f(\mathbf{N},t)$
$-\frac{2\gamma\lambda k_B T}{\mu_0} \int d^3\mathbf{N}\mathbf{N}^{\alpha} f(\mathbf{N},t) = -\frac{2\gamma\lambda k_B T}{\mu_0} \mathbf{m}$

By recalling Equation C.4 and replacing the term that we have just analyzed above with its last form, a primitive equation of motion for the spin polarization vector can be obtained;

$$\dot{\mathbf{m}} = \frac{\partial \mathbf{m}}{\partial t} = \gamma \left[\mathbf{m} \times \mathbf{H} \right] - \Lambda_{\mathbf{N}} \mathbf{m} - \gamma\lambda \left\langle \mathbf{s} \times \left[\mathbf{s} \times \mathbf{H} \right] \right\rangle \tag{C.11}$$

where $\Lambda_{\mathbf{N}} = \frac{2\gamma\lambda k_B T}{\mu_0}$

However, when we look at the last term of the equation, this can be regarded as an equation of motion for the magnetization dynamics which is coupled to the second moments of the distribution function. The derivation of a more concrete equation depends on further analysis of this last term. Therefore, for the non-equilibrium state of magnetization, this will be studied in detail by deriving a driven equation so called LLB equation.

If the distribution function is chosen as $f(\mathbf{N}) = {\exp(\xi_{\mathbf{o}} \cdot \mathbf{N})}/{\mathrm{Z}(\xi_{\mathrm{o}})}$ where $\mathrm{Z}(\xi_{\mathrm{o}}) = 4\pi \left({\sinh(\xi_{\mathrm{o}})}/{\xi_{\mathrm{o}}}\right)$ is the partition function and $\xi_{\mathbf{o}} = \beta\mu_o \mathbf{H}_{mfa}$is reduced magnetic field. Therofore, for the non-equilibrium condition one can assume that $f(\mathbf{N}) = {(\exp(\xi \cdot \mathbf{N}))}/{\mathrm{Z}(\xi)}$ where ξ=ξ(t) non equilibrium reduced magnetic field. By recalling Equation C.2, we obtain;

$$\tilde{\mathbf{m}}_j = \langle \mathbf{s}_j \rangle = \int d^3N \mathbf{N}_j f(\mathbf{N}, t) = \int d^3N \mathbf{N}_j \left({\exp(\xi_j \cdot \mathbf{N})}/{Z(\xi)}\right)$$

As it can be seen from Equation C.11, the second moments of the distribution function requires analysis in detail. To do so, we initially try to write down a relation for the 2^{nd} order differentiation of the distribution function in terms of Langevin function $B(\xi) = \coth(\xi) - {1}/{\xi}$;

$$\begin{aligned} &\tfrac{\partial}{\partial \xi_i} Z(\xi) = \tfrac{\partial}{\partial \xi_i} \left(\int d^3N \exp(\xi_i \cdot \mathbf{N}) \right) = \int d^3N \mathbf{N}_i \exp(\xi_i \cdot \mathbf{N}) \\ &= Z(\xi) \left(\int d^3N \mathbf{N}_i f(\mathbf{N}, t) \right) = Z(\xi) \tilde{\mathbf{m}}_i \end{aligned}$$

where we used $f(\mathbf{N}, t) = \left({(\exp(\xi_j \cdot \mathbf{N}))}/{Z(\xi)}\right)$ relation. When we take the 2^{nd} derivative of partition function with respect the reduced field, we obtain an important relation before we reach the classical LLB equation of motion.

$$\begin{aligned} &\tfrac{\partial}{\partial \xi_k} (f(\mathbf{N}, t)) = \tfrac{\partial}{\partial \xi_k} \left(\left({\exp(\xi \cdot \mathbf{N})}/{Z(\xi)} \right) \right) = \tfrac{\mathbf{N}_k (\exp(\xi \cdot \mathbf{N})) Z(\xi) - \frac{\partial (Z(\xi))}{\partial \xi_k} \exp(\xi \cdot \mathbf{N})}{Z(\xi) Z(\xi)} \\ &= \tfrac{\mathbf{N}_k (\exp(\xi \cdot \mathbf{N})) - \tilde{\mathbf{m}}_i \exp(\xi \cdot \mathbf{N})}{Z(\xi)} = \tfrac{\mathbf{N}_k (\exp(\xi \cdot \mathbf{N})) - \tilde{\mathbf{m}}_k \exp(\xi \cdot \mathbf{N})}{Z(\xi)} \\ &= \mathbf{N}_k (f(\mathbf{N}, t)) - (f(\mathbf{N}, t)) \tilde{\mathbf{m}}_k \end{aligned}$$

Thus,

$$\frac{\partial}{\partial \xi_k} (f(\mathbf{N}, t)) = \mathbf{N}_k (f(\mathbf{N}, t)) - (f(\mathbf{N}, t)) \tilde{\mathbf{m}}_k \tag{C.12}$$

The following equations are exploited in the derivation of the Equation C.12 which is written above.

$$\begin{aligned}
&\triangleright\ \tfrac{\partial}{\partial \xi_i} Z(\xi) = Z\left(\xi\right) \tilde{\mathbf{m}}_i \\
&\triangleright\ \tilde{\mathbf{m}}_i = B(\xi)\tfrac{\xi_i}{\xi} \\
&\triangleright\ f\left(\mathbf{N}, t\right) = \left(\exp\left(\xi_j \cdot \mathbf{N}\right)/_{Z\left(\xi\right)}\right)
\end{aligned}$$

The first thing is to write down $\frac{\partial \tilde{\mathbf{m}}_i}{\partial \xi_i}$;

$$\begin{aligned}
&\tfrac{\partial}{\partial \xi_j}\left(B(\xi)\tfrac{\xi_i}{\xi}\right) = \tfrac{\partial B(\xi)}{\partial \xi_j}\tfrac{\xi_i}{\xi} + B(\xi)\tfrac{\partial \xi_i}{\partial \xi_j}\tfrac{1}{\xi} + B(\xi)\xi_i \tfrac{\partial}{\partial \xi_j}\left(\tfrac{1}{\xi}\right) \\
&= \tfrac{\partial B(\xi)}{\partial \xi_j}\tfrac{\xi_i}{\xi} + B(\xi)\delta_{ij}\tfrac{1}{\xi} - B(\xi)\xi_i \tfrac{1}{{\xi_j}^2} = \left(\tfrac{\partial B(\xi)}{\partial \xi_j} - \tfrac{B(\xi)}{\xi}\right)\tfrac{\xi_i \xi_j}{\xi^2} + B(\xi)\tfrac{1}{\xi}\delta_{ij}
\end{aligned}$$

$$\frac{\partial B(\xi)}{\partial \xi_j}\frac{\xi_i}{\xi} = \left(\frac{\partial B(\xi)}{\partial \xi_j} - \frac{B(\xi)}{\xi}\right)\frac{\xi_i \xi_j}{\xi^2} + \frac{B(\xi)}{\xi}\delta_{ij} \tag{C.13}$$

where $\frac{\partial \xi_i}{\partial \xi_j} = \delta_{ij}$. By using the following trivial relation: $B^2 = 1 - B'(\xi) - 2\frac{B(\xi)}{\xi}$, we can reach our goal which is to write an extended relation for the second moments of the distribution function.

$$\langle \mathbf{s}_i \mathbf{s}_j \rangle = \left(\frac{\partial}{\partial \xi_j} B(\xi)\right)\frac{\xi_i}{\xi} + \tilde{m}_i \tilde{m}_j = \frac{B(\xi)}{\xi}\left(\left(\frac{\xi}{B(\xi)} - 3\right)\frac{\xi_i \xi_j}{\xi^2} + \delta_{ij}\right) \tag{C.14}$$

By taking the advantage of both Equation C.12 and Equation C.13, the second order differentiation of the partition function can be obtained:

$$\begin{aligned}
&\tfrac{\partial}{\partial\xi_j}\left(\tfrac{\partial}{\partial\xi_i}Z(\xi)\right) = \tfrac{\partial}{\partial\xi_j}\left(Z\left(\xi\right)\tilde{m}_i\right) = Z\left(\xi\right)\tfrac{\partial}{\partial\xi_j}\left(\tilde{m}_i\right) + \tilde{m}_i\tfrac{\partial}{\partial\xi_j}\left(Z\left(\xi\right)\right) \\
&= Z\left(\xi\right)\tfrac{\partial}{\partial\xi_k}\left(\tilde{m}_i\right) + \left(\tfrac{\partial}{\partial\xi_k}Z\left(\xi\right)\right)\tilde{m}_i \\
&= Z\left(\xi\right)\tfrac{\partial}{\partial\xi_k}\left(\int d^3N N_i f\left(N,t\right)\right) + \tfrac{\partial}{\partial\xi_k}\left(\int d^3N\left(\xi\cdot N\right)\right)\tilde{m}_i \\
&= Z\left(\xi\right)\left(\int d^3N N_k \tfrac{\partial}{\partial\xi_k}\left(f\left(N,t\right)\right)\right) + \tilde{m}_i\left(\int d^3N N_k\left(\xi\cdot N\right)\right) \\
&= Z\left(\xi\right)\left(\int d^3N N_i\left(N_k\left(f\left(N,t\right)\right) - \left(f\left(N,t\right)\right)\tilde{m}_k\right)\right) + \tilde{m}_i\left(\int d^3N N_k Z\left(\xi\right) f\left(N,t\right)\right) \\
&= \tilde{m}_i\left(\int d^3N N_k f\left(N,t\right)\right) Z\left(\xi\right) - Z\left(\xi\right)\tilde{m}_k\left(\int d^3N N_i\left(f\left(N,t\right)\right)\right) \\
&+ Z\left(\xi\right)\left(\int d^3N N_i N_k\left(f\left(N,t\right)\right)\right) \\
&= Z\left(\xi\right)\left(\tilde{m}_i\tilde{m}_k - \tilde{m}_k\tilde{m}_i\right) + \tilde{m}_i\left(\int d^3N N_k f\left(N,t\right)\right) Z\left(\xi\right) \\
&= Z\left(\xi\right)\left[\tilde{m}_i,\tilde{m}_k\right] + \left(\int d^3N N_i N_k f\left(N,t\right)\right) Z\left(\xi\right)
\end{aligned}$$

We obtain the following relation where we used the commutation relation $[\tilde{m}_i, \tilde{m}_j] = 0$

$$\frac{1}{Z\left(\xi\right)}\frac{\partial}{\partial\xi_j}\left(\frac{\partial}{\partial\xi_i}Z(\xi)\right) = \left(\int d^3N \mathbf{N}_i\mathbf{N}_k f\left(\mathbf{N},t\right)\right) = \left\langle s_i s_k\right\rangle \tag{C.15}$$

At that stage, the first thing is to write down the Equation C.11 by using tensors. Thus, we get rid of the vectoral form since tensors conceal the vectoral form of the equation.

$$\begin{aligned}
\dot{m} &= \tfrac{\partial m}{\partial t} = \gamma\left[m\times H\right] - \Lambda_N m - \gamma\lambda\left\langle s\times\left[s\times H\right]\right\rangle \\
&= \gamma\varepsilon_{ijk}\left\langle s_j\right\rangle H_k - \Lambda_N\left\langle s_i\right\rangle - \tfrac{\Lambda_N}{2}\varepsilon_{ijn}\varepsilon_{lmn}\left\langle s_j s_m\right\rangle\xi_{0_n}
\end{aligned}$$

By using both a simple equation for reduced magnetic field $\xi_0 = \frac{\mu_0 H}{k_B T}$ and the relations that were derived above Equation C.12, Equation C.14, and Equation C.15,

we can do the following calculations;

$$\frac{\partial m}{\partial t} = \gamma\varepsilon_{ijk}\left\langle s_j\right\rangle H_k - \Lambda_N\left\langle s_i\right\rangle - \frac{\Lambda_N}{2}\varepsilon_{ijn}\varepsilon_{lmn}\left\{\frac{B(\xi)}{\xi}\left(\left(\frac{\xi}{B(\xi)}-3\right)\frac{\xi_j\xi_m}{\xi^2}+\delta_{jm}\right)\right\}\xi_0$$
$$= \gamma\varepsilon_{ijk}\left\langle s_j\right\rangle H_k - \Lambda_N\left\langle s_i\right\rangle - \frac{\Lambda_N}{2}\varepsilon_{ijn}\varepsilon_{lmn}\frac{B(\xi)}{\xi}\left(\frac{\xi}{B(\xi)}-3\right)\frac{\xi_j\xi_m}{\xi^2}\xi_{0_n} - \frac{\Lambda_N}{2}\varepsilon_{ijn}\varepsilon_{lmn}\frac{B(\xi)}{\xi}\delta_{jm}\xi_{0_n}$$
$$= \gamma\varepsilon_{ijk}\left\langle s_j\right\rangle H_k - \Lambda_N\left\langle s_i\right\rangle - \frac{\Lambda_N}{2}\varepsilon_{ijn}\varepsilon_{lmn}\left(1-\frac{3m}{\xi}\right)\frac{m_jm_m}{m^2}\xi_{0_n} - \frac{\Lambda_N}{2}\varepsilon_{ijn}\varepsilon_{lmn}\delta_{jm}\frac{m}{\xi}\xi_{0_n}$$

Moreover, by using the Levi Civita mathematical formalism;

$$\varepsilon_{imn}\varepsilon_{ijk}a_nb_jc_k = \left(\delta_{mj}\delta_{nk}-\delta_{mk}\delta_{nj}\right)a_nb_jc_k = a_mb_kc_k - c_ma_jb_j$$
$$-\varepsilon_{ijn}\varepsilon_{lmn}\xi_m\xi_j\xi_{0_n} = -\left(\delta_{im}\delta_{jn}-\delta_{in}\delta_{jm}\right)\xi_m\xi_j\xi_{0_i} = \xi^2\xi_{0_i} - \left(\xi_j\xi_i\right)\xi_{0_i}$$

The reduced magnetic field turns into the following form;

$$\xi_{0_i} = \frac{\left(\xi_j\xi_{0_j}\right)}{\xi^2}\xi_i - \varepsilon_{ijn}\varepsilon_{lmn}\frac{\xi_j\xi_m}{\xi^2}\xi_{0n} \tag{C.16}$$

Fortunately, we have another important relation $\frac{\xi_j}{\xi} = \frac{m_j}{m}$ leads to modify Equation C.16:

$$\xi_{0_i} = \frac{(m\xi_0)}{\xi^2}\xi_i - \varepsilon_{ijn}\varepsilon_{lmn}\frac{m_jm_m}{m^2}\xi_{0_n}$$

When we plug the relation above, we can obtain LLB equation . Yet, it is not able to describe the motion of the spin polarization vector, clearly;

$$\frac{\partial m_i}{\partial t} = \gamma\varepsilon_{ijk}m_jH_k - \Lambda_N\left(1-\frac{m\cdot\xi_0}{m\xi}\right)m_i - \gamma\lambda\left(1-\frac{m}{\xi}\right)\varepsilon_{ijn}\varepsilon_{lmn}\frac{m_mm_j}{m^2}H_n$$

In the vectoral form;

$$\frac{\partial m}{\partial t} = \gamma m\times H - \Lambda_N\left(1-\frac{m\cdot\xi_0}{m\xi}\right)m - \gamma\lambda\left(1-\frac{m}{\xi}\right)\frac{(m\times(m\times H))}{m^2} \tag{C.17}$$

Now, we do some further analysis of each term of Equation C.17. During the analysis, we will perturb the magnetization by applying an external field ($\boldsymbol{H}$). For small deviations from the equilibrium where $m \cong m_0$ and $m \cong m_0 \equiv B(\xi_0)\frac{\xi_0}{\xi_0}$, one can put LLB

equation into more compact form using $H = \frac{k_B T}{\mu_0}\xi_0$ and $m - m_0 \cong B'(\xi_0)(\xi - \xi_0)$

(i) The 1^{st} term becomes $\gamma(m \times H)$

(ii) The 2^{nd} term is $-\Lambda_N \left(1 - \frac{m\cdot\xi_0}{m\xi}\right) m\, m \cong m_0 \equiv B(\xi_0)\frac{\xi_0}{\xi_0} \Rightarrow \begin{cases} \frac{m_0}{\xi_0} = \frac{B(\xi_0)}{\xi_0} \\ \frac{m}{\xi} = \frac{B(\xi)}{\xi} \end{cases}$ which led us to get the following relation that describes the deviation from the equilibrium state.

$$m - m_0 \cong B'(\xi)(\xi - \xi_0)$$

Simultaneously, the second term is called longitudinal relaxation term of LLB equation will turn into a different form by considering the relations written above.

$$\begin{aligned} &-\Lambda_N \left(1 - \tfrac{m\cdot\xi_0}{m\xi}\right) m = -\Lambda_N \left(\tfrac{m(\xi-\xi_0)}{m\xi}\right) m = -\Lambda_N \left(\frac{m\left(\frac{m-m_0}{B'(\xi)}\right)}{m\xi}\right) m \\ &= -\tfrac{\Lambda_N}{B'(\xi_0)} \left(\tfrac{m^2 - m m_0}{m\xi}\right) m = -\tfrac{\Lambda_N}{B'(\xi_0)} \left(1 - \tfrac{m m_0}{m^2}\right) \tfrac{m^2}{\xi} \\ &= -\tfrac{\Lambda_N}{B'(\xi)} \tfrac{B(\xi)}{\xi} \left(1 - \tfrac{m m_0}{m^2}\right) m = -\Gamma_1 \left(1 - \tfrac{m m_0}{m^2}\right) m \end{aligned}$$

In this way, we obtain

$$-\Lambda_N \left(1 - \frac{m \cdot \xi_0}{m\xi}\right) m = -\Gamma_1 \left(1 - \frac{m m_0}{m^2}\right) m \tag{C.18}$$

where $\Gamma_1 = \left(\frac{\Lambda_N}{B'(\xi!)}\right)\left(\frac{B(\xi)}{\xi}\right)$ is called as the coefficient of the longitudinal relaxation term.

(iii) The 3^{rd} term is $-\gamma\lambda \left(1 - \frac{m}{\xi}\right) \frac{(m\times(m\times H))}{m^2}$

For the detailed analysis of the transverse relaxation term the two relations written below play a key role since they will describe the initial condition of the

magnetization before the perturbation made by the external magnetic field;

$$\left.\begin{array}{c} H = \frac{k_B T}{\mu_0}\xi_0 \\ m \cong m_0 \equiv B(\xi_0)\frac{\xi_0}{\xi_0} \end{array}\right\} H = \frac{k_B T}{\mu_0}\xi_0 = \frac{k_B T}{\mu_0}\frac{\xi_0}{B(\xi_0)}m_0$$

$$-\gamma\lambda\left(1-\frac{m}{\xi}\right)\frac{(m\times(m\times H))}{m^2} = -\gamma\lambda\left(1-\frac{m}{\xi}\right)\left(\frac{1}{m^2}\right)\left(m\times\left(m\times\frac{k_B T}{\mu_0}\frac{\xi_0}{B(\xi_0)}m_0\right)\right)$$

$$= -\gamma\lambda\frac{k_B T}{\mu_0}\frac{\xi_0}{B(\xi_0)}\left(1-\frac{m}{\xi}\right)\frac{(m\times(m\times m_0))}{m^2} = -\frac{\Lambda_N}{2}\left(\frac{\xi_0}{B(\xi_0)}\right)\left(1-\frac{m}{\xi}\right)\frac{(m\times(m\times m_0))}{m^2}$$

$$= -\frac{\Lambda_N}{2}\left(\left(\frac{\xi_0}{B(\xi_0)}\right)-()\right)\frac{(m\times(m\times m_0))}{m^2} = -\frac{\Lambda_N}{2}\left(\left(\frac{\xi_0}{B(\xi_0)}\right)-1\right)\frac{(m\times(m\times m_0))}{m^2}$$

Thus, the third term of LLB equation turns into the following form;

$$-\gamma\lambda\left(1-\frac{m}{\xi}\right)\frac{(m\times(m\times H))}{m^2} = -\Gamma_2\frac{(m\times(m\times m_0))}{m^2} \tag{C.19}$$

where $\Gamma_2 = \frac{\Lambda_N}{2}\left(\left(\frac{\xi_0}{B(\xi_0)}\right)-1\right)$ is coefficient of transverse relaxation term.

As a conclusion, when we plug Equation C.16 and Equation C.17 into Equation C.19, we obtain the classical LLB equation by using the quantum generalization methods.

$$\frac{\partial m}{\partial t} = \gamma\left(m\times H\right) - \Gamma_1\left(1-\frac{m m_0}{m^2}\right)m - \Gamma_2\frac{(m\times(m\times m_0))}{m^2} \tag{C.20}$$

LLB equation for ferromagnetic materials which is including the analysis of the critical behavior of the magnetization dynamics below and above Curie Temperature. Up to now, we aim at obtaining an isolated equation of motion for the spin polarization without considering any interaction between the magnetic moments (which can be referred as isolated magnetic moments). That simulates the situation in pure paramagnetism. Due to thermal agitations, we expect a random orientation of the dipoles which do not have interaction with one another, in the absence of an external field which brings about the zero net magnetic moment (paramagnetic case). But, individual moments have random orientations initially and in the presence of an external magnetic field which is able to deal with the thermal excitations. A new alignment of magnetization vector driven by the external magnetic field can be acquired [6]. More-

over, this can be characterized by the equation that we derived above.

Now, we will revise the LBB equation by considering the case where the magnetic moments are not-isolated and are instead exchange coupled to each other. Furthermore, the interaction between the moments will be assumed as isotropic and the first nearest neighbor interactions are going to be taken into account. For the sake of clarity, the system Hamiltonian will include just external magnetic field-spin (magnetic field coupling) and the exchange interaction (spin–spin or Heisenberg exchange interaction):

$$H = -\mu_0 \sum_{i,i} H_i s_i - \frac{1}{2} \sum_{i,j} J_{ij} \left(\eta_x s_{xi} s_{xj} + \eta_y s_{yi} s_{yj} + s_{zi} s_{zj} \right) \tag{C.21}$$

η_y and η_x are the anisotropy factors which are η_x,$\eta_y \leq 1$

It is impossible to treat the spin-spin interactions fully without some approximations. Garanin took the advantage of Mean Field Approximation (MFA) [6] in the description of effective field corresponding to each lattice site. Semi-classical spin dynamics leads us to get the interaction field of the system by presenting the following equation for the single spin Hamiltonian:

$$\begin{gathered} \tfrac{ds}{dt} = \dot{s} = \gamma(s \times H(s)) \\ -g\mu_B H(s) = \tfrac{\delta H}{\delta s} \Rightarrow H(s) = -\tfrac{1}{g\mu_B} \left(\tfrac{\delta H}{\delta s} \right) \\ \Rightarrow \tilde{H}(s) = -\left(\tfrac{\delta H}{\delta s} \right) \end{gathered}$$

The last equation is in CGS unit and $g\mu_B$ is inserted inside of the effective field. In SI unit system, we need to divide it to the permeability of free space μ_0 which will

have the following form;

$$\begin{aligned} {H_i}^{MFA} &= -\tfrac{1}{\mu_0}\tfrac{\partial H}{\partial s} \\ &= -\tfrac{1}{\mu_0}\tfrac{\partial}{\partial s_i}\left(-\mu_0 \textstyle\sum_{i,i} H_i s_i - \frac{1}{2}\sum_{i,i} J_{ij}\left(\eta_x s_{xi} s_{xj} + \eta_y s_{yi} s_{yj} + s_{zi} s_{zj}\right)\right) \\ &= H_i + \tfrac{1}{\mu_0}\textstyle\sum_j J_{ij}\left(\eta_x s_{xj} + \eta_y s_{yi} + s_{zi}\right) \end{aligned}$$

The MFA field can be written in a more compact form;

$${H_i}^{MFA} = {H_i}^{E} + H_i = \frac{J_0}{\mu_0} m_i + H_i \tag{C.22}$$

One of the most prominent features of the ferromagnetic materials is the case of very strong and homogenous exchange field which can be said for the temperature below Curie point: $\left|{H_i}^{E}\right| \gg |H_i|$ Above of Cruie temperature (T_c) which is the phase transition temperature for the ferromagnetic material so the spontaneous magnetization does not exist because ferromagnetic material behaves like a paramagnet.

$$H^{MFA} = H^E + H = H^E\left(1 + \frac{H \cdot H^E}{(H^E)^2}\right)$$

By using the special form of Taylor expansion called Maclaurin expansion one can get a special relation for $\frac{1}{\mathrm{H}^{MFA}}$ which is the modulus of MFA field;
If $x \ll 1$
$(1/1 - x\,) = (1+x)^{-1} = 1 + x + x^2 + x^3 + x^{4.} \ldots$
$x \to -x$
$(1/1 + x\,) = (1+x)^{-1} = 1 - x + x^2 - x^3 + x^{4.} \ldots$

$$\begin{aligned} \tfrac{1}{H^{MFA}} &\cong \tfrac{1}{H^E}\left(1 - \tfrac{H\cdot H^E}{(H^E)^2} + \left(\tfrac{H\cdot H^E}{(H^E)^2}\right)^2 - \left(\tfrac{H\cdot H^E}{(H^E)^2}\right)^3 + \ldots\right) \\ &\cong \tfrac{1}{H^E}\left(1 - \tfrac{H\cdot H^E}{(H^E)^2}\right) \end{aligned} \tag{C.23}$$

After that the relations below are written for general expressions of Equation C.24 exchange interaction field, Equation C.25 magnetization vector at the non-equilibrium case and Equation C.26 the relation between the reduced magnetic field and the MFA field, respectively.

$$H^E = \frac{J_0}{\mu_0} m \tag{C.24}$$

$$m = B\left(\xi_0\right) \frac{\xi_0}{\xi_0} \tag{C.25}$$

$$\xi_0 = \beta \mu_0 H^{MFA} \tag{C.26}$$

Thus, we can obtain the following relation between the Langevin function and the magnetization at equilibrium case;

$$m_0 = B\left(\beta \mu_0 H^{MFA}\right) \left(\frac{H^{MFA}}{H^{MFA}}\right) = B\left(\beta \mu_0 H^{MFA}\right) \left(\frac{H^{MFA}}{H^{MFA}}\right)$$
$$B\left(\beta \mu_0 H^{MFA}\right) = \frac{m_0}{\left(\frac{H^{MFA}}{H^{MFA}}\right)}$$

By taking advantage of Mean Field Approximation, the Langevin function is expanded up to first order and it has the following form;

$$B\left(\xi_0\right) \cong B\left(\beta \mu_0 H^E\right) + B'\left(\beta \mu_0 H^E\right) \frac{H \cdot H^E}{\left(H^E\right)^2} \tag{C.27}$$

Meanwhile, the main goal is to obtain a relation for the equilibrium magnetization and its small deviation case from the equilibrium due to the effect of applied magnetic

field.

$$\frac{m_0}{\left(\frac{H^{MFA}}{H^{MFA}}\right)} \cong B\left(\beta\mu_0 H^E\right) + B'\left(\beta\mu_0 H^E\right)\left(\frac{H\cdot H^E}{\left(H^E\right)^2}\right) \tag{C.28}$$

Therefore, we obtain a compact equation;

$$m_0 \cong \left(B\left(\beta\mu_0 H^E\right) + B'\left(\beta\mu_0 H^E\right)\frac{H\cdot H^E}{\left(H^E\right)^2}\right)\left(\frac{H^{MFA}}{H^{MFA}}\right) \tag{C.29}$$

Yet, Equation C.29 entails to be extended by using the relation of exchange field and the MFA field together with some mathematical relations about the conversion of dot product into the vector product (Equation C.8 and Equation C.10). By utilizing these equations, the last form of m_0 is obtained;

$$m_0 \approx \frac{B}{m}m + B'\beta\mu_0\frac{(m\cdot H)\,m}{m^2} - \frac{B\mu_0}{mJ_0}\frac{(H\times m)\times m}{m^2} \tag{C.30}$$

Now, we can continue with the new stage which will lead us to reach LLB equation of motion for ferromagnets that is capable of showing the behavior of the magnetization vector for the finite temperature regime.

In that stage, we analyze the coefficients (Γ_1 and Γ_2) of the terms of LLB equation shown in Equation C.20. In these analyses the vital role is to plug the relation of m_0 (Equation C.30) into Equation C.20.

(i) Transverse relaxation term: $-\Gamma_2\frac{(m\times(m\times m_0))}{m^2}$ where $\Gamma_2 = \frac{\Lambda_N}{2}\left(\left(\frac{\xi_0}{B(\xi_0)}\right) - 1\right)$

By using the following three principal relations that are studied above;

- $\Lambda_N = \frac{2\gamma\lambda k_B T}{\mu_0}$
- $m = B\left(\xi_0\right)\frac{\xi_0}{\xi_0}$
- $\xi_0 = \beta\mu_0 H^{MFA}$

The coefficient of the transverse relaxation term Γ_2 is obtained in the following form;

$$\begin{aligned}\Gamma_2 &= \tfrac{\Lambda_N}{2}\left(\left(\tfrac{\xi_0}{B(\xi_0)}\right)-1\right)\\ &= \tfrac{\frac{\gamma\lambda k_B T}{\mu_0}}{}\left(\left(\tfrac{\xi_0}{B(\xi_0)}\right)-1\right)\\ &= \tfrac{\gamma\lambda k_B T}{\mu_0}\left(\left(\tfrac{\xi_0}{B(\xi_0)}\right)-1\right)\\ &= \tfrac{\gamma\lambda k_B T}{\mu_0}\left(1-\left(\tfrac{B(\xi_0)}{\xi_0}\right)\right)\tfrac{\beta\mu_0 H^{MFA}}{B(\xi_0)}\end{aligned}$$

Having strong exchange interaction causes to consider the applied magnetic field-spin interaction as the perturbation so the MFA field turns into the following form;

$$H^E \gg H \Leftrightarrow H^{MFA} = H^E + H = \frac{J_0}{\mu_0}m + H \approx \frac{J_0}{\mu_0}m \wedge \beta = 1/k_B T$$

$$\begin{aligned}\Gamma_2 &= \tfrac{\gamma\lambda \cancel{k_B T}}{\mu_0}\left(1-\left(\tfrac{B(\xi_0)}{\xi_0}\right)\right)\tfrac{1/\cancel{k_B T}\;\cancel{\mu_0}\frac{J_0}{\cancel{\mu_0}}m}{B(\xi_0)}\\ &= \tfrac{\gamma\lambda}{\mu_0}\left(1-\left(\tfrac{B(\xi_0)}{\xi_0}\right)\right)\tfrac{J_0 m}{B(\xi_0)} = \gamma\alpha_\perp \tfrac{m}{B(\xi_0)}\tfrac{J_0}{\mu_0}\end{aligned}$$

Thus,

$$\Gamma_2 = \gamma\alpha_\perp \frac{m}{B(\xi_0)}\frac{J_0}{\mu_0} \tag{C.31}$$

where $\alpha_\perp = \lambda\left(1-\left(\frac{B(\xi_0)}{\xi_0}\right)\right)$ The transverse relaxation (or damping) term (Equation C.31) of LLB equation turns out to be in a different form when the Equation C.32 which is written below is used.

$$\left.\begin{aligned} H &= \left(\tfrac{k_B T}{\mu_0}\right)\xi_0 \\ m &\cong m_0 \equiv B(\xi_0)\tfrac{\xi_0}{\xi_0}\end{aligned}\right\} H = \left(\frac{k_B T}{\mu_0}\right)\left(\frac{\xi_0}{B(\xi_0)}\right)m_0 \tag{C.32}$$

By means of the Equation C.32, we can obtain the following equation:

$$
\begin{aligned}
&-\Gamma_2 \tfrac{(m\times(m\times m_0))}{m^2} = -\tfrac{\Lambda_N}{2}\left(\left(\tfrac{\xi_0}{B(\xi_0)}\right)-1\right)\tfrac{(m\times(m\times m_0))}{m^2} \\
&= -\gamma\alpha_\perp \tfrac{m}{B(\xi_0)}\tfrac{J_0}{\mu_0}\tfrac{(m\times(m\times m_0))}{m^2} \\
&= -\gamma\alpha_\perp \tfrac{m}{B(\xi_0)}\tfrac{J_0}{\mu_0}\tfrac{\left(m\times\left(m\times\left(\frac{\mu_0}{k_BT}\frac{B(\xi_0)}{\xi_0}\right)H\right)\right)}{m^2} \\
&= -\gamma\alpha_\perp \tfrac{m}{\cancel{B(\xi_0)}}\tfrac{J_0}{\cancel{\mu_0}}\left(\tfrac{\cancel{B(\xi_0)}}{k_BT}\tfrac{\cancel{\mu_0}}{\xi_0}\right)\tfrac{(m\times(m\times H))}{m^2}
\end{aligned}
$$

Then, by using the relations that are written below, give the last shape to the transverse relaxation term.

$$
\left.\begin{aligned}
\xi_0 &= \beta\mu_0 H^{MFA} \\
H^{MFA} &= \tfrac{J_0}{\mu_0} m
\end{aligned}\right\} \xi_0 = \beta J_0 m
$$

$$
\begin{aligned}
&-\Gamma_2 \tfrac{(m\times(m\times m_0))}{m^2} = -\gamma\alpha_\perp\left(\tfrac{m}{k_BT}\tfrac{J_0}{\xi_0}\right)\tfrac{(m\times(m\times H))}{m^2} \\
&= -\gamma\alpha_\perp\left(\tfrac{\cancel{m}}{\cancel{k_BT}}\tfrac{\cancel{J_0}}{\cancel{\beta J_0 m}}\right)\tfrac{(m\times(m\times H))}{m^2} \\
&= -\gamma\alpha_\perp \tfrac{(m\times(m\times H))}{m^2}
\end{aligned}
$$

As a result, the transverse relaxation term is obtained;

$$
-\Gamma_2 \frac{(m\times(m\times m_0))}{m^2} = -\gamma\alpha_\perp \frac{(m\times(m\times H))}{m^2} \tag{C.33}
$$

(ii) The longitudinal relaxation term: $-\Gamma_1\left(1-\frac{mm_0}{m^2}\right)m$ where $\Gamma_1 = \frac{\Lambda_N}{B'(\xi)}\frac{B(\xi)}{\xi}$
The magnetization of the whole system at the equilibrium case Equation C.30 was

$$
m_0 \cong \left(B\left(\beta\mu_0 H^E\right) + B'\left(\beta\mu_0 H^E\right)\frac{H\cdot H^E}{\left(H^E\right)^2}\right)\left(\frac{H^{MFA}}{H^{MFA}}\right)
$$

First of all, this crucial relation is plugged into the longitudinal relaxation term

of LLB equation;

$$
\begin{aligned}
&-\Gamma_1\left(1-\tfrac{mm_0}{m^2}\right)m = -\Gamma_1\left(1-\frac{m\left\{\frac{B}{m}m+B'\beta\mu_0\frac{(m\cdot H)m}{m^2}-\frac{B\mu_0}{mJ_0}\frac{(H\times m)\times m}{m^2}\right\}}{m^2}\right)m \\
&= -\Gamma_1\left(1-\frac{\left\{\frac{B}{m}m^2+B'\beta\mu_0\cancel{m^2}\frac{(m\cdot H)}{\cancel{m^2}}-\frac{B\mu_0}{mJ_0}m\frac{(H\times m)\times m}{m^2}\right\}}{m^2}\right)m \\
&= -\Gamma_1\left(1-\frac{\frac{B}{m}\cancel{m^2}}{\cancel{m^2}}+B'\beta\mu_0\frac{(m\cdot H)}{m^2}\right)m \\
&= -\Gamma_1 B'\beta\mu_0\left(\frac{1-B\diagup m}{B'\beta\mu_0}+\frac{(m\cdot H)}{m^2}\right)m
\end{aligned}
$$

Thus,

$$
-\Gamma_1\left(1-\frac{mm_0}{m^2}\right)m = -\gamma\alpha_{//}\left(\frac{1-B\diagup m}{B'\beta\mu_0}+\frac{(m\cdot H)}{m^2}\right)m \tag{C.34}
$$

where $\alpha_{//}=\frac{\Gamma_1}{\gamma}B'\beta\mu_0=\frac{\Lambda_N}{\cancel{B'(\xi)}}\frac{B(\xi)}{\gamma\xi}\cancel{B'(\xi)}\beta\mu_0=\frac{2\cancel{\gamma}\lambda\cancel{k_B}\cancel{T}}{\cancel{\mu_0}}\frac{B(\xi)}{\cancel{\gamma}\xi}\cancel{\mu_0}\beta=2\lambda\frac{B(\xi)}{\xi}$
is called the longitudinal damping parameter.

To gain more concrete relation for the longitudinal damping parameter we again resort to Mean Field Approximation which gives us the following relation;

$$
J_0 = 3k_BT_C \tag{C.35}
$$

By using Equation C.35 and the other three relations (which are written below), we can obtain a crucial relation for $\frac{B(\xi_0)}{\xi_0}$;

$$
\left.\begin{aligned}
m &= B\left(\xi_0\right)\tfrac{\xi_0}{\xi_0} \\
\xi_0 &= \beta\mu_0 H^{MFA} \\
H^{MFA} &= \tfrac{J_0}{\mu_0}m
\end{aligned}\right\}
\frac{B\left(\xi_0\right)}{\xi_0}=\frac{m}{\xi_0}=\frac{m}{\beta\mu_0 H^{MFA}}=\frac{\cancel{m}}{\beta\cancel{\mu_0}\frac{J_0}{\cancel{\mu_0}}\cancel{m}}=\frac{\cancel{k_B}T}{3\cancel{k_B}T_C}=\frac{T}{3T_C}
$$

As a result, the longitudinal damping parameter has the following form;

$$
\alpha_{//}=2\lambda\frac{B(\xi)}{\xi}=\lambda\frac{2T}{3T_C} \tag{C.36}
$$

It is important to note that up to now we were interested in the temperature below Curie point. Yet, what if we exceed the phase transition point? $\left(1-\frac{B}{m}\right)$ is a small quantity proportional to the deviation from the equilibrium. Thus, B is expanded around around the equilibrium magnetization m_e up to the first order in $\delta m = m - m_e$

$$B(\xi) = B(\xi_e) + \beta J_0 B'(\xi)\delta m \tag{C.37}$$

Therefore,

$$\begin{aligned} &1-\tfrac{B(\xi)}{m} = 1-\tfrac{B(\xi_e)+\beta J_0 B'(\xi)\delta m}{m} \\ &= 1-\tfrac{B(\xi)}{m} - \beta J_0 B'(\xi_e)\tfrac{\delta m}{m} = \tfrac{\delta m}{m}\left(1-\beta J_0 B'(\xi_e)\right) \end{aligned}$$

Accordingly, we can expand $\delta m = m - m_e$ around ${m_e}^2$ up to first order;

$$\frac{\delta m}{m} \approx \frac{1}{2}\left(\frac{m^2 - {m_e}^2}{{m_e}^2}\right) \tag{C.38}$$

In view of these two important approximations Equation C.37 and Equation C.38, we analyze the following term;

$$\frac{1-\frac{B(\xi)}{m}}{\beta\mu_0 B'(\xi_e)} \cong \left(\frac{1-\beta J_0 B'(\xi_e)}{\beta\mu_0 B'(\xi_e)}\right)\frac{1}{2}\left(\frac{m^2-{m_e}^2}{{m_e}^2}\right) = \frac{1}{2\chi_{//}}\left(\frac{m^2-{m_e}^2}{{m_e}^2}\right) \tag{C.39}$$

where $\chi_{//} = \left(\frac{1-\beta J_0 B'(\xi_e)}{\beta\mu_0 B'(\xi_e)}\right)$ is is the longitudinal susceptibility. Therefore, we can rewrite the longitudinal relaxation term by using these new relations;

$$-\gamma\alpha_{//}\left(\frac{1-B/m}{B'\beta\mu_0}+\frac{(m\cdot H)}{m^2}\right)m = -\gamma\alpha_{//}\left(\frac{m\cdot\left(\frac{1}{2\chi_{//}}\left(\frac{m^2-{m_e}^2}{{m_e}^2}\right)+H\right)}{m^2}\right)m \tag{C.40}$$

In a critical region where the phase transition happens, the relations requires some modifications to reflect the reality of the case above the Curie point so that by taking the advantage of the Taylor expansion, the Langevin function can be expanded

but the main contribution comes from the first two terms thus,

$$B(\xi) \cong \frac{1}{3}\xi - \frac{1}{45}\xi^3 + \frac{2}{295}\xi^5 - \frac{1}{4725}\xi^7 \cdots \approx \frac{1}{3}\xi\left(1 - \frac{1}{15}\xi^2\right) \tag{C.41}$$

In addition to this by resorting to Mean Field Approximation, we obtain

$$\left.\begin{array}{r} \xi^2 \cong 15\varepsilon \\ \\ \varepsilon = 1 - \frac{T}{T_c} \end{array}\right\} \begin{array}{l} \frac{B(\xi)}{\xi} = \frac{1}{3}\left(1 - \frac{1}{15}\xi^2\right) = \frac{1}{3}\left(1 - \frac{\cancel{1}}{\cancel{15}}\cancel{15}\quad\varepsilon\right) \\ \qquad = \frac{1}{3}\left(\cancel{1} - \cancel{1} + \frac{T}{T_c}\right) = \frac{T}{3T_c} \end{array} \tag{C.42}$$

As a result, both longitudinal and transverse damping parameters have the same relation above T_c

$$\alpha_{//} = \alpha_{\perp} = 2\lambda\frac{T}{3T_c} \tag{C.43}$$

Moreover, the longitudinal susceptibility and the field-like-term which is responsible for the fluctuations in the magnetization length are also revised. ${m_e}^2 \cong \frac{5}{3}\varepsilon$ is again a modification of MFA to the equilibrium magnetization. Thus,

$$\frac{1 - B/m}{B'\beta\mu_0} \cong \left(\frac{1 - \beta J_0 B'(\xi_e)}{\beta\mu_0 B'(\xi_e)}\right)\frac{1}{2}\left(\frac{m^2 - {m_e}^2}{{m_e}^2}\right) \cong \frac{J_0}{\mu_0}\left(\frac{3}{5}m^2 - \varepsilon\right) = \frac{J_0}{\mu_0}\left(\frac{3}{5}m^2 - 1 + \frac{T}{T_c}\right)$$

To sum up, LLG equation is not able to describe high temperature effects on the magnetization dynamics. Whereas, the LLB equation is a more generalized form of the conventional LLG equation of motion. In this appendix, we derive LLB equation of motion for ferromagnetic materials by using some results taken from the Mean Field Approximation. We should not forget the fact that LLB equation is a perturbative approach to the Fokker Planck Equation and it is valid at non-equilibrium state of magnetization dynamics. At the equilibrium case this equation is coupled to Curie Weiss Equation to continue to give sufficiently accurate and physical results.

By using the Equation C.33, Equation C.34, Equation C.36, Equation C.40, and Equation C.43 we can conclude this long and complex derivation with an equation which is able drive the magnetization at finite temperature even above the Curie temperature.

It is important to note that the whole derivation has been carried out when the effective mean field is including both external magnetic field (Zeeman field) and exchange field (which is extremely strong for ferromagnetic materials). Moreover, the external applied field was considered as a perturbation to the exchange field.

However, in general when the field is simulating the real field acting on the magnetization vector, it includes many field components in addition to the applied and exchange field. Therefore, this new field can be addressed as effective field $\boldsymbol{H}_{eff}$ as written below.

$$H_{eff} = H_{appl} + H_{an} + \begin{cases} \frac{1}{2\chi_{//}} \left(1 - \frac{m^2}{m_e^2}\right) m & T \leq T_c \\ \\ \frac{1}{2\chi_{//}} \left[\frac{3}{5} \left(\frac{T_c}{T_c - T}\right) m^2 - 1\right] m & T \geq T_c \end{cases} \tag{C.44}$$

where $\tilde{\gamma} = \frac{\gamma}{1+{\alpha_G}^2}$ and $\boldsymbol{H}_{appl}$ applied magnetic field and $\boldsymbol{H}_{an}$ anisotropy field including both in plane and out of plane anisotropy. The temperature dependence of the transverse and longitudinal damping parameters are given by:

$$\alpha_{//} = \alpha_G \left(\frac{2T}{3T_c}\right); \alpha_{\perp} = \begin{cases} \alpha_G \left(1 - \frac{T}{3T_c}\right) & T < T_c \\ \\ \alpha_G \left(\frac{2T}{3T_c}\right) & T \geq T_c \end{cases} \tag{C.45}$$

LLB equation is obtained and it is written in the following form;

$$\frac{\partial m}{\partial t} = -\tilde{\gamma} \left[m \times H_{eff}\right] + \frac{\tilde{\gamma}\alpha_{//}}{|m|^2} \left[\left[m \cdot H_{eff}\right] m\right] - \frac{\tilde{\gamma}\alpha_{\perp}}{|m|^2} \left[m \times \left[m \times H_{eff}\right]\right] \tag{C.46}$$

APPENDIX D: LLB BASED MACROSPIN MODEL USING COMSOL MULTIPHYSICS

The first thing to model the magnetization dynamics in COMSOL Multiphysics program is the detailed mathematical analysis of the LLB equation of motion.
Magnetization vector has three spatial components:
$m = (m_x,m_y,m_z)$ and it can be pointed out like

$$m = m_x\widehat{i} + m_y\widehat{j} + m_z\widehat{k} \tag{D.1}$$

The square of spin polarization vector is

$$m^2 = {m_x}^2 + {m_y}^2 + {m_z}^2 and m^2 \leq 1$$

Like the spatial components of the spin polarization vector, the effective terms of the spatial components should be written for this purpose;

$$H_{eff} = {H_x}^{eff}\hat{i} + {H_y}^{eff}\hat{j} + {H_z}^{eff}\hat{k} = H_{app}+H_{an}+H_L+H_{long} \tag{D.2}$$

After, we determine the terms of the effective field above, we can also write the spatial components of each term of the effective field, as follows;
The applied field term "H_{app}":

$$H_{app} = H_x\hat{i} + H_y\hat{j} + H_z\hat{k}$$

The longitudinal damping field term "H_{long}":

$$H_{long} = \begin{cases} \left(\frac{1}{2\chi_{\parallel}}\right)\left(1-\frac{m^2}{{m_e}^2}\right)m & T_C > T \\ -\left(\frac{1}{\chi_{\parallel}}\right)\left(1+\frac{3T_c}{5(T-T_c)}m^2\right)m & T_C \leq T \end{cases} = {H_x}^{long} + {H_y}^{long} + {H_z}^{long}$$

$$= \begin{cases} \left(\frac{1}{2\chi_{\parallel}}\right)\left(1-\frac{m^2}{{m_e}^2}\right)\left(m_x\widehat{i}+m_y\widehat{j}+m_z\widehat{k}\right) & T_C > T \\ -\left(\frac{1}{\chi_{\parallel}}\right)\left(1+\frac{3T_c}{5(T-T_c)}m^2\right)\left(m_x\widehat{i}+m_y\widehat{j}+m_z\widehat{k}\right) & T_C \leq T \end{cases} \tag{D.3}$$

The anisotropy field term "H_{app}":

$$H_{an} = -\left(\frac{1}{\chi_{\perp}}\right)(m_x\hat{e}_x + m_y\hat{e}_y + m_z\hat{e}_z) = {H_x}^{an} + {H_y}^{an} + {H_z}^{an} \tag{D.4}$$

The Langevin field term $H_L = M_s h_{th}$;

$$|h_{th}| = \frac{1}{\sqrt{2\pi}}\left(\frac{e^{-\left(\frac{t^2}{2}\right)}}{M_s}\right)\sqrt{2\left(\frac{\alpha K_B T_s}{\mu_0\gamma_0\Delta V M_s \Delta T}\right)} \tag{D.5}$$

By the way, the stochastic Langevin field is dimensionless. It affects the motion of the magnetization vector, randomly and thermally. Like the other terms of effective field, Langevin field has three spatial but uncorrelated components.

We turn all of them into dimensionless form by normalizing them to saturation magnetization. The new field can be called as reduced field and can be written as follows;

$$h_{eff} = \frac{H_{eff}}{M_s}$$

In this way, we make the effective field as dimensionless. As we write effective field in the reduced effective field form, we are able to sum the Langevin field with our effective field because Langevin field is already in the dimensionless form.

$$h_{eff} = \frac{H_{eff}}{M_s} + h_{th} \tag{D.6}$$

Therefore, the following equation which is the last form of LLB equation where all variables are dimensionless when the spin polarization vector (m) is used as our dependent variable.

$$\frac{dm}{dt} = -\gamma \left(m \times H_{eff}\right) + \gamma\alpha_{\parallel} \left(\frac{\left(m \cdot H_{eff}\right) m}{m^2}\right) - \alpha_{\perp}\gamma \left(\frac{m \times \left(H_{eff} \times m\right)}{m^2}\right) \tag{D.7}$$

As a result, now we know that LLB equation of motion has 3 components except the spin torque term that is only taken into account when the current is applied to it. Therefore; the expanded form of these terms of LLB equation can be easily entered into the simulation program. Here, the effective magnetic field unit also exists and equals to "A/m". Yet "$\overrightarrow{m}$" is the spin polarization vector is dimensionless and gyromagnetic ratio was taken from our above simulation results as "C/kg" but we will anymore take the unit of it as $\left(\frac{m}{A \cdot s}\right)$ and then we will solve below PDE by taking these units into consideration. By the way, the unit of the field should still be 'A/m" because when we solve the unit inconsistency between the terms of the effective field we should also break down the unit consistency among the components of LLB equation by multiplying the new form of effective field with the saturation magnetization again. Then, here we make the expansion of the terms of LLB equation:

The first term is the precessional torque term:

$$
\begin{aligned}
(m \times H_{eff}) &= \begin{pmatrix} \widehat{i} & \widehat{j} & \widehat{k} \\ m_x & m_y & m_z \\ {H_x}^{eff} & {H_y}^{eff} & {H_z}^{eff} \end{pmatrix} \\
&= \widehat{i}\,(m_y {H_z}^{eff} - m_z {H_y}^{eff}) \\
&+ \widehat{j}\,(m_z {H_x}^{eff} - m_x {H_z}^{eff}) \\
&+ \widehat{k}\,(m_x {H_y}^{eff} - m_y {H_x}^{eff})
\end{aligned}
$$

The second term is to consider the longitudinal relaxation of the macrospin:

$$
\begin{aligned}
&(m \cdot H_{eff})\, m = (m_x {H_x}^{eff} + m_y {H_y}^{eff} + m_z {H_z}^{eff}) \left(m_x \widehat{i} + m_y \widehat{j} + m_z \widehat{k} \right) \\
&= m_x\,(m_x {H_x}^{eff} + m_y {H_y}^{eff} + m_z {H_z}^{eff})\,\widehat{i} \\
&+ m_y\,(m_x {H_x}^{eff} + m_y {H_y}^{eff} + m_z {H_z}^{eff})\,\widehat{j} \\
&+ m_z\,(m_x {H_x}^{eff} + m_y {H_y}^{eff} + m_z {H_z}^{eff})\,\widehat{k}
\end{aligned}
$$

The third one is the transverse damping torque term:

$$
\begin{aligned}
m \times (H_{eff} \times m) &= \begin{pmatrix} \widehat{i} & \widehat{j} & \widehat{k} \\ m_x & m_y & m_z \\ (m_y {H_z}^{eff} - m_z {H_y}^{eff}) & (m_z {H_x}^{eff} - m_x {H_z}^{eff}) & (m_x {H_y}^{eff} - m_y {H_x}^{eff}) \end{pmatrix} \\
&= (m_y\,(m_x {H_y}^{eff} - m_y {H_x}^{eff}) - m_z\,(m_z {H_x}^{eff} - m_x {H_z}^{eff}))\,\widehat{i} \\
&+ (m_z\,(m_y {H_z}^{eff} - m_z {H_y}^{eff}) - m_x\,(m_x {H_y}^{eff} - m_y {H_x}^{eff}))\,\widehat{j} \\
&+ (m_x\,(m_z {H_x}^{eff} - m_x {H_z}^{eff}) - m_y\,(m_y {H_z}^{eff} - m_z {H_y}^{eff}))\,\widehat{k}
\end{aligned}
$$

Then, if we again plug these expanded forms of the torque terms in LLB equation, we get a clear and comprehensible form of this equation.

We can write the first derivative of spin polarization vector with respect to the time as;

$$
\frac{dm}{dt} = \frac{\partial m_x}{\partial t}\widehat{i} + \frac{\partial m_y}{\partial t}\widehat{j} + \frac{\partial m_z}{\partial t}\widehat{k} = \frac{\partial m_x}{\partial t} + \frac{\partial m_y}{\partial t} + \frac{\partial m_z}{\partial t}
$$

Thus, we separated the spin polarization vector into its three spatial components $\boldsymbol{m}\left(m_x, m_y, m_z\right)$ and in this way we get three partial differential equations:

$$\frac{\partial m_x}{\partial t} = -\gamma\left(m_y {H_z}^{eff} - m_z {H_y}^{eff}\right) + \left(\frac{\gamma\alpha_{//}}{m^2}\right)\left[m_x\left(m_x {H_x}^{eff} + m_y {H_y}^{eff} + m_z {H_z}^{eff}\right)\right]$$
$$-\left(\frac{\gamma\alpha_{\perp}}{m^2}\right)\left[\left(m_y\left(m_x {H_y}^{eff} - m_y {H_x}^{eff}\right) - m_z\left(m_z {H_x}^{eff} - m_x {H_z}^{eff}\right)\right)\right]$$

$$\frac{\partial m_y}{\partial t} = -\gamma\left(m_z {H_x}^{eff} - m_x {H_z}^{eff}\right) + \left(\frac{\gamma\alpha_{//}}{m^2}\right)\left[m_y\left(m_x {H_x}^{eff} + m_y {H_y}^{eff} + m_z {H_z}^{eff}\right)\right]$$
$$-\left(\frac{\gamma\alpha_{\perp}}{m^2}\right)\left[\left(m_z\left(m_y {H_z}^{eff} - m_z {H_y}^{eff}\right) - m_x\left(m_x {H_y}^{eff} - m_y {H_x}^{eff}\right)\right)\right]$$

$$\frac{\partial m_z}{\partial t} = -\gamma\left(m_x {H_y}^{eff} - m_y {H_x}^{eff}\right) + \left(\frac{\gamma\alpha_{//}}{m^2}\right)\left[m_z\left(m_x {H_x}^{eff} + m_y {H_y}^{eff} + m_z {H_z}^{eff}\right)\right]$$
$$-\left(\frac{\gamma\alpha_{\perp}}{m^2}\right)\left[\left(m_x\left(m_z {H_x}^{eff} - m_x {H_z}^{eff}\right) - m_y\left(m_y {H_z}^{eff} - m_z {H_y}^{eff}\right)\right)\right]$$

We can see that our LLB equation is an ordinary coefficient form of differential equation and now we ready to enter this equation into the COMSOL Multiphysics. However, we need to have an ordinary coefficient form of differential equation that is recognized by COMSOL.

Actually, COMSOL Multiphysics separates all types of differential equations into the different forms. It also has boundary conditions if someone wants to add a condition as the COMSOL solves the partial differential equation.

As we said before COMSOL can solve given partial differential equations. Here, as we mentioned before that LLB equation is in the Coefficient PDE form, so if look at the default equation for the Coefficient Form PDE interface in COMSOL Multiphysics;

$$e_a\left(\frac{\partial^2 u}{\partial t^2}\right) + d_a\left(\frac{\partial u}{\partial t}\right) + \nabla\cdot\left(-c\left(\nabla u\right) - \alpha u + \gamma\right) + \beta\left(\nabla u\right) + au = f \qquad \text{(D.8)}$$

As we can see that the dependent variable "u" and independent variable is "t" for this default PDE. The other all terms are the coefficients of the PDE. The names of these coefficients are; Therefore, at first we should determine that which term will be

Table D.1. The symbols and the their corresponding meanings in the default ordinary differential equation which is shown in the LLB equation.

Symbol	**Coefficient Name**
e_a	The mass coefficient
d_a	A damping coefficient or a mass coefficient
c	The diffusion coefficient
α	The conservative flux convection coefficient
γ	The conservative flux source term
β	The convection coefficient
a	The absorption coefficient
f	The source term

the dependent variable and which will be independent variable in our modeling. Then, the whole equation must be rearranged according to this kind of above arrangement of default PDE in the COMSOL. Besides, if we need we can also add constraint(s) to the modeling by using the subdomain setting, subdomain expressions, boundary settings and also the boundary expressions pages of COMSOL Multiphysics which are opened for this purpose of all PDE types.

If we want to make a simulation that relies on an original PDE (which looks like only from the framework of the PDEs) for our case we should at first arrange our PDE to determine clearly the coefficients of the default form Coefficient Partial Differential Equation in the COMSOL. In other words to enter our PDE in the COMSOL one of the first things that should be done is to arrange the PDE according to the explanations about the default form of this PDE s in the COMSOL. Below equations are the last

cases of the LLB that are ready to be entered to the COMSOL.

$$-\frac{\partial m_x}{\partial t} + m_x\left[\left(\frac{\gamma\alpha_{\parallel}}{m^2}\right)\left(m_x {H_x}^{eff} + m_y {H_y}^{eff} + m_z {H_z}^{eff}\right) - \left(\frac{\gamma\alpha_{\perp}}{m^2}\right)\left(m_y {H_y}^{eff} + m_z {H_z}^{eff}\right)\right]$$
$$= -\left[-\gamma\left(m_y {H_z}^{eff} - m_z {H_y}^{eff}\right) + \left(\frac{\gamma\alpha_{\perp}}{m^2}\right)\left({m_y}^2 {H_x}^{eff} + {m_z}^2 {H_x}^{eff}\right)\right]$$

$$-\frac{\partial m_y}{\partial t} + m_y\left[\left(\frac{\gamma\alpha_{\parallel}}{m^2}\right)\left(m_x {H_x}^{eff} + m_y {H_y}^{eff} + m_z {H_z}^{eff}\right) - \left(\frac{\gamma\alpha_{\perp}}{m^2}\right)\left(m_z {H_z}^{eff} + m_x {H_x}^{eff}\right)\right]$$
$$= -\left[-\gamma\left(m_z {H_x}^{eff} - m_x {H_z}^{eff}\right) + \left(\frac{\gamma\alpha_{\perp}}{m^2}\right)\left({m_z}^2 {H_y}^{eff} + {m_x}^2 {H_y}^{eff}\right)\right]$$

$$-\frac{\partial m_z}{\partial t} + m_z\left[\left(\frac{\gamma\alpha_{\parallel}}{m^2}\right)\left(m_x {H_x}^{eff} + m_y {H_y}^{eff} + m_z {H_z}^{eff}\right) - \left(\frac{\gamma\alpha_{\perp}}{m^2}\right)\left(m_x {H_x}^{eff} + m_y {H_y}^{eff}\right)\right]$$
$$= -\left[-\gamma\left(m_x {H_y}^{eff} - m_y {H_x}^{eff}\right) + \left(\frac{\gamma\alpha_{\perp}}{m^2}\right)\left({m_x}^2 {H_z}^{eff} + {m_y}^2 {H_z}^{eff}\right)\right]$$

Moreover, as we mentioned before in default general coefficient form of PDE in the COMSOL Multiphysics program, there are several coefficients so that if we look at the values of these coefficients for our case;

$e_a = 0$
$c = 0$
$\alpha = 0$
$\gamma = 0$
$\beta = 0$

$$d_a = \begin{bmatrix} -1 & 0 & 0 \\ 0 & -1 & 0 \\ 0 & 0 & -1 \end{bmatrix}$$

$$a = \begin{bmatrix} (1,1) & 0 & 0 \\ 0 & (2,2) & 0 \\ 0 & 0 & (3,3) \end{bmatrix}$$

$$(1,1) = \left[\left(\frac{\gamma\alpha_{\parallel}}{m^2}\right)\left(m_x {H_x}^{eff} + m_y {H_y}^{eff} + m_z {H_z}^{eff}\right) - \left(\frac{\gamma\alpha_{\perp}}{m^2}\right)\left(m_y {H_y}^{eff} + m_z {H_z}^{eff}\right)\right]$$
$$(2,2) = \left[\left(\frac{\gamma\alpha_{\parallel}}{m^2}\right)\left(m_x {H_x}^{eff} + m_y {H_y}^{eff} + m_z {H_z}^{eff}\right) - \left(\frac{\gamma\alpha_{\perp}}{m^2}\right)\left(m_z {H_z}^{eff} + m_x {H_x}^{eff}\right)\right]$$
$$(3,3) = \left[\left(\frac{\gamma\alpha_{\parallel}}{m^2}\right)\left(m_x {H_x}^{eff} + m_y {H_y}^{eff} + m_z {H_z}^{eff}\right) - \left(\frac{\gamma\alpha_{\perp}}{m^2}\right)\left(m_x {H_x}^{eff} + m_y {H_y}^{eff}\right)\right]$$

$$f = \begin{bmatrix} (1,1) & 0 & 0 \\ 0 & (2,2) & 0 \\ 0 & 0 & (3,3) \end{bmatrix}$$

$$(1,1) = -\left[-\gamma\left(m_y {H_z}^{eff} - m_z {H_y}^{eff}\right) + \left(\frac{\gamma\alpha_{\perp}}{m^2}\right)\left({m_y}^2 {H_x}^{eff} + {m_z}^2 {H_x}^{eff}\right)\right]$$
$$(2,2) = -\left[-\gamma\left(m_z {H_x}^{eff} - m_x {H_z}^{eff}\right) + \left(\frac{\gamma\alpha_{\perp}}{m^2}\right)\left({m_z}^2 {H_y}^{eff} + {m_x}^2 {H_y}^{eff}\right)\right]$$
$$(3,3) = -\left[-\gamma\left(m_x {H_y}^{eff} - m_y {H_x}^{eff}\right) + \left(\frac{\gamma\alpha_{\perp}}{m^2}\right)\left({m_x}^2 {H_z}^{eff} + {m_y}^2 {H_z}^{eff}\right)\right]$$

After the determination of coefficients, we should do another thing which is turning them into codes to enter the PDE in the COMSOL.

These codes are;

Table D.2. Code names corresponding to the symbols and symbols which are used in the LLB equations.

Name	**Symbol**	**Code**
Gyromagnetic ratio	γ	Gamma
Damping parameter	α	Alpha
Longitudinal damping parameter	$\alpha_{\parallel}$	alpha_pll
Transverse damping parameter	$\alpha_{\perp}$	alpha_tr
Effective Magnetic field	H	H
Magnetic field x direction	H_X	HX
Magnetic field y direction	H_Y	HY
Magnetic field z direction	H_Z	HZ
Temperature ratio	$r = T/T_c$	r
Damping parameter difference	Δd	d_a
Permeability of Free Space	μ_0	M_0
Saturation Magnetization	M_S	M_S
Square of Spin Polarization Vector	m^2	m_square
Curie Temperature of the Material	T_c	TC
Boltzman Constant	k_B	KB
Logitudinal Susceptibility	$\chi_{//}$	Xll
Transverse Susceptibility	$\chi_{\perp}$	Xt

Model Navigator:

(i) Start Comsol MultiPhysics

(ii) From the space dimension, select 3D and from application modes select: COMSOL Multiphysics/PDE Modes/PDE, Coefficient Form→Time-dependent analysis

(iii) In the Dependent variables field, enter " mx my mz ", with space in between the components

(iv) Click OK

Options and Settings:

(i) From Options menu, select Constants

(ii) Define the following constants

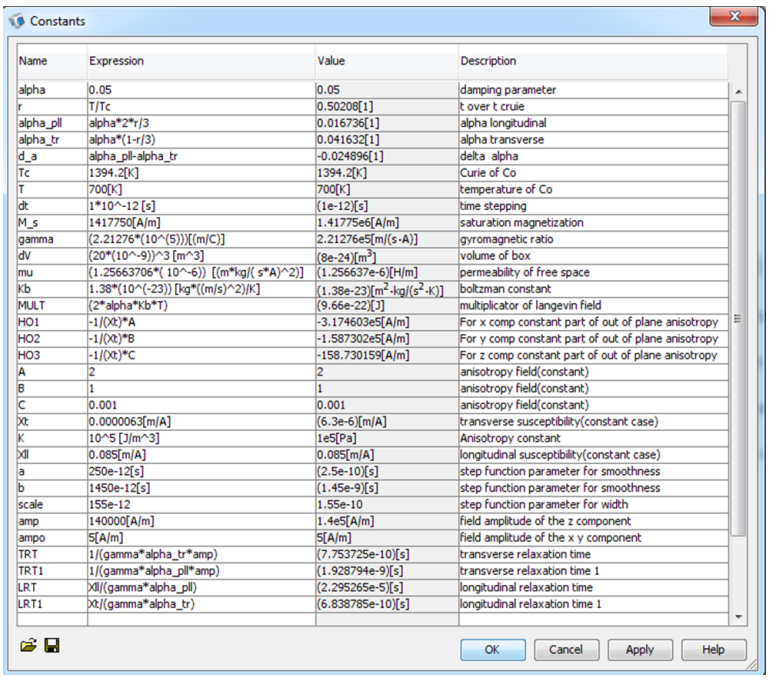

Name	Expression	Value	Description
alpha	0.05	0.05	damping parameter
r	T/Tc	0.50208[1]	t over t cruie
alpha_pll	alpha*2*r/3	0.016736[1]	alpha longitudinal
alpha_tr	alpha*(1-r/3)	0.041632[1]	alpha transverse
d_a	alpha_pll-alpha_tr	-0.024896[1]	delta alpha
Tc	1394.2[K]	1394.2[K]	Curie of Co
T	700[K]	700[K]	temperature of Co
dt	1*10^-12 [s]	(1e-12)[s]	time stepping
M_s	1417750[A/m]	1.41775e6[A/m]	saturation magnetization
gamma	(2.21276*(10^(5)))[(m/C)]	2.21276e5[m/(s·A)]	gyromagnetic ratio
dV	(20*(10^-9))^3 [m^3]	(8e-24)[m^3]	volume of box
mu	(1.25663706*(10^-6)) [(m*kg/(s*A)^2)]	(1.256637e-6)[H/m]	permeability of free space
Kb	1.38*(10^(-23)) [kg*((m/s)^2)/K]	(1.38e-23)[m^2·kg/(s^2·K)]	boltzman constant
MULT	(2*alpha*Kb*T)	(9.66e-22)[J]	multiplicator of langevin field
HO1	-1/(Xt)*A	-3.174603e5[A/m]	For x comp constant part of out of plane anisotropy
HO2	-1/(Xt)*B	-1.587302e5[A/m]	For y comp constant part of out of plane anisotropy
HO3	-1/(Xt)*C	-158.730159[A/m]	For z comp constant part of out of plane anisotropy
A	2	2	anisotropy field(constant)
B	1	1	anisotropy field(constant)
C	0.001	0.001	anisotropy field(constant)
Xt	0.0000063[m/A]	(6.3e-6)[m/A]	transverse susceptibility(constant case)
K	10^5 [J/m^3]	1e5[Pa]	Anisotropy constant
Xll	0.085[m/A]	0.085[m/A]	longitudinal susceptibility(constant case)
a	250e-12[s]	(2.5e-10)[s]	step function parameter for smoothness
b	1450e-12[s]	(1.45e-9)[s]	step function parameter for smoothness
scale	155e-12	1.55e-10	step function parameter for width
amp	140000[A/m]	1.4e5[A/m]	field amplitude of the z component
ampo	5[A/m]	5[A/m]	field amplitude of the x y component
TRT	1/(gamma*alpha_tr*amp)	(7.753725e-10)[s]	transverse relaxation time
TRT1	1/(gamma*alpha_pll*amp)	(1.928794e-9)[s]	transverse relaxation time 1
LRT	Xll/(gamma*alpha_pll)	(2.295265e-5)[s]	longitudinal relaxation time
LRT1	Xt/(gamma*alpha_tr)	(6.838785e-10)[s]	longitudinal relaxation time 1

Figure D.1. This is screen shot of Constant Interface in COMSOLMultiphysics.

Geometry Modeling:

(i) From Draw menu, select Block

(ii) Specify properties according to the following tables; when done click OK

It should be center based box because the arrow that we will see after the COMSOL solves the PDE. One point of the arrow starts from the center to the one corner of the box.

Length value can ben determined as follows;

$$x = 2, y = 2, z = 2$$

Here, we work on SI Unit system so that the unit of the length is taken meter

Axis base point can ben determined as follows;

$$x = -1, y = -1, z = -1$$

(iii) From Options menu, select Suppress/ Suppress Boundaries

(iv) Select all boundaries from the list and click Select Current Suppression

(v) Click OK

We want to suppress the boundaries because after COMSOL solves the PDE for a time interval that we determine before we want to see the arrow's position.

(vi) From Options/ Expressions, select Subdomain Expressions

(vii) Select Subdomain 1, enter the following in the edit fields:

Physics Settings:

(i) From Physics menu, select Subdomain Settings

(ii) Select Subdomain 1, enter the following values

Below Figure D.3, Figure D.4 and Figure D.5 shows us where and how our coefficients of the PDE are entered to the COMSOL Multiphysics Program.

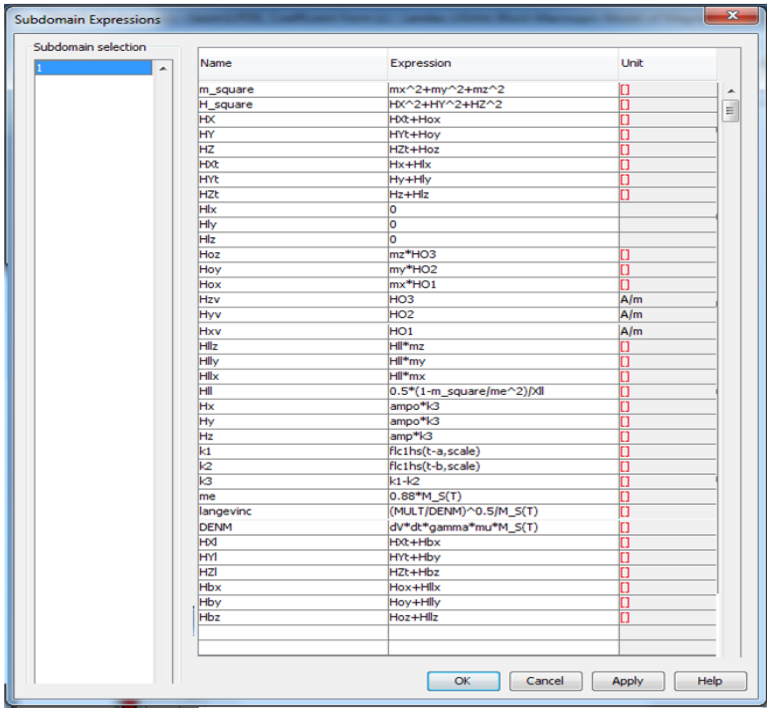

Figure D.2. This is a screen shot of Subdomain Expressions Interface in COMSOL Multiphysics.

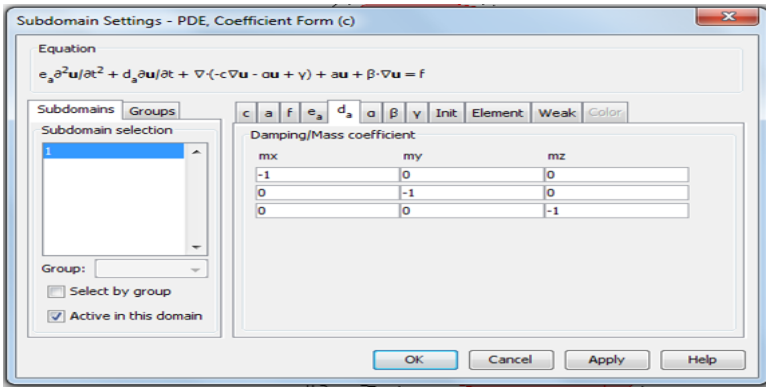

Figure D.3. This is a screen shot of Subdomain Settings Interface in COMSOL Multiphysics. This tab shows only "da" cofficient values of the entire equation.

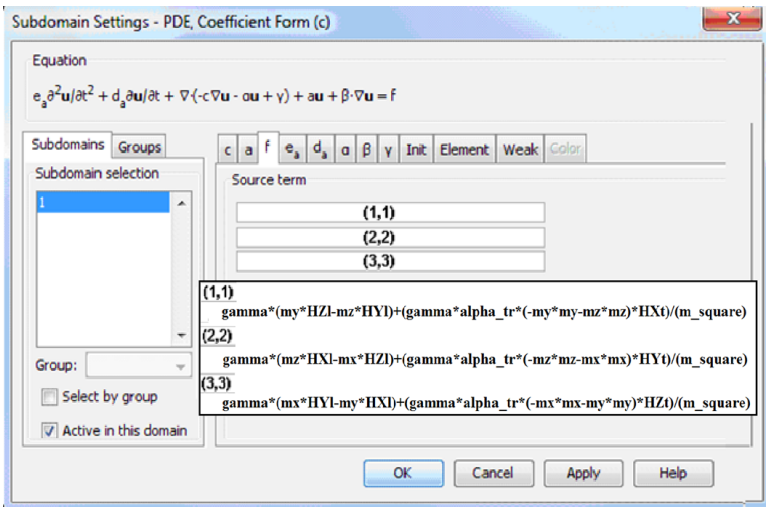

Figure D.4. This is a screen shot of Subdomain Settings Interface in COMSOL Multiphysics. This tab shows only "f" cofficient values of the entire equation.

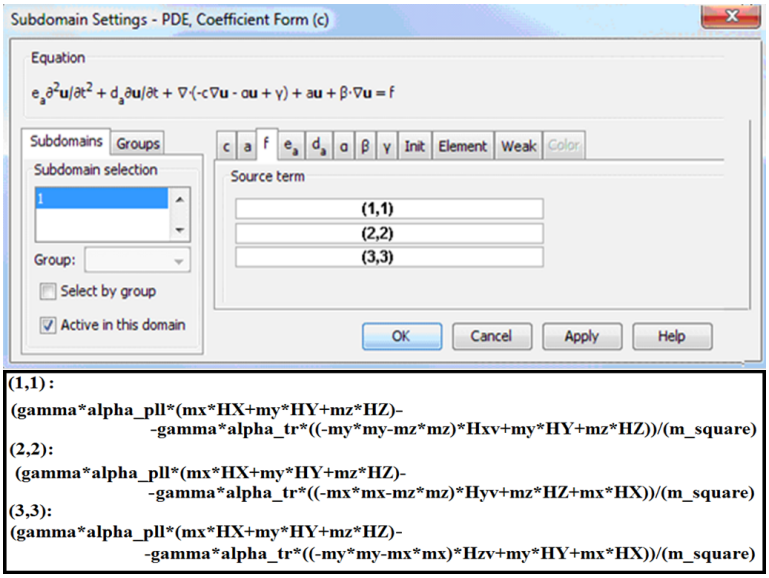

Figure D.5. This is a screen shot of Subdomain Settings Interface in COMSOL Multiphysics. This shows only "a" cofficient values of the entire equation.

We should also give an initial condition to the PDE as COMSOL starts to solve the PDE by using this initial condition.

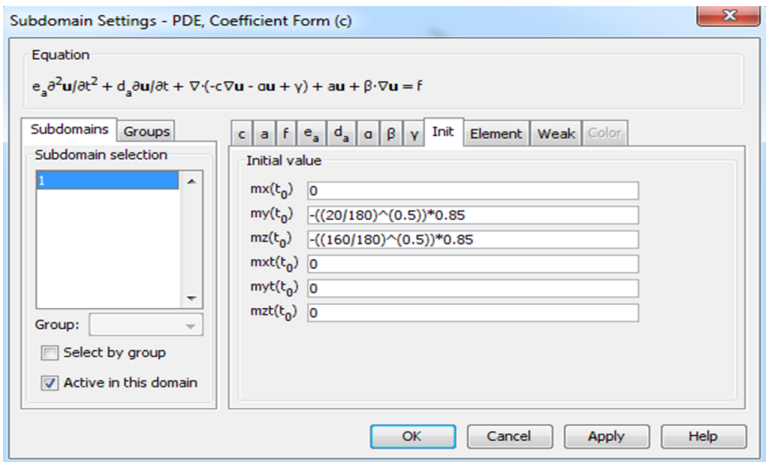

Figure D.6. This is a screen shot of Subdomain Settings Interface in COMSOL Multiphysics. This tab shows the initial conditions of the entire model.

An alternative way of inclusion of functions which depends on the same independent variable of the system is to insert listed values of the function corresponding to this independent variable.

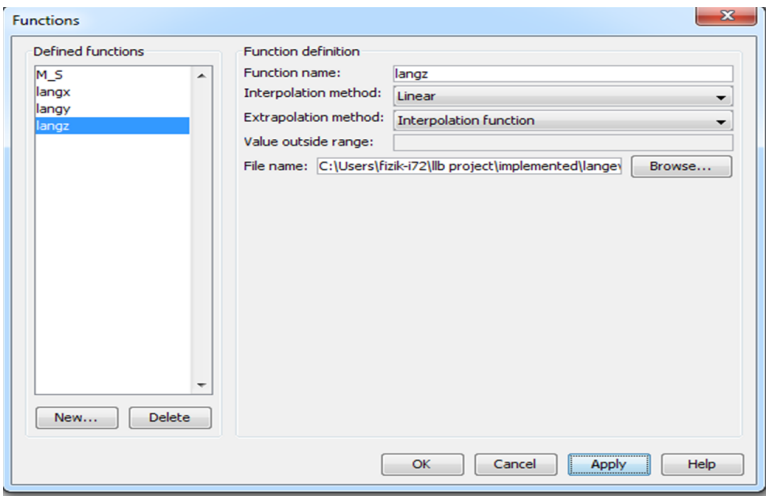

Figure D.7. This is a screen shot of interpolating function inclusion Interface in COMSOL Multiphysics. COMSOL Multiphysics allows both a mathematical equation inclusion and the list of function values.

Mesh Generation:

(i) From Mesh menu, select Swept Mesh Parameters
(ii) Select Subdomain 1
(iii) On the Predefined Mesh Size list, select Extremely Coarse
(iv) On the Element Layers page, check the Manual Specification of element layers field
(v) In the Number of Element Layers edit field, enter value 1
(vi) Click Remesh
(vii) Click OK

Computing the Solutions:

(i) From Solve menu, select Solver Parameters
(ii) Select Time- dependent Solver from the Solver list
(iii) Enter range(0,0.0000000000002,0.00000000005) in the Times edit field
(iv) Click OK
(v) Click Solve

Postprocessing and Visualization:

(i) From Postprocessing menu, select Plot Parameters
(ii) Uncheck all plot types
(iii) In the Arrow page, check the Arrow plot field
(iv) On the Subdomain Data field, enter mx, my, mz in the x, y, z edit fields, respectively
(v) In the Arrow positioning field, enter value 1 for Number of points field for x, y, z points
(vi) In the Arrow parameters field, select arrow from Arrow Type list and Proportional from Arrow Length List
(vii) Click Color button and select Red color
(viii) Click Ok

Plotting the Result:

(i) From Postprocessing menu, select Cross Section Plot Parameters

(ii) In the Plot Type list, check Point plot

(iii) In the Solutions to use list, select Stored Output times

(iv) From time list, select all the time values

(v) Check the Keep current plot field

(vi) Click the Title/Axis button

(vii) The default values of Title/ Axis are Auto. In the Second Axis Label, check the empty field and enter: "magnetization ¡i¿mx/mx(t=0)"

(viii) Click OK

(ix) Click on the Point tab

(x) On the Point page, enter "mx/M_s" in the Expression field. By doing this, we normalize the component.

(xi) Enter 0 for x, y, z coordinates

(xii) Check that the x-axis data is selected as Auto

(xiii) Click the Line Settings button

(xiv) Select Color from the Line color list. Then, click Color button and select random color

(xv) From the Line Style list, select a style

(xvi) Click OK

(xvii) Click OK. A plot of variation of magnetization component mx with time appears. Minimize the plot. BE CAREFUL. DO NOT CLOSE THIS PLOT.

(xviii) On the COMSOL Multiphysics program, enter Options/Constants. Change the value of r to "0.3". Click OK.

However, the plottings of the COMSOL are at the undesirable level so that we give up to use of the post processing and visualization part of COMSOL Multiphysics. Then, we only take the data of the coordinates of the normalized magnetization versus time graph as a ".dat" file. After that by using Mathematica 7.0 version first we import the data from this dat file and we plot the data how we want such as we can put a legend with more visible and presentable case and we can adjust the image size etc.

APPENDIX E: LLB BASED MACROSPIN MODEL USING MATHEMATICA

In this appendix, our goal is to express in-detail the non stochastic LLB equation based macrospin model together with its outputs.

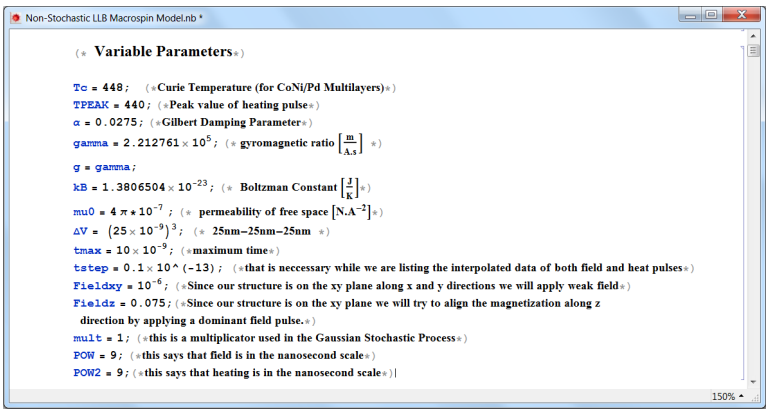

Figure E.1. The screenshot shows the constants which will be used in the LLB based model developed by using Mathematica.

The codes written above are staple constants of the LLB simulations. Before writing the main equations these constant needs to be recognized by the program.

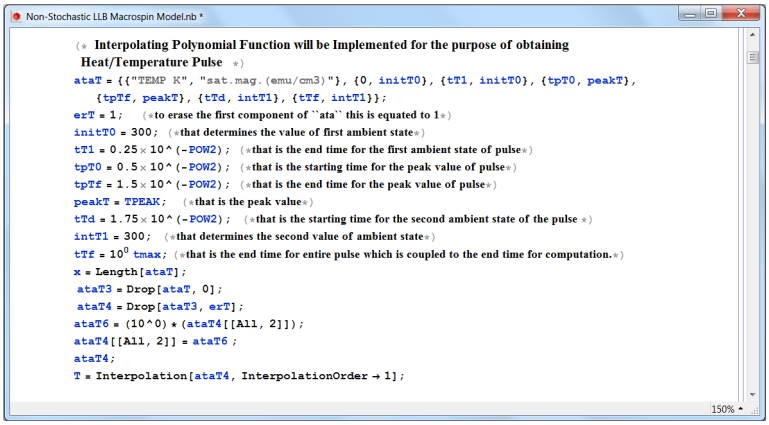

Figure E.2. This screenshot shows that how we can create an adjustable heating pulse by using Mathamatica algorithms.

By using the commands which are shown above, we created an interpolated heating pulse with adjustable width amplitude and the slope.

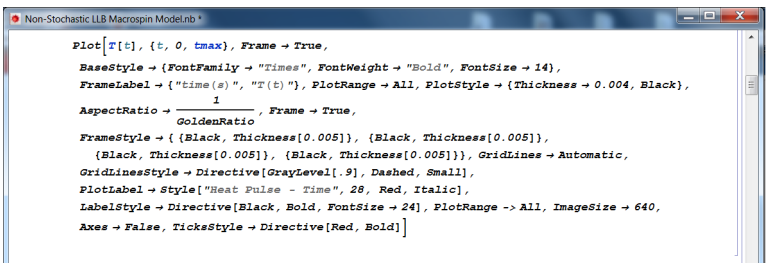

Figure E.3. This screenshot shows the required command for plotting the heating pulse.

After the development of heating pulse and the inclusion of vital constants we can insert the intrinsic parameters which are possessed by CoNi/Pd multilayer systems.

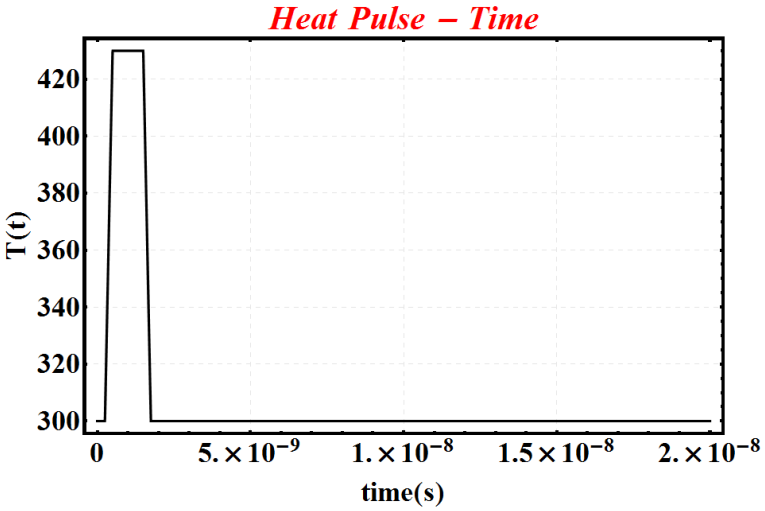

Figure E.4. This is an output of commands written above. In this output, it is shown that an example heating pulse with 1.25 ns width and 425 K amplitude.

Saturation magnetization and the zero field equilibrium magnetization are the among the crucial inputs of our model. By using the experimental data that we have obtained from the experiments does not include all the values which can be chosen by the user, arbitrarily. To do so, we need to create interpolated forms of both the saturation magnetization and the zero field equilibrium magnetization (remanance). What is more, since LLB equation is a time dependent ordinary differential equation, these two intrinsic parameters need to be the interpolating functions of both temperature and time, separately. The following codes are written for that purpose.

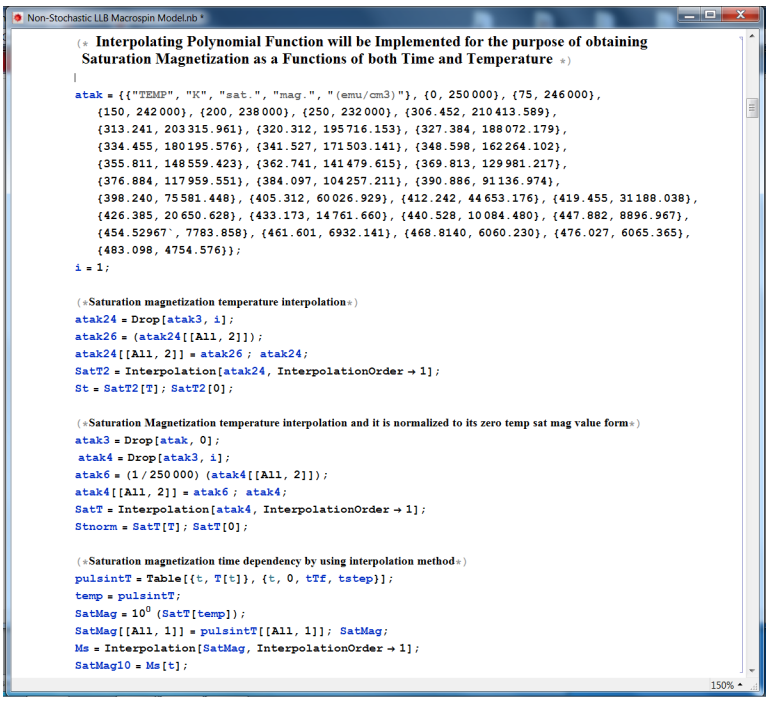

Figure E.5. This is the screen shot which shows the required commands to create interpolation functions of intrinsic parameters.

The intrinsic parameters(saturation magnetization and zero field equilibrium magnetization) are included into the LLB model as interpolation functions. The interpolation is created by using the experimental data. The dependencies of these parameters are time and temperature.

After this step, we need to see whether the saturation magnetization and the zero field equilibrium magnetization are functions of both temperature and time, separately or not. To see them, we plot each case by using the following commands.

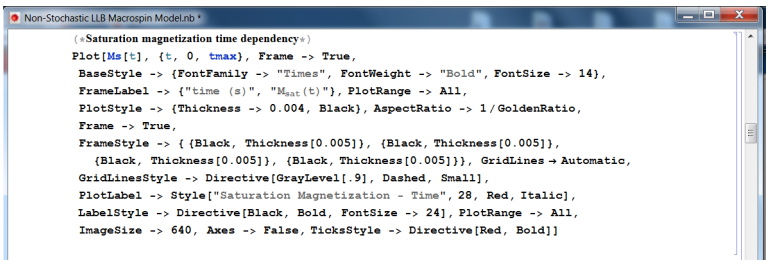

Figure E.6. This is the screenshot which shows the necessary commands for plotting the saturation magnetization with respect to time.

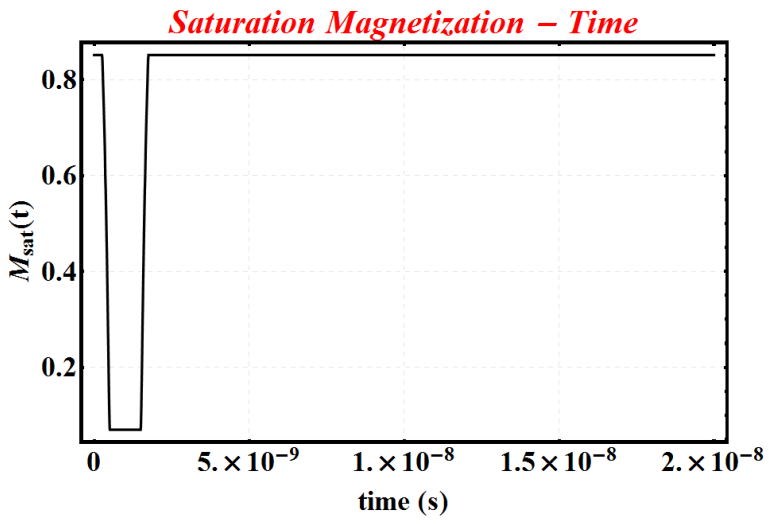

Figure E.7. This is an output of the commands shown above. The time dependent saturation magnetization.

Saturation magnetization is a time dependent function because the system temperature is changing in time. The change in temperature has a direct influence on the saturation magnetization value of the sample.

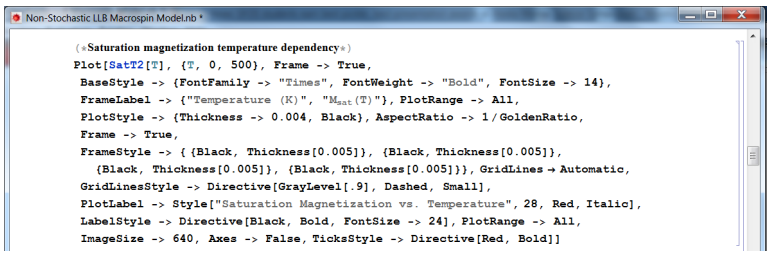

Figure E.8. This is the screenshot which shows the necessary commands for plotting the saturation magnetization with respect to temperature.

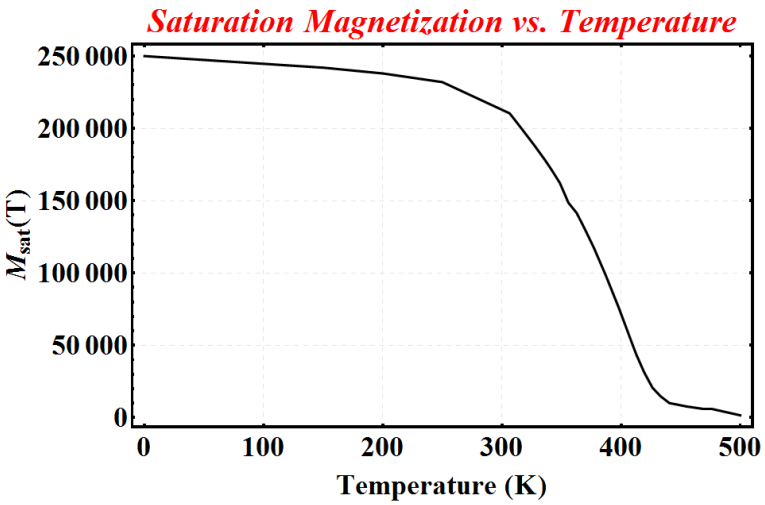

Figure E.9. This is an output of the commands which are shown above. The temperature dependent saturation magnetization.

As the temperature of the system is increased up to Curie temperature, the saturation magnetization value of the material decreases considerably. Since magnetic moments are starting to move independently, significant decrease in the value of average magnetization can be observed.

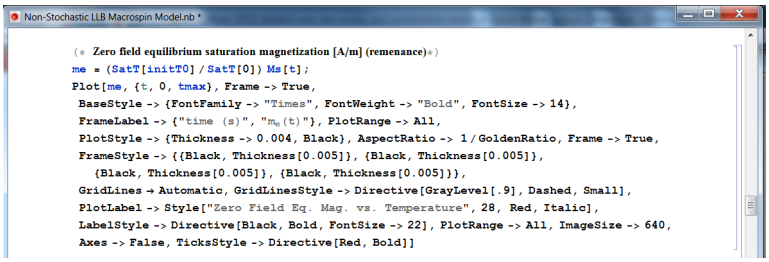

Figure E.10. That is a screenshot which is taken from the LLB model is developed by using Mathematica and this screen shot shows the change in the zero field equilibrium magnetization value with respect to time.

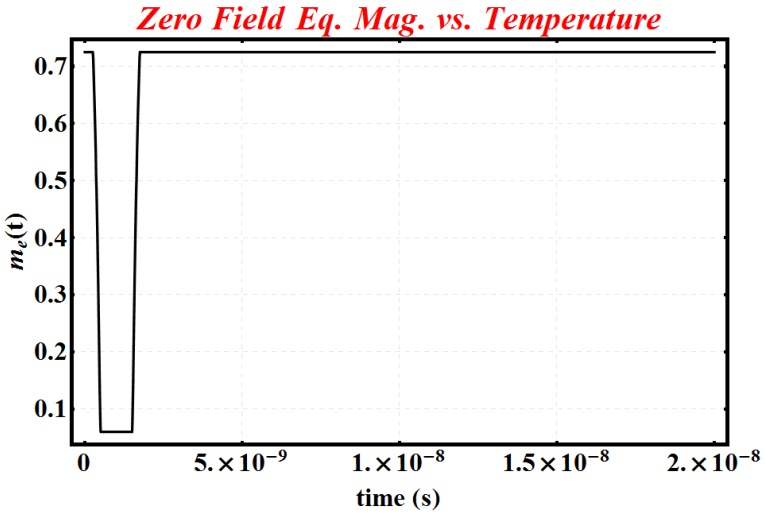

Figure E.11. This is an output of commands written above which shows the time dependence of zero field equilibrium saturation magnetization.

Including the intrinsic parameters as an interpolation function of either time or temperature in the LLB based macrospin model is one of the crucial parts. By means of these implementations, our LLB model gains experimental inputs.

The single fitting of our entire model was the longitudinal susceptibility. First, we plugged both the coercivity values of CoNi/Pd MLs and its temperature values into the model as DC magnetic field and heating pulse, respectively. Thus, we had extracted the temperature dependence of longitudinal susceptibility. After these significant steps, to proceed ourselves to another crucial stage, we need to include the longitudinal susceptibility in the model as an interpolating function of both time and temperature, separately. The following commands are created for this purpose.

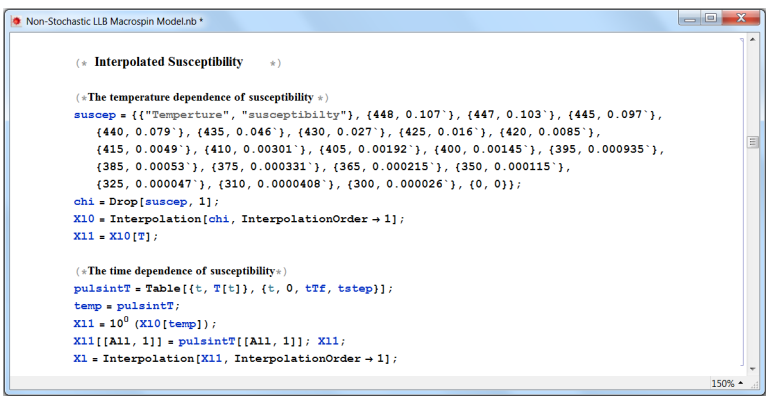

Figure E.12. This is the screenshot which shows the necessary codes to insert the longitudinal susceptibility as an interpolation function in the LLB based macrospin model.

After that, again we need to see whether the codes written above is working correctly or not. We plot these two interpolating functions.

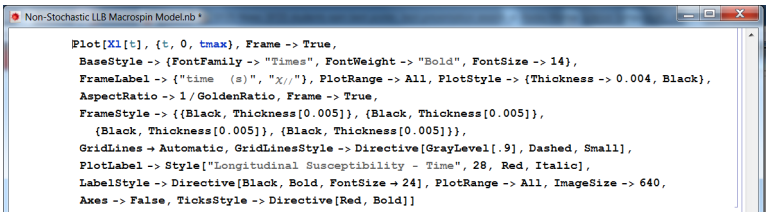

Figure E.13. That is the screenshot of the necessary codes to plot the longitudinal susceptibility with respect to time. This screenshot is taken from the codes written in Mathematica.

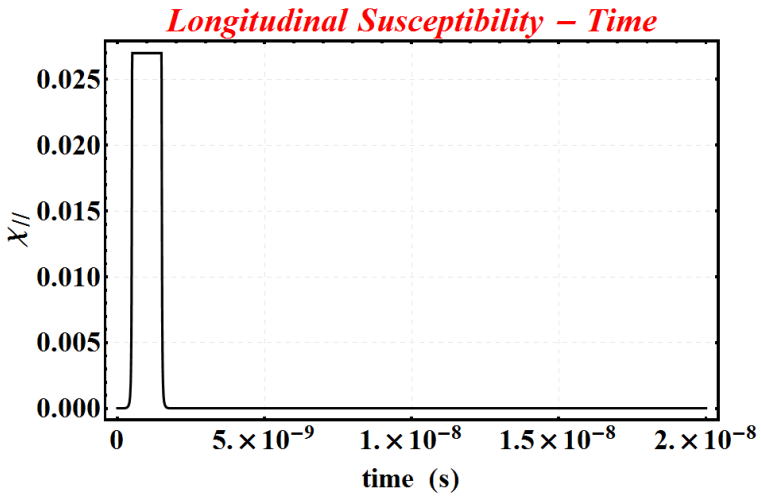

Figure E.14. That is the output of the commands which are written above shows the time dependent longitudinal susceptibility.

The system temperature varies in time causes to regard the longitudinal susceptibility as a functional of time.

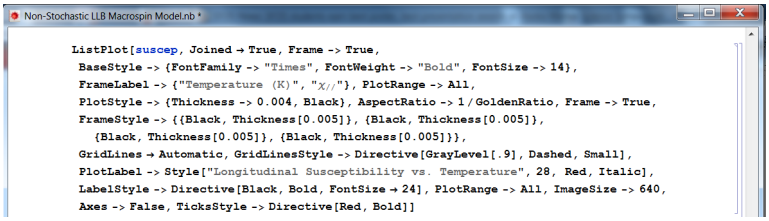

Figure E.15. The screenshot of the command window in Mathematica which is written to plot the longitudinal susceptibility with respect the temperature.

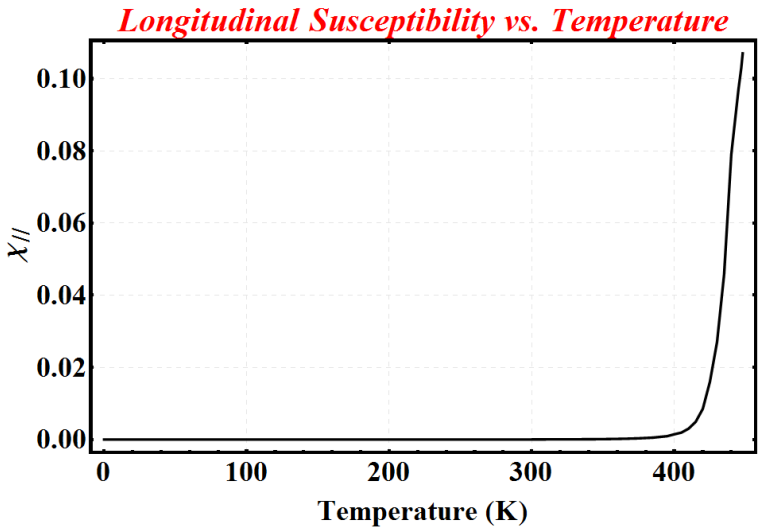

Figure E.16. That is an output of commands written above.It shows the behavior of longitudinal susceptibility against to the temperature increase.

As the temperature increases the magnetic moments are more susceptible to the magnetic field. This is exploited by the HAMR system because in this system by increasing the system temperature close phase transition point this technique makes the magnetic layer more susceptible to magnetic field leads to achieve the magnetic moments alignment along a specified direction with the less magnetic field application.

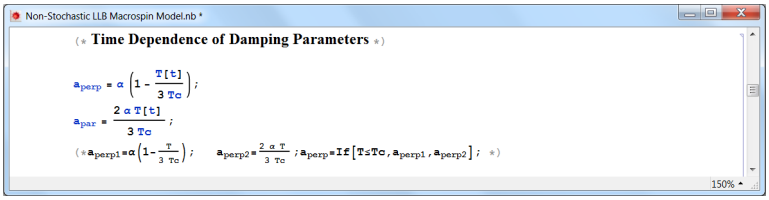

Figure E.17. That is a command window screen shot which is created to develop the temperature dependence of the damping parameters.

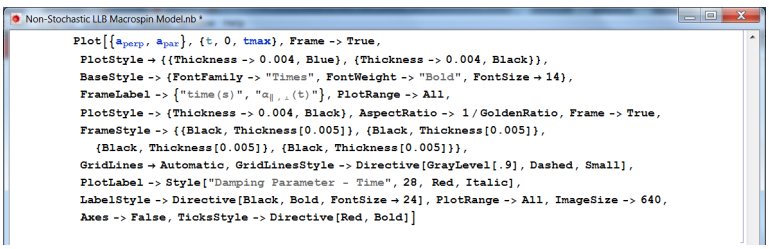

Figure E.18. That is a screen shot which shows the necessary commands to plot the damping parameters with respect to time.

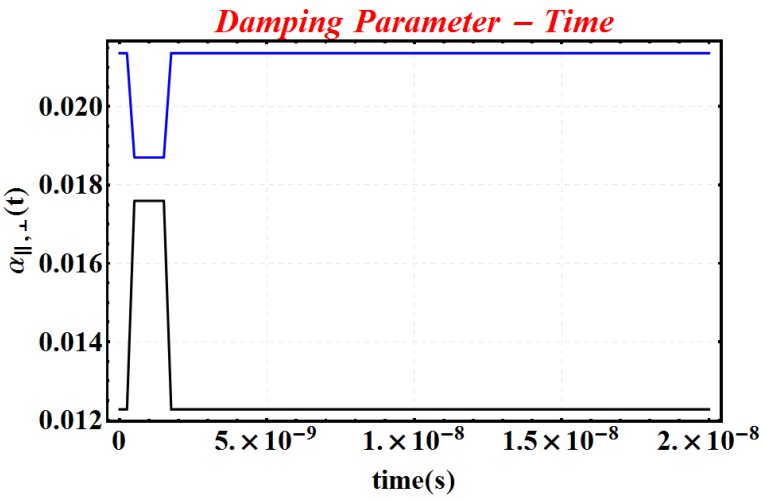

Figure E.19. That is the output of the commands written above. The longitudinal damping parameter (blue solid line) and the the transverse damping parameter (black solid line) are plotted in the same figure. Gilbert damping parameter is taken as 0.0275.

As it has been stated before that the LLB framework considers two different damping parameters which are longitudinal and transverse damping parameters and they are describing the longitudinal and transverse relaxations of the magnetization, respectively. Here, by using the codes which are shown above, these two vital parameters are included in the model as the functions of both temperature and time.

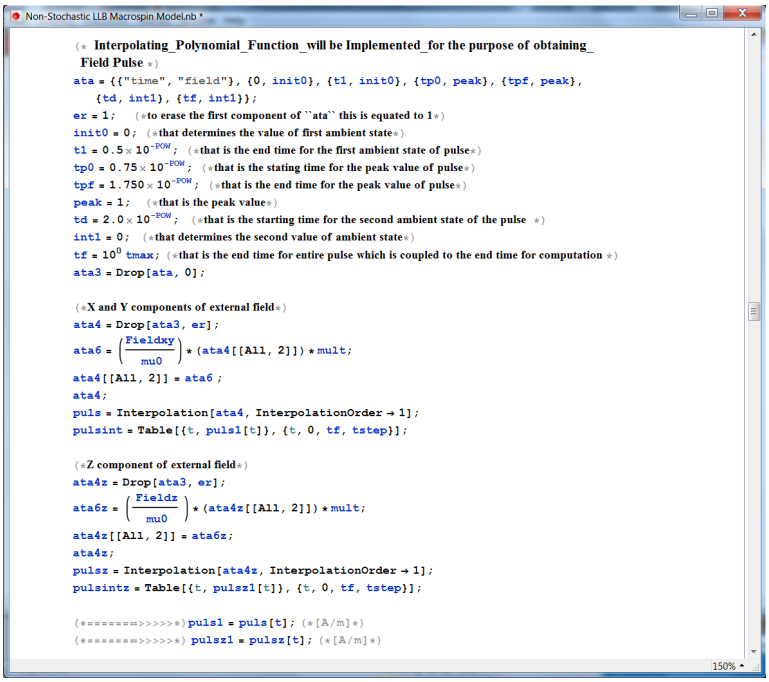

Figure E.20. That is the screenshot and it shows that the creation of magnetic field pulse with adjustable width, amplitude and fall and rise slopes.

We are applying weak external magnetic field along x and y direction in addition to a dominant magnetic field along the z direction (perpendicular to the plane of the thin film structure). The reason behind choosing the dominant field application direction as z direction is because of the having a magnetic media with high perpendicular anisotropy.

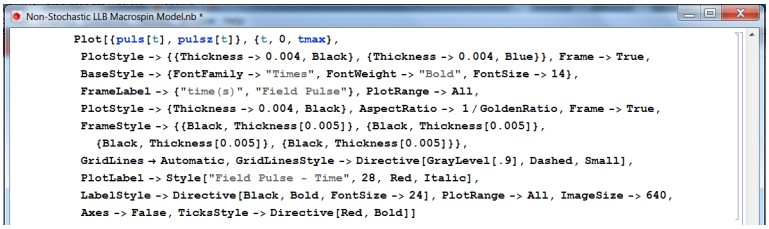

Figure E.21. That is the screenshot of the required commands to plot the external magnetic field.

The external magnetic field pulse is a simplification of the straying field applied to the recording layer by the writing head.

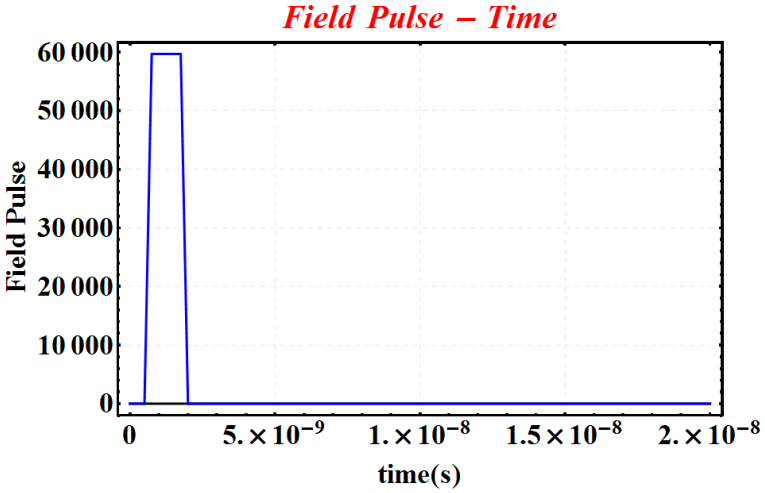

Figure E.22. That is an output of the commands written above which shows an example of the applied magnetic field pulse.

The blue solid line in the figure shows the dominant magnetic field pulse (the z component of the external magnetic field pulse). The black solid line shows the weak magnetic field pulse applied along both x and y directions.

The total effective field which is helping in describing the behavior of the magnetization vector while it is evolving in time. The first component of the effective magnetic field is applied external magnetic field or so called Zeeman field. The codes

below are written for the purpose of creating a pulsed shape field pulse. Like in the case of heating pulse, the field pulse has the properties of adjustable width, amplitude and the slope.

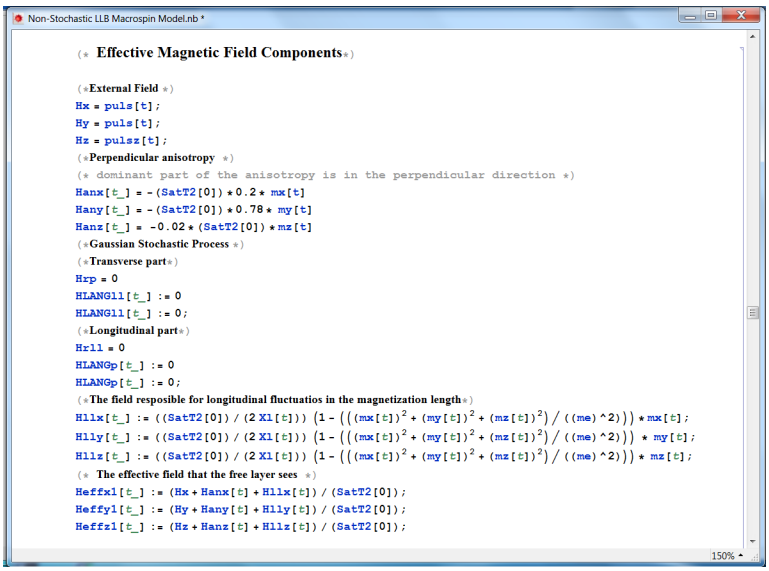

Figure E.23. This screenshot shows the exigent commands to include the total effective field of the LLB macrospin model.

In the effective magnetic field, the individual interaction between the magnetic moments are disregarded. In the macrospin model all spins are strongly coupled to each other and they are creating a coherent motion as they are under the influence of magnetic field.

The last thing which needs to be done is to create field pulse. Due to that reason, we wrote down the above codes. Since the whole model is in three dimensions, we created three applied magnetic field pulses corresponding to each spatial component.

Moreover, the perpendicular anisotropy is the dominant anisotropy of our system. This makes the plane of the thin film sample energetically unfavorable. The codes are describing this fact, as well.

Another important component of the effective field is Gaussian stochastic process. In this case we did not consider the stochasticity. Yet, it has just been turned off. In other words, our modeling is the stochastic form LLB modeling and we can have the flexibility of turning the random fluctuations off or on at any time. Considering that is a nonstochastic LLB based macrospin model, the Gaussian stochastic process is set to zero. To see the relations of them see the Appendix F.

The last term is included controls the longitudinal fluctuations in the magnetization length. In the final analysis, we created our effective magnetic field, for which three spatial components are described.

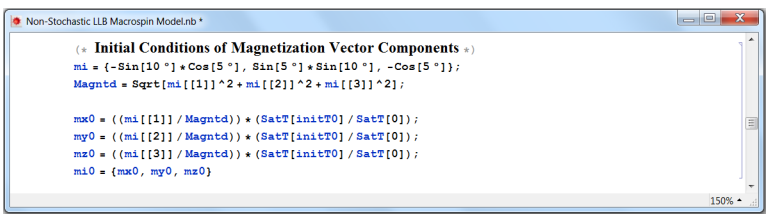

Figure E.24. That is the command window screenshot which shows the initial condition of magnetization vector.

In this model, due to the preference of the high perpendicular anisotropy magnetic media, the easy axis of the magnetic moment (which is the inherently preferred direction of magnetic moments as they are not under the influence anything) is along the out of plane direction. It is normalized to its magnitude at a given ambient temperature.

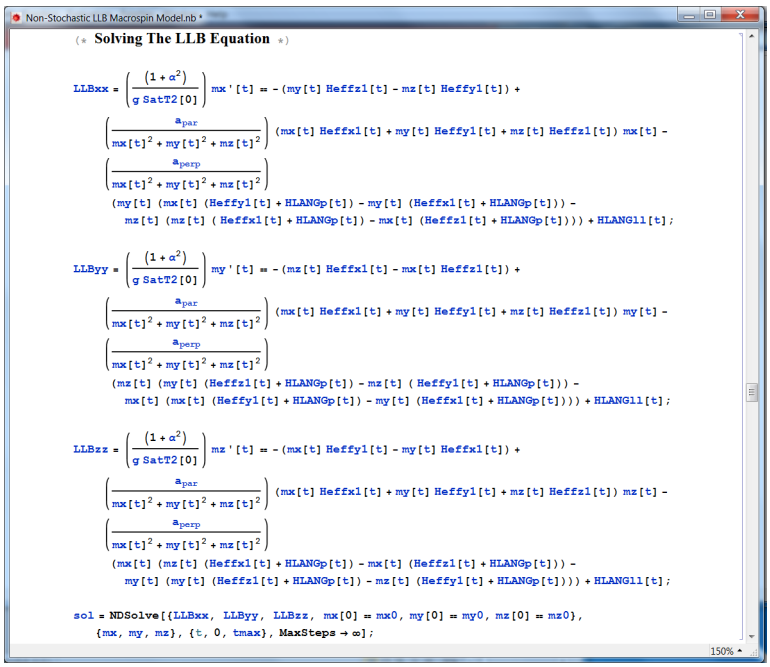

Figure E.25. This is the screenshot which shows the spatial components of the main LLB equation.

The LLB equation is a second order ordinary time dependent differential equation. By means of the codes written above we can solve the LLB equation.

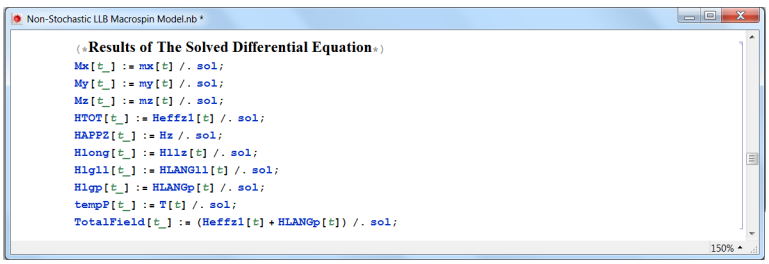

Figure E.26. That is the screenshot which shows the required codes to analyze the behavior of the magnetization vector depending on the solution of the differential equation written above.

By using the codes written above we can plot the time evolution of all parameters used in the LLB model. In other words, when the codes written above has found a solution for this ODE, the results are allocated to the new variables to see their time

evolution. Such as x component of magnetization vector was called in the codes as "mx" but after solving the differential equation, the time evolution of mx is allocated to "Mx" variable. The codes written above carry out this allocation for other variables. Now, we wiil show some of the example figures which rely on the solution of the LLB based macrospin model.

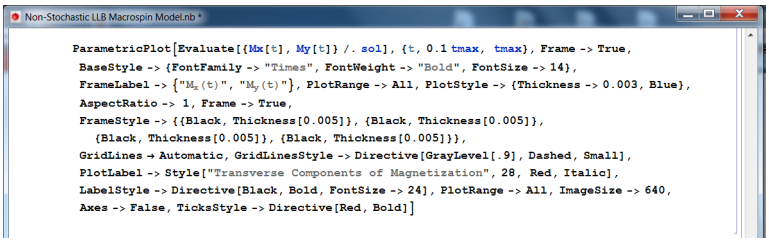

Figure E.27. That is the screenshot which shows the necessary codes to plot the time evolution of transverse components of magnetization vector.

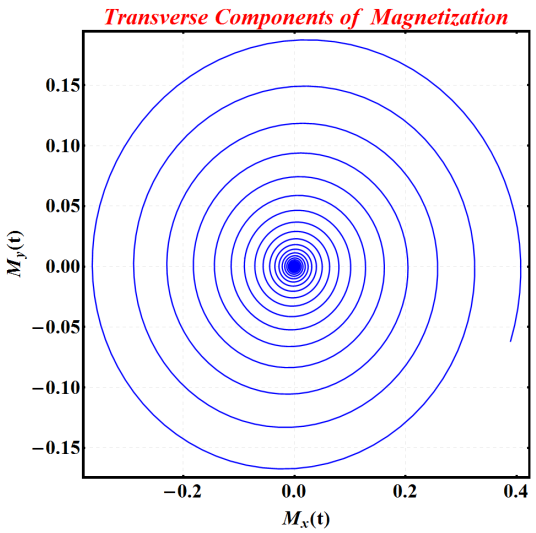

Figure E.28. That is the output of the codes written above. It shows that the time evolution of the transverse components.

The figure above is the plot of transverse components of magnetization vector. The magnetic field is applied through the $+z$ direction. That is why, these two components damp to zero.

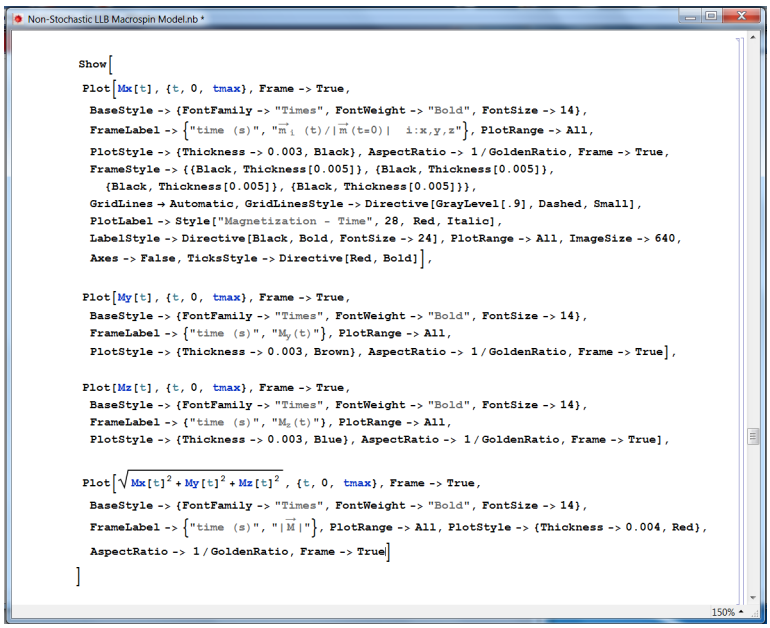

Figure E.29. That is the screenshot of the required commands to plot the spatial components together with the magnetization magnitude in the same figure.

The Figure E.30 shows the time evolution of the magnetization vector together with the time evolution of the magnetization magnitude. Since the external magnetic field is applied through the $+z$ direction, x and y components (black and brown colored solid lines, respectively) of the magnetization vector die out. Yet, the z component of the magnetization (blue colored solid line) relaxes to the same direction with the external magnetic field. During the time evolution, the change in the magnetization magnitude is apparent. The external magnetic field pulse amplitude is 60 kA/m and the width of the pulse is 1.25 ns. The heating pulse amplitude is 440 K and the width of the heating pulse is 1.25. The delay between the heating the field pulses is 0.5ns.

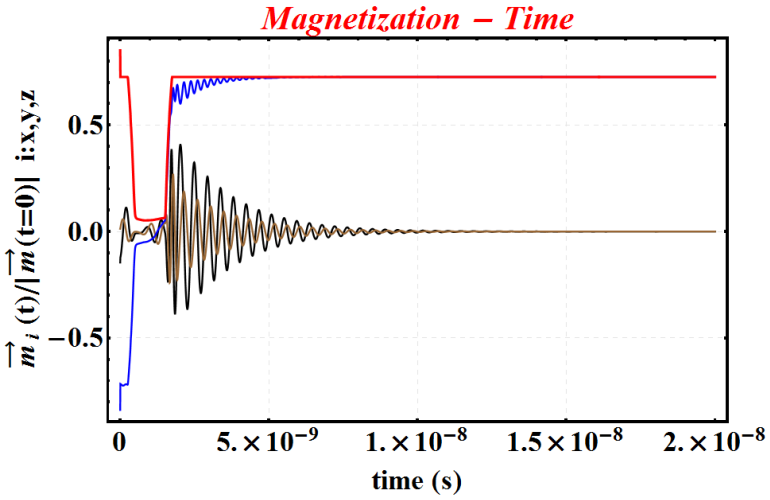

Figure E.30. That is the output of the codes written above which shows the time evolution of magnetization vector components (x, y, and z components brown, black and blue solid line and the magnetization magnitude is the red solid line).

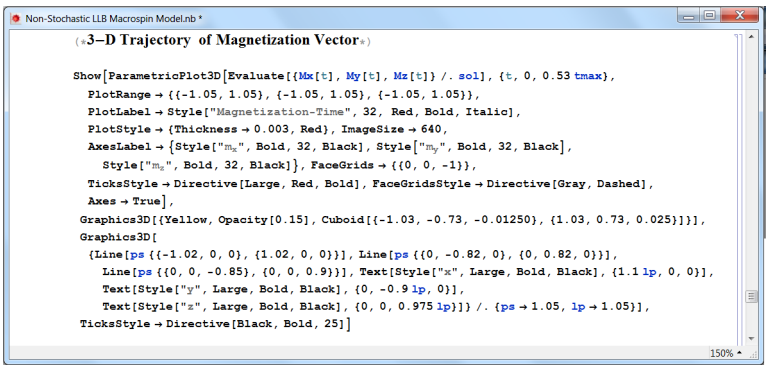

Figure E.31. That is the required command to plot 3D trajectory of the magnetization vector.

By using the commands which are shown above will not only show the 3Dtrajectory of the magnetization vector but also the thin film.

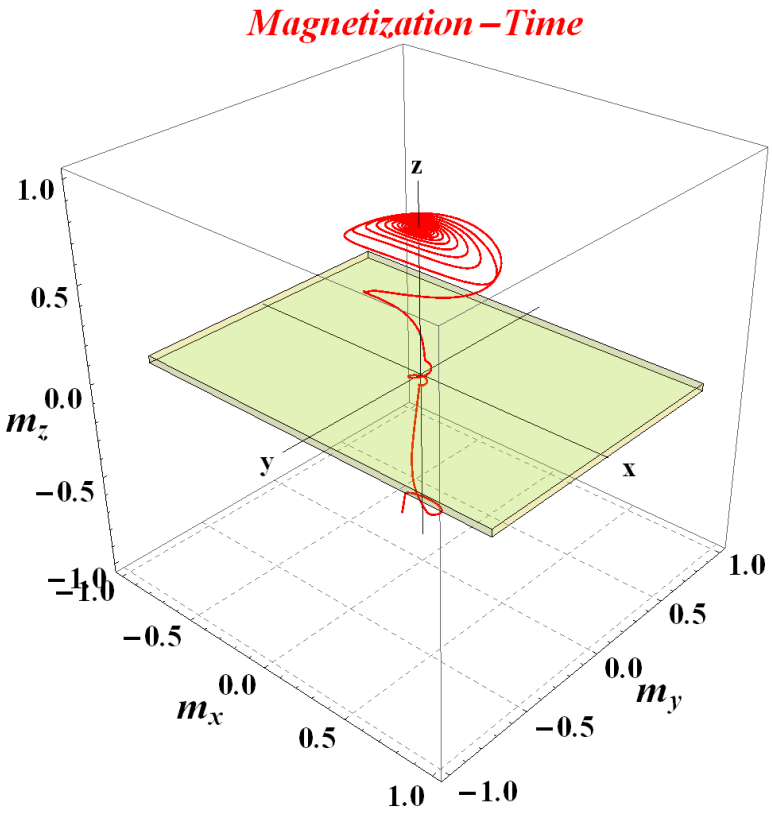

Figure E.32. That is the output of the codes written above which shows the switching process of the magnetization vector.

The figure above shows the three dimensional trajectory of the magnetization vector. Due to possession of high perpendicular anisotropy makes the out of plane of the thin film energetically favorable. Therefore, the magnetization tendency is not to spend much time on the plane of the thin film sample.

Figure E.33. That is the command window screenshot which shows how to extract the time evolutions of spatial components or the other parameters as as a list.

By using the codes written above we can save the evolution of crucial parameters as txt file and after that we can plot them even we close the LLB based model.

APPENDIX F: SWITCHING TIME DISTRIBUTION MODEL IN MATHEMATICA

In this appendix the goal is to show how to create the switching time distribution as a function of both heating and external field pulses.

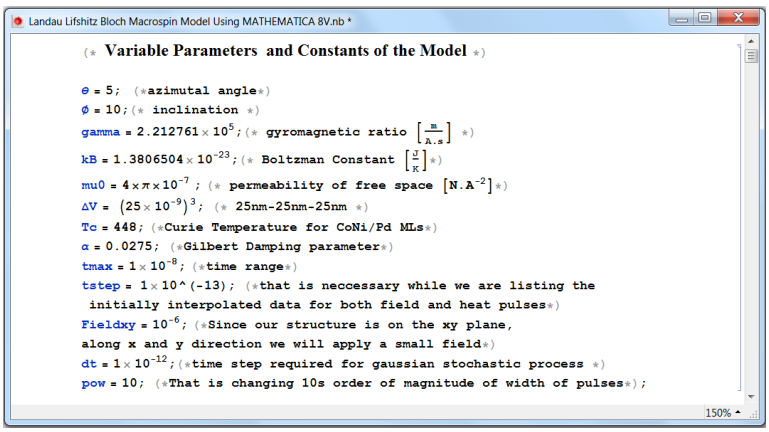

Figure F.1. The screenshot taken from constants which are used in the S-LLB II model.

The first thing is to determine the constants of the LLB equation based macrospin model. Since the switching time distribution depends on both heating and magnetic field pulse amplitudes, the amplitudes of these two pulses are considered as individual variables.

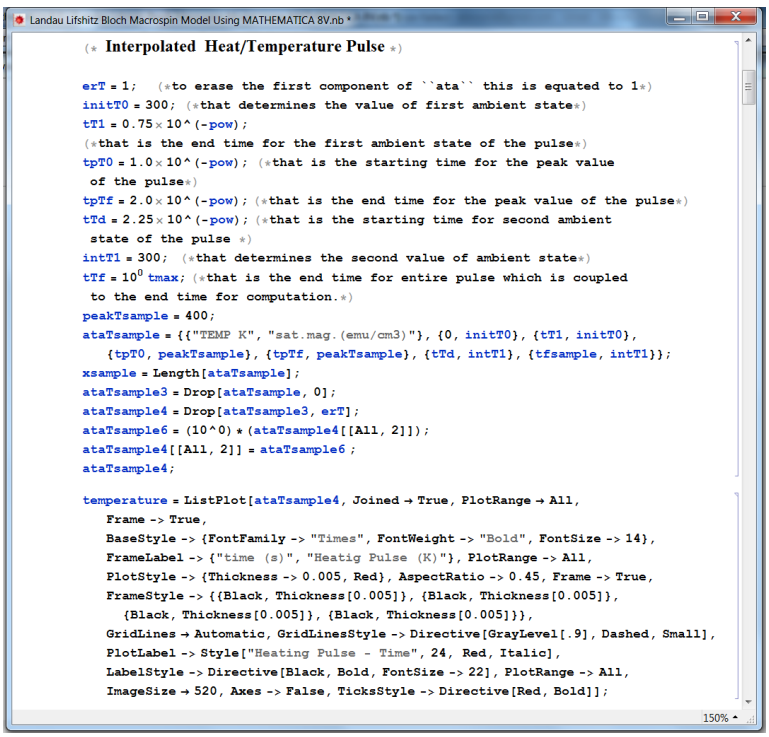

Figure F.2. The screenshot of written codes of the S-LLB II model. In this part, the creation of interpolation function for an adjustable heating pulse.

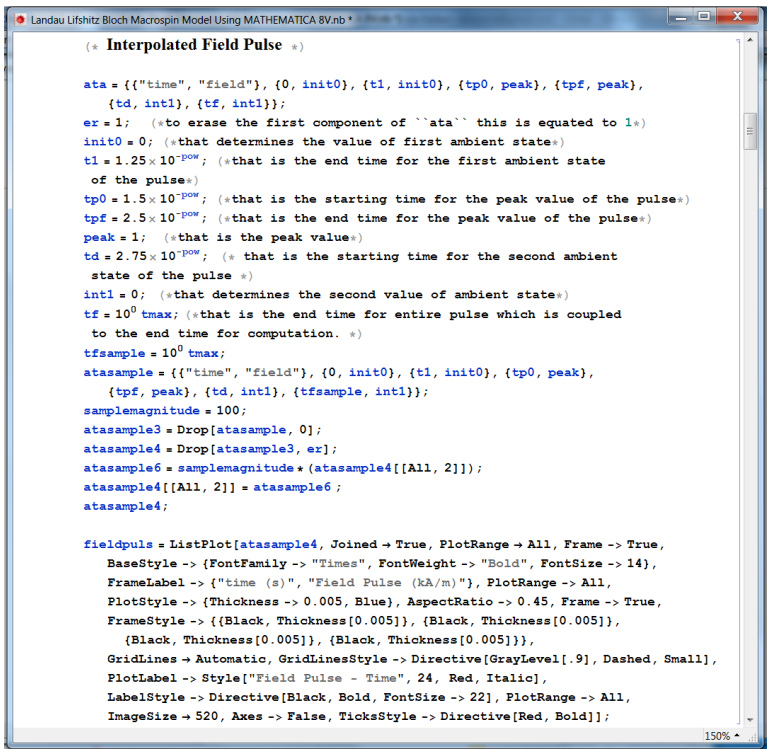

Figure F.3. The screenshot of written codes of the S-LLB Model. In this part, the creation of interpolation function for an adjustable field pulse.

After creating both magnetic field and heating pulses to show their characteristic behavior, we plot them in the same figure by using the following commands. By the way of these commands the figure gains a representational form.

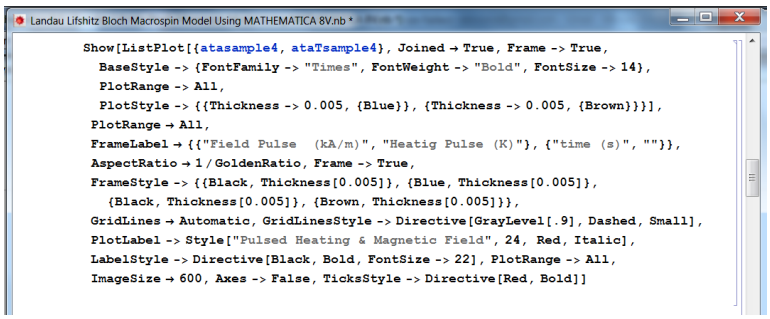

Figure F.4. That is the screenshot which shows the codes for the plot of heating and field pulse in the same figure.

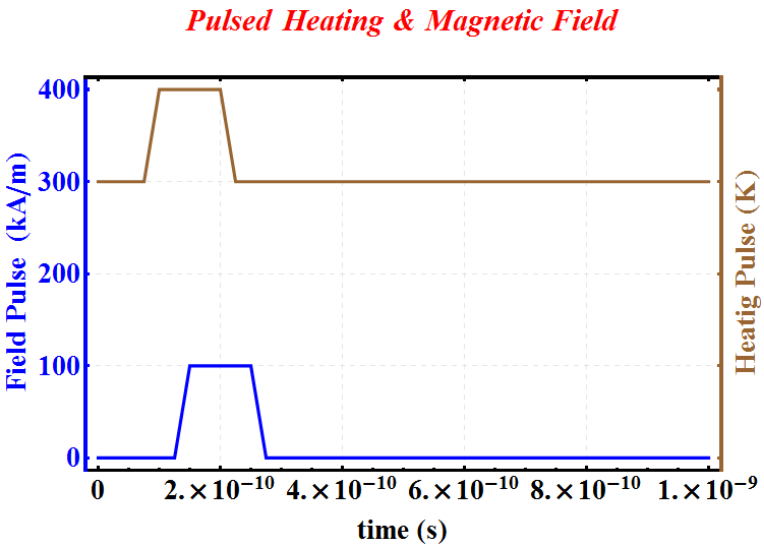

Figure F.5. That is the plot of interpolating functions of both heating and field pulses (brown solid line is the heating pulse and blue solid line is the magnetic field pulse).

As in the case HAMR technique the employed heating pulse is opened first, after that (in our case the delay between two pulses is 0.5 ns) the external magnetic field pulse is turned on to align the magnetic moments along the direction of the external magnetic field pulse. In this example set, the amplitudes of both heating and magnetic field pulses are 400 K and 100kA/m, respectively.

Another important component of the effective field is Gaussian stochastic process. In this case, we considered the stochasticity. In other words, our modeling is the stochastic form LLB modeling and we can have the flexibility of turning the random

fluctuations off or on at any time. The codes below are written for the purpose of creating the Gaussian stochastic process which is described indetail in Chapter I. The Gaussian stochastic process is described in two different ways but here we will use the recently proposed stochastic process. Conforming the properties of this new fromalism makes the name of our equation as S-LLB II equation which satisfies the Boltzman Distribution even at the temperature values close to Curie temperature. This process has two parts and the following two screenshots are showing the codes written for the accurate description of stochastic behavior of magnetization vector.

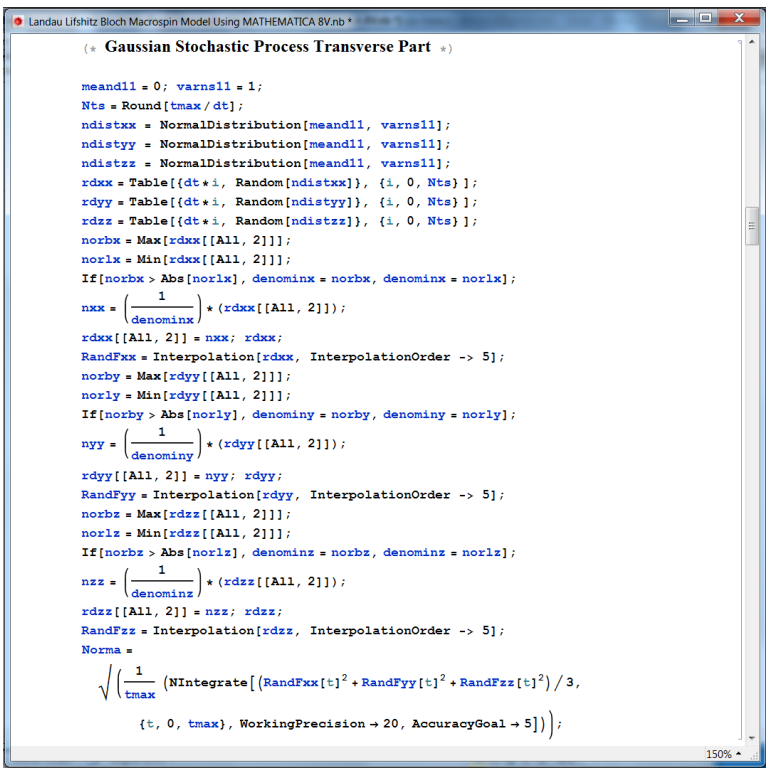

Figure F.6. The codes which are required for the creation of the transverse part of the Gaussian stochastic process.

The first one is acting on the system as a component in the transverse damping torque term. This is included as a field term in the effective field.

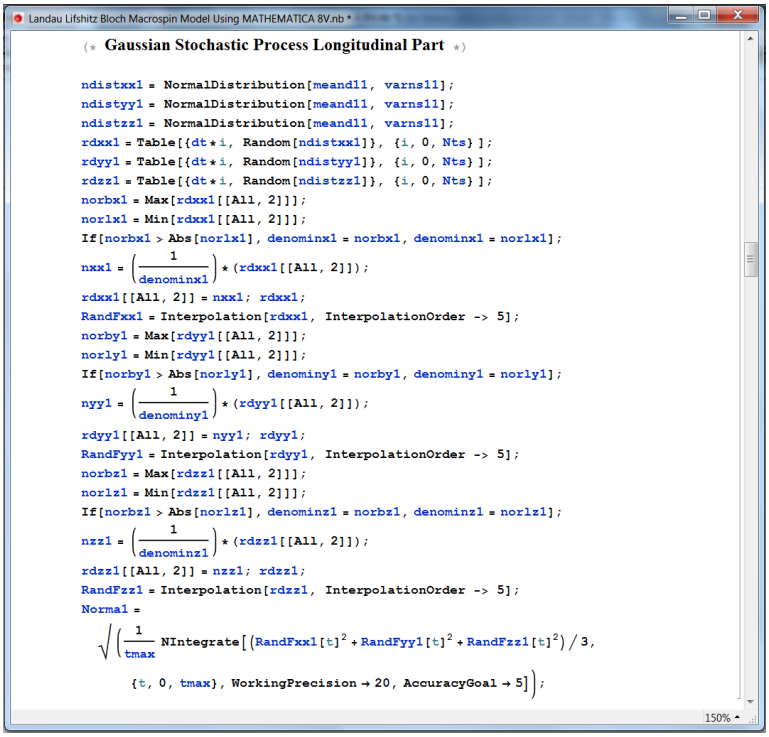

Figure F.7. The codes which are required for the creation of longitudinal part of the Gaussian stochastic process.

The second one is the acting on the system as an additional torque term. These are creating random functions by considering the properties of the Gaussian distribution function. These randomly fluctuating functions have zero mean and unit variance. Further, by the codes written above we created six uncorrelated randomly fluctuating functions. While three of them are for the Gaussian stochastic processes in the effective field which is just acting on the transverse damping torque term. The remaining three are for the additional torque terms. Each of these three corresponds to one spatial component. After that, these functions need to be in the forms of a field and a torque. For that purpose, we described their relations (which are written between (* and *)). These two things are the unit analysis of the Gaussian stochastic processes. While the first one is in unitless form (because our effective field is reduced effective field (normalized to the zero temperature saturation magnetization)), the second one is in s^1 unit (because all terms of LLB equation are in s^1 unit).

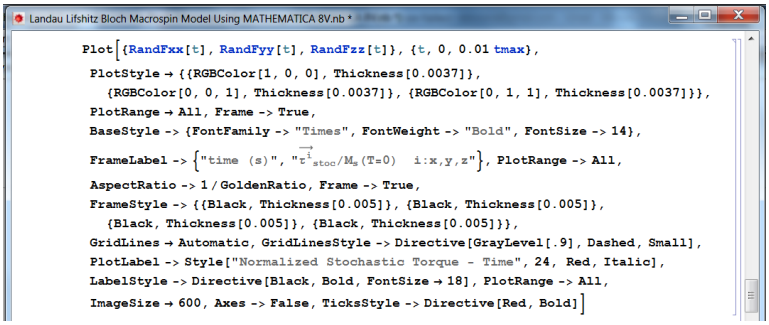

Figure F.8. The codes written for the purpose of showing the spatial components of Gaussian stochastic torque in one figure.

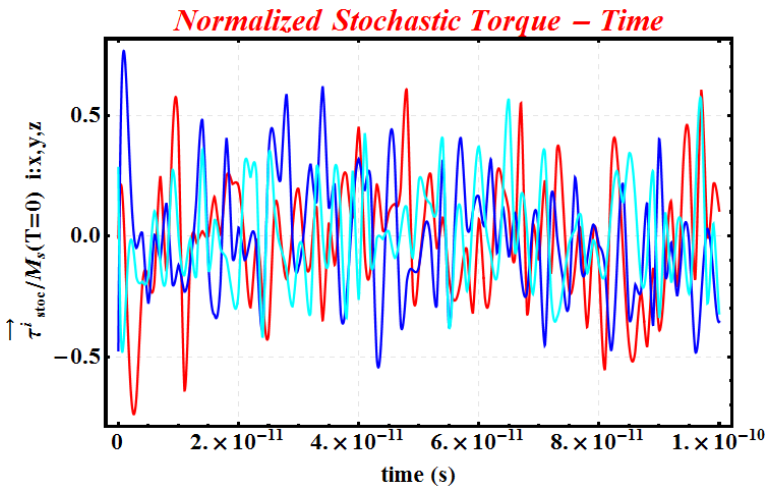

Figure F.9. The spatial components of normalized Gaussian stochastic torque.

The spatial components of the torque form of the Gaussian stochastic process are mainly a randomly fluctuating based upon Gaussian function.

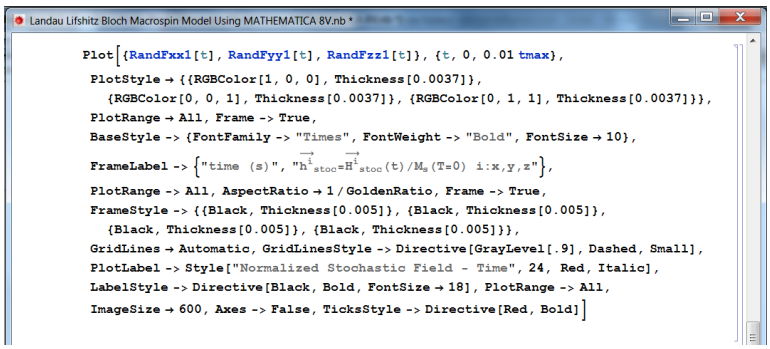

Figure F.10. The codes written for the purpose of showing the spatial components of Gaussian stochastic field in one figure.

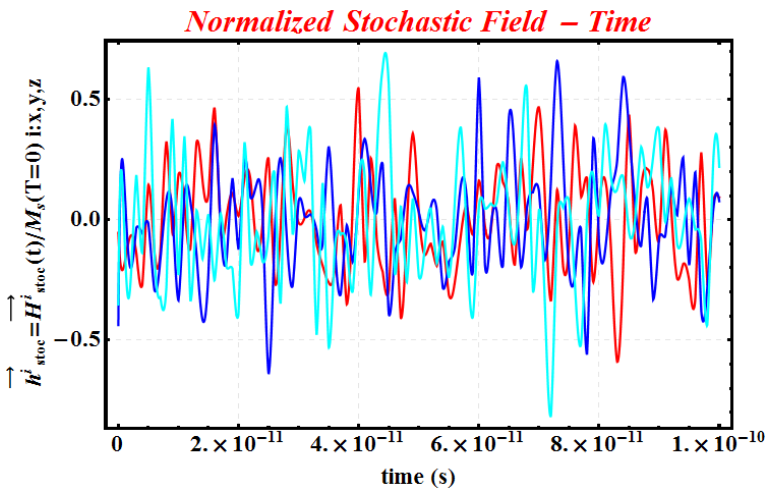

Figure F.11. The spatial components of normalized Gaussian stochastic field.

The spatial components of the field form of the Gaussian stochastic process are mainly a randomly fluctuating based upon Gaussian function.

When the descriptions of both transverse and longitudinal Gaussian stochastic processes are implemented the last thing is to manipulate the amplitudes of the external magnetic field pulse and heating pulse. Below screen shots are components of these manipulations.

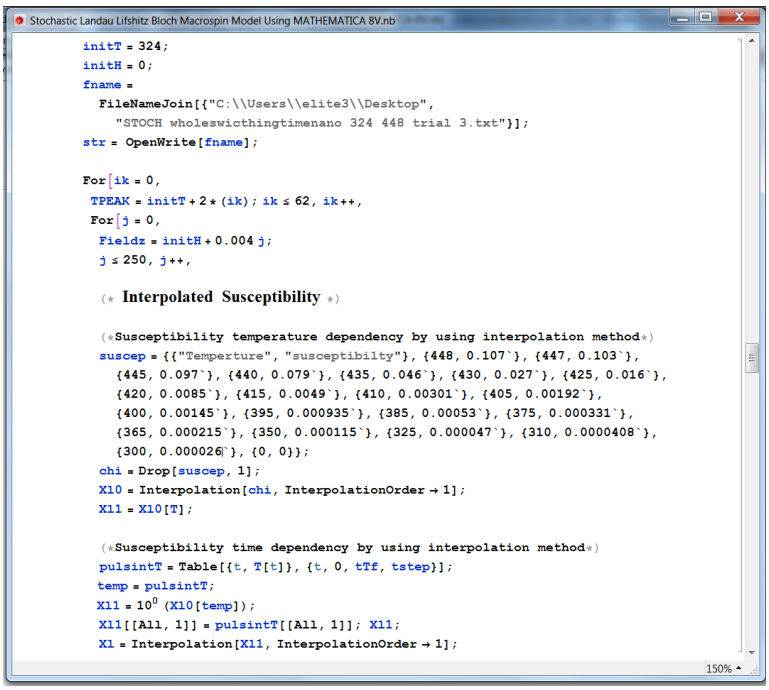

Figure F.12. This is the screen shot which shows the required codes for both the creation of the different combinations of field and heating pulses and interpolating susceptibility.

The first thing is to set a directory for a document in which all data will be saved in. The screen shot shown above is showing the way of creating a file with a specified directory. After that the parameters which are affected by the manipulated variables must be inserted inside of this manipulation command. Moreover, one of them is longitudinal susceptibility. The screenshot above shows also this inclusion.

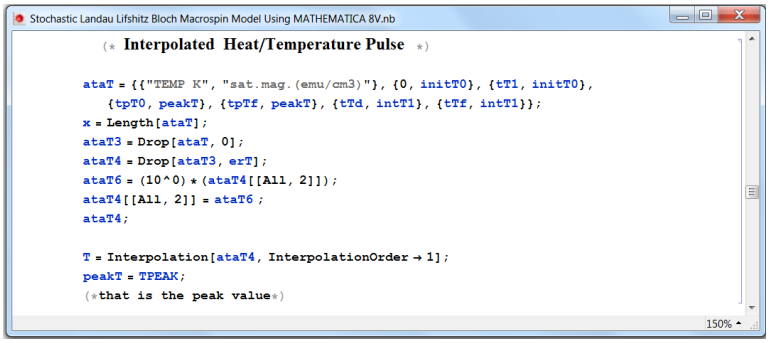

Figure F.13. These are the codes for the creation of heating pulse.

One of the variables of the switching time distribution model is heating pulse. Whist the width of the heating pulse is kept constant, the amplitude will be varied by using manipulation command. The saturation magnetization and zero field equilibrium magnetization depend on temperature. Since the system temperature is a function of time. These two intrinsic parameters are time dependent, as well. Moreover, to include them in the manipulation command is also a requirement.

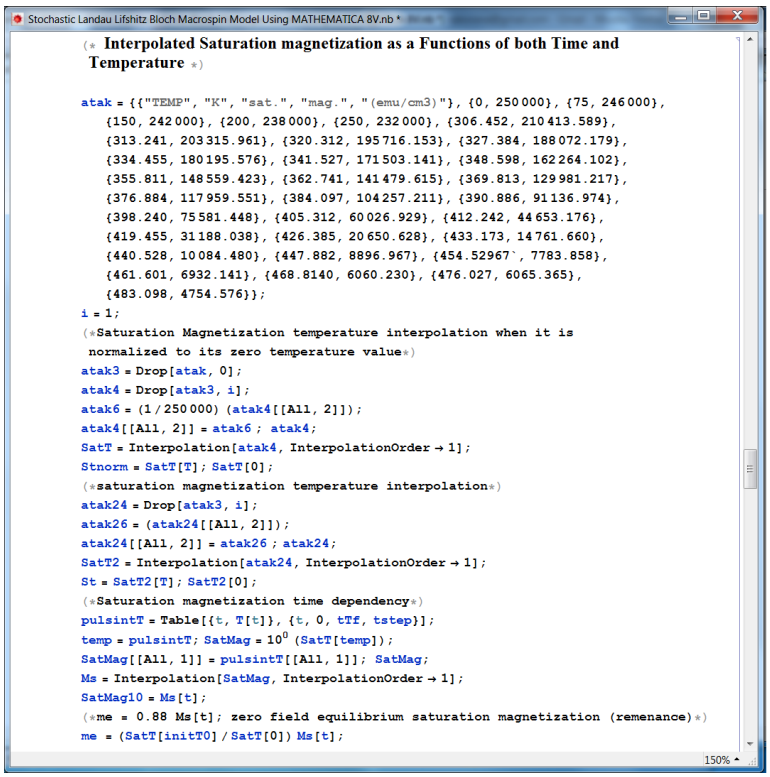

Figure F.14. This is the screen shot for the creation of time and temperature dependence of saturation magnetization.

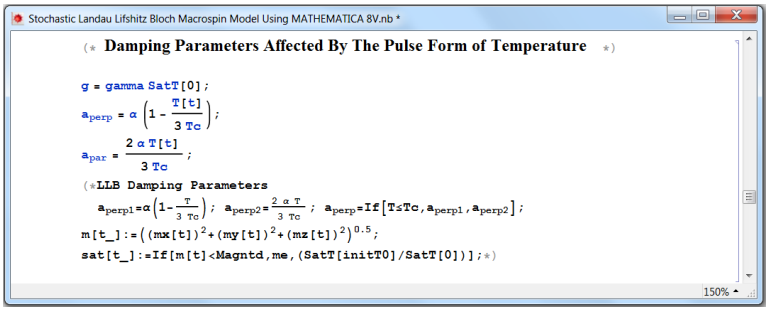

Figure F.15. This is the screen shot for the creation of time and temperature dependence of damping parameters.

Another two temperature dependent parameters are parallel and transverse damping parameters. Due to their dependence on temperature, their values are changing in time, as well. Moreover, these two parameters are inserted in the manipulation.

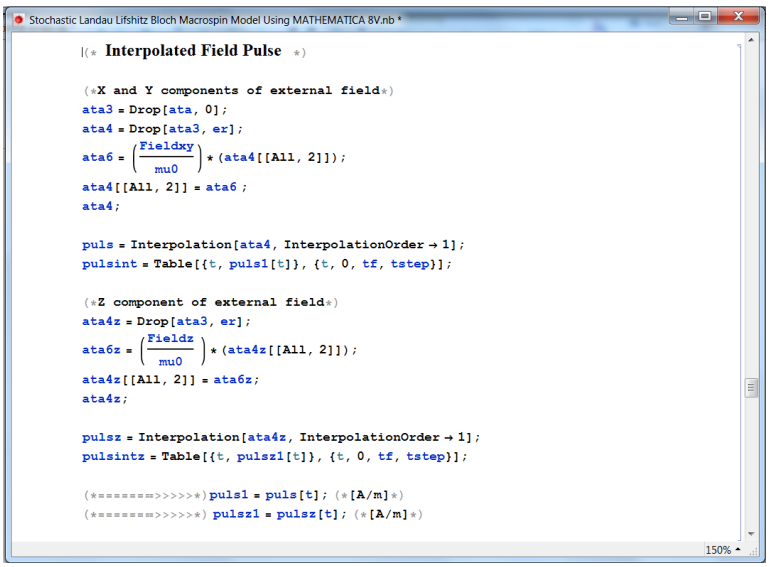

Figure F.16. The screen shot shows the necessary codes which are written to create an adjustable interpolating field pulse.

The second variant of the manipulation is the amplitude of magnetic field pulse. The screenshot above shows the necessary commands to create an adjustable field pulse. Since the manipulation depends on the amplitude of field pulse, the codes written for the creation of a magnetic field is inserted in the manipulation.

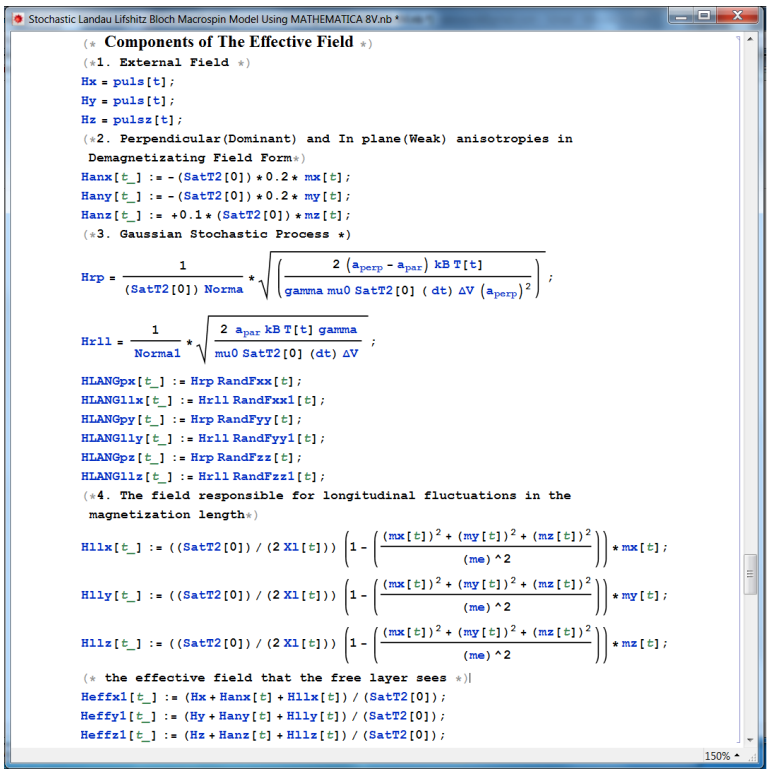

Figure F.17. The screen shot shows the necessary codes for the identifications of components of effective field.

The effective magnetic field does not only depend on the temperature of the system but also the external magnetic field is one of the components of the effective field. The screenshot above shows the codes of the effective magnetic field.

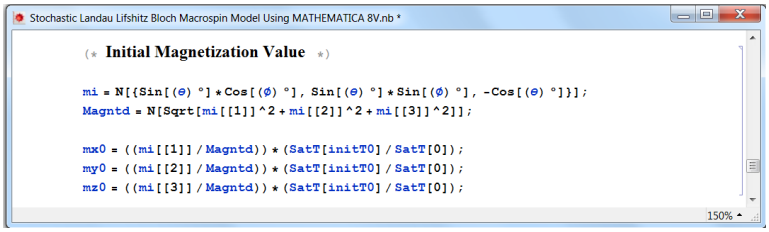

Figure F.18. The screen shot shows the necessary codes to identify the initial condition of the magnetization vector.

The determination of the initial condition of magnetization vector is definitely important. In our case, the preference of highly perpendicular anisotropy magnetic media makes the preferential direction of the magnetic moments perpendicular to the plane. Yet, for the ferromagnetic materials, there are more than one magnetic anisotropies. While one of them is dominant, others weakly exist. That is why the initial condition of the magnetization vector is tilted a little from perpendicular direction to the thin film plane.

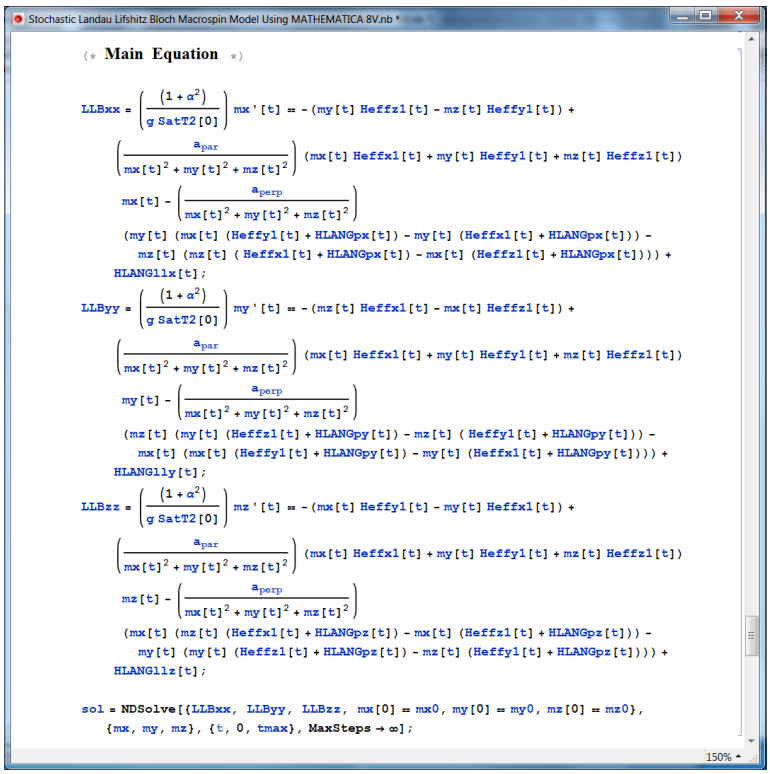

Figure F.19. The screen shot shows the required codes to describe the main equation (S-LLB II formalism).

The LLB equation is distinguished into three spatial components. They are also included in the manipulation because, in the end, all variables are plugged into this main equation.

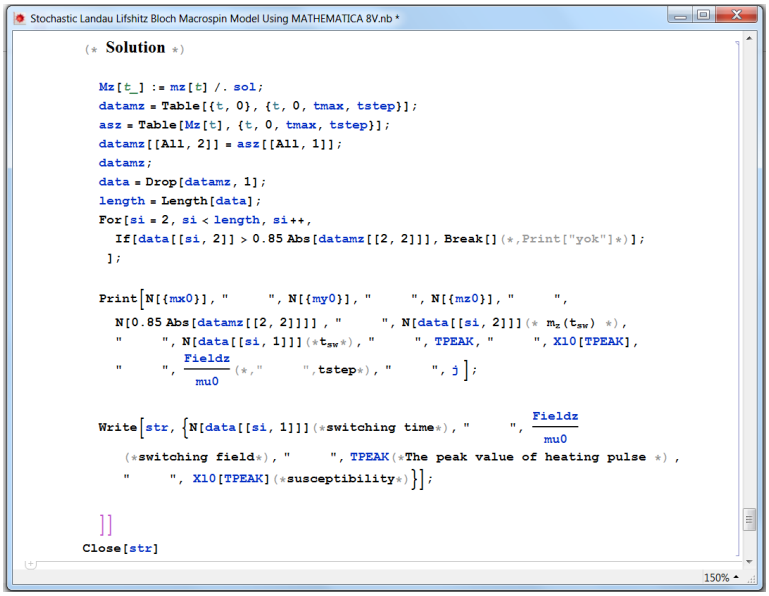

Figure F.20. The screen shot which is taken from the S-LLB II model created in Mathematica. This part is exigent for extracting the outputs from this model.

The last part of the manipulation is related to outputs. After the determinations of the outputs of the LLB based macrospin model, using the codes which are shown in the screenshot above, we write the outputs in a file whose directory is determined in the beginning.

APPENDIX G: SOFTWARE INTERFACE OF MACROSPIN LLB MODEL FOR CONI/PD MLS

In this section, by manipulating some crucial parameters in the macrospin model, we end up with a minimal but sufficient interface of the LLB macrospin modeling. The following figure is the screen shot of the interface. It enables us having user friendly and

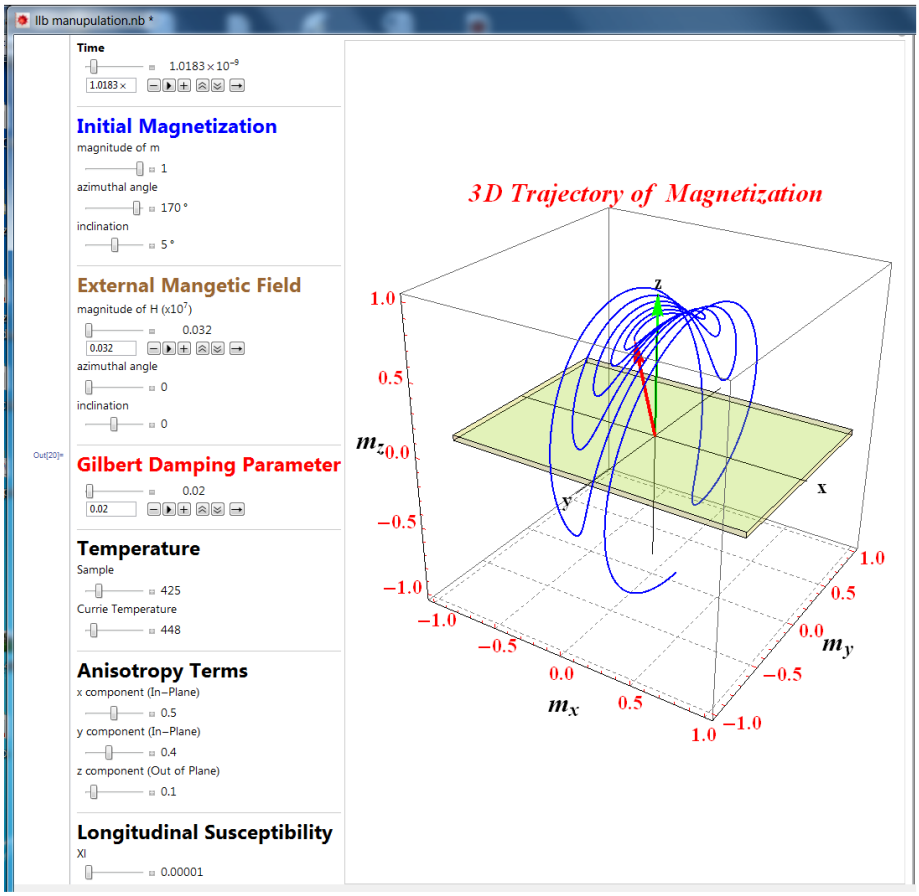

Figure G.1. An extensive manipulation of the LLB based macrospin model.

interactive applications by setting some inputs. So that modifying the implemented codes for each time is not necessary. In pursuit of this goal, we can observe the behavior of the magnetization vector as it is under the influence of an external magnetic field. Besides as response of the magnetization to the given parameters, we can follow the magnetization vector trajectory in each time step.

APPENDIX H: EXPERIMENTAL ANALYSIS (VSM MEASUREMENT TECHNIQUE)

One of our staple goals is to use the experimentally determined temperature dependence of intrinsic properties of a magnetic structure. As it has been stated before that we preferred CoNi/Pd magnetic multilayer structure which possesses high perpendicular anisotropy which makes it a potential recording layer candidate for the HAMR system. In this appendix, we will try to give some detailed information about the experimental work.

The first thing which needs to be identified is that CoNi/Pd multilayer structure is obtained by using sputtering technique. The Figure H.1 is the schematic illustration of the whole structure. This multilayer system is sputter deposited onto Si/SiO2 substrate with a structure of Ta (1.5)/Pd (3)/ [$Co_{55}Ni_{45}$ (0.22) / Pd (1.2)] x 22 repeats /Pd (2) (where all thicknesses are in nanometer scale). Temperature dependence of hysteresis loops, saturation magnetization, and coercive field of the whole structure were measured by using vibrating sample magnetometry (VSM). It is worth noting that the temperature of the system ranges from room temperature (300 K) up to the Curie temperature of the sample (T_c=448K) [7] In this appendix, the VSM measure-

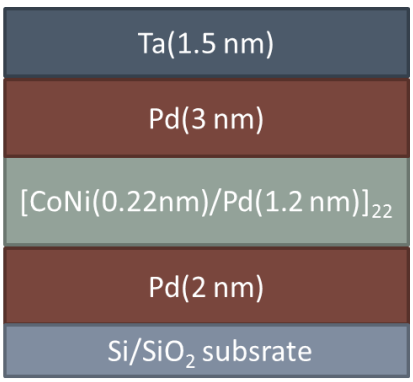

Figure H.1. Schematic representation of the CoNi/Pd MLs structure.

ment technique will be presented in-detail. A VSM is used to measure the magnetic

behavior of magnetic materials and it is based on the measurement of magnetic flux change in a coil when a magnetized sample is vibrated near it. The magnetic sample is attached to one end of a nonmagnetic rod (it is a kind of versatile sample holder), the other end of which is connected to a driving system (a loudspeaker cone Figure H.2) or another kind of mechanical vibrator). This driving system is in charge of the vibration of the sample. Moreover, the magnetic dipole moments create a magnetic field around the sample and it is called the magnetic stray field. As the sample is moved up and down, this magnetic stray field changes as a function of time and can be sensed by a set of pick-up coils. The vibration of the magnetic sample results in an oscillating magnetic field and this induces an alternating electromotive force (emf) in the coils. Furthermore, the magnitude of the induced emf is proportional to the magnetic moment of the sample. The (small) alternating emf is usually amplified via a lock-in amplifier. This amplifier is adjusted to sense only the signals with the specified vibration frequency. In other words, a reference signal at the frequency of vibration is required for the lock-in amplifier, which can come from an optical, magnetic, or capacitive sensor coupled to the driving system. There are many types of driving systems [22]. One of them is in the mechanical form which is carried out by a cam or crank (which is a rotating disk shaped to convert circular motion into linear motion). In this case, the vibration frequency is generally below 40 Hz, and the vibration amplitude is a few millimeters. The amplitude is fixed by the geometry of the mechanical system.

By the advent of new technologies, the mechanical driving system is replaced by the linear motor based driving system. Moreover, the amplitude is fixed by the drive signal to the linear motor. Alternatively, another driving system which is based on a loudspeaker, as in Figure H.2. In this case, the frequency is generally about 100 Hz, and the amplitude is near 0.1 mm. Therefore, the latter driving technique is more sensitive than the preceding one. However, in this case, depending on the mass of the sample and its interaction with the magnetic field, the amplitude may vary. To control and monitor both the variations in the amplitude and the frequency, there must be some provisions. One method for this is to attach a small permanent magnet to the sample rod, outside the varying field region, with a second set of sensing coils Figure H.2. The important maintenance is to minimize vibration of the sensing coils in the magnetic

field, and to keep the measuring field from influencing other parts of the system. It is important to note that the VSM measures the magnetic moment (m) of the sample, and therefore the magnetization M, whereas the fluxmeter method ordinarily measures the flux density B.

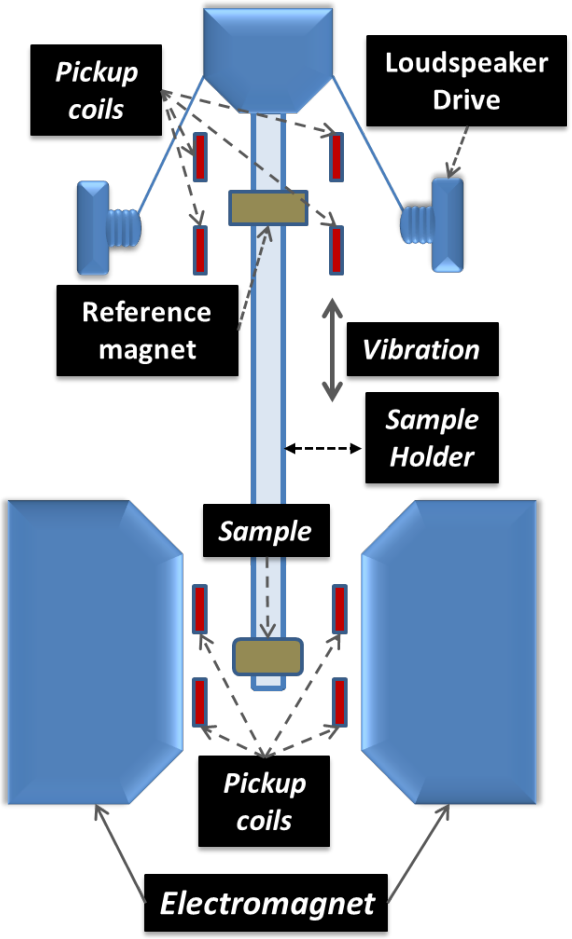

Figure H.2. Schematic representation of the VSM technique.

As a consequence, the VSM is very versatile and sensitive. It may be used for both weakly and strongly magnetic substances, and standard versions can detect a magnetic moment of about 10^{-5} emu = 1 erg/Oe or 10^{-8} Am^2. This corresponds to the saturation magnetization of about 0.04 mg of iron, which suggests the attention to cleanliness. That is definitely necessary when measuring small or weakly magnetic samples [22].

The VSM must be used with care in the determination of the magnetization curves or hysteresis loops of magnetically soft materials. The specimen has to be short and the demagnetizing field may then be such a large fraction of the applied field that the true field is uncertain. However, if the sample is or can be made very thin, as is often the case in spintronic devices, the demagnetizing correction can be small or negligible. The demagnetizing correction is also generally unimportant in the determination of saturation magnetization M_S [22]. The VSM can be adapted for measurements at high and low temperatures, since only the sample and the vibrating rod must be heated or cooled. VSMs are limited to small samples, generally less than 1 g. In addition to these, the various components of VSM technique are hooked up to a computer interface. By means of the interfaces which are controlling and monitoring software, the VSM system can tell you more accurately how much the sample is magnetized and how its magnetization depends on the strength of the constant magnetic field.

REFERENCES

1. Atxitia, U., O. Chubykalo-Fesenko, N. Kazantseva, D. Hinzke, U. Nowak and R. W. Chantrell, "Micromagnetic Modeling Of Laser-Induced Magnetization Dynamics Using The Landau-Lifshitz-Bloch Equation", *Applied Physics Letters*, Vol. 91, No. 23, p. 232507, 2007.

2. Wiederrecht, G., *Handbook Of Nanoscale Optics And Electronics*, Academic Press, Amsterdam, 2010.

3. Evans, R., R. Chantrell, U. Nowak, A. Lyberatos and H. Richter, "Thermally Induced Error: Density Limit For Magnetic Data Storage", *Applied Physics Letters*, Vol. 100, No. 10, pp. 102402–102402, 2012.

4. Nagata, K., Y. Kawakubo, D. Kato and T. Sugiyama, "Durability Of Thermally Assisted Magnetic Recording Disk", *Magnetic Recording Conference, 2002. Digest of the Asia-Pacific*, pp. TU–TU, IEEE, 2002.

5. Rottmayer, R., S. Batra, D. Buechel, W. Challener, J. Hohlfeld, Y. Kubota, L. Li, B. Lu, C. Mihalcea, K. Mountfield *et al.*, "Heat-assisted Magnetic Recording", *Magnetics, IEEE Transactions on*, Vol. 42, No. 10, pp. 2417–2421, 2006.

6. Garanin, D., "Fokker-Planck And Landau-Lifshitz-Bloch Equations For Classical Ferromagnets", *Physical Review B*, Vol. 55, No. 5, p. 3050, 1997.

7. Ozatay, O., T. Hauet, S. H. Florez, J. A. Katine, A. Moser, J.-U. Thiele, L. Folks and B. D. Terris, "Probing Activation Energy Barrier Distribution For Reversal Of Strongly Exchange-Coupled Magnetic Multilayer Thin Films", *Applied Physics Letters*, Vol. 95, No. 17, p. 172502, 2009.

8. Comsol, A., "Comsol Multiphysics User's Guide", *Version: September*, 2005.

9. Landau, L. D. and E. M. Lifshitz, "On The Theory Of The Dispersion Of Magnetic Permeability In Ferromagnetic Bodies.", *Phys. Z. Sowietunion*, Vol. 8, pp. 153–169, 1935.

10. Helmut Kronmüller, S. P., *Handbook Of Magnetism And Advanced Magnetic Materials*, WILEY, 2007.

11. McDaniel, T., "Application Of Landau-Lifshitz-Bloch Dynamics To Grain Switching In Heat-Assisted Magnetic Recording", *Journal of Applied Physics*, Vol. 112, No. 1, pp. 013914–013914, 2012.

12. Evans, R. F. L., D. Hinzke, U. Atxitia, U. Nowak, R. W. Chantrell and O. Chubykalo-Fesenko, "Stochastic Form Of The Landau-Lifshitz-Bloch Equation", *Phys. Rev. B*, Vol. 85, p. 014433, Jan 2012.

13. Spaldin, N., *Magnetic Materials: Fundamentals And Device Applications*, Cambridge University Press, Cambridge, 2003.

14. Chubykalo-Fesenko, O., U. Nowak, R. Chantrell and D. Garanin, "Dynamic Approach For Micromagnetics Close To The Curie Temperature", *Physical Review B*, Vol. 74, No. 9, p. 094436, 2006.

15. Atxitia, U., O. Chubykalo-Fesenko, J. Walowski, A. Mann and M. Munzenberg, "Tracing The Thermal Mechanism In Femtosecond Spin Dynamics", *arXiv preprint arXiv:0904.4399*, 2009.

16. Taylor, B., P. Mohr and M. Douma, "NIST Reference On Constants, Units, And Uncertainty", *National Institute of Standards and Technology*, 2000.

17. Finocchio, G., L. Torres, G. Consolo, M. Carpentieri and B. Azzerboni, "Magnetic Vortex Driven By Non-uniform Injection Of Spin-polarized Current In Nano-scale Spin Valves", *Journal of Magnetism and Magnetic Materials*, Vol. 321, No. 6, pp. 602 – 606, 2009, ¡ce:title¿Current Perspectives: Perpendicular Recording¡/ce:title¿.

18. Finocchio, G., I. N. Krivorotov, X. Cheng, L. Torres and B. Azzerboni, "Micromagnetic Understanding Of Stochastic Resonance Driven By Spin-Transfer-Torque", *Phys. Rev. B*, Vol. 83, p. 134402, Apr 2011.

19. Jr., W. F. B., "Thermal Fluctuations Of A Single-Domain Particle", *Physical Review*, Vol. 130, pp. 1677–1686, 1963.

20. Kilic, U., G. Finocchio, T. Hauet, S. H. Florez, G. Aktas and O. Ozatay, "Magnetic Switching Driven By Nanosecond Scale Heat And Magnetic Field Pulses: An Application Of Macrospin Landau-Lifshitz-Bloch Model", *Applied Physics Letters*, Vol. 101, No. 25, p. 252407, 2012.

21. Kimel, A., A. Kirilyuk, P. Usachev, R. Pisarev, A. Balbashov and T. Rasing, "Ultrafast Non-thermal Control Of Magnetization By Instantaneous Photomagnetic Pulses", *Nature*, Vol. 435, No. 7042, pp. 655–657, 2005.

22. Cullity, B. D. and C. D. Graham, *Introduction To Magnetic Materials*, Wiley-IEEE Press, 2 edn., 2008.